ANNEX 1

SOLVENT EXTRACTION AND ION EXCHANGE, 18(2), 345–374 (2000)

KINETICS OF RELEASE OF CALCIUM AND FLUORIDE IONS FROM ION-EXCHANGE RESINS IN ARTIFICIAL SALIVA

Dmitri Muraviev[1*], Anna Torrado and Manuel Valiente
Unidad de Química Analítica, Universitat Autònoma de Barcelona
E-08193 Bellaterra (Barcelona), Spain.

ABSTRACT

The paper reports the results obtained by studying the kinetics of release of anti-carious ions, such as Ca^{2+} and F^-, from a carboxylic cation exchanger, Lewatit S8528, and a weak base resin, Lewatit MP62, and their binary mixtures of different compositions in contact with solution of artificial saliva. The release of ions from the resins was studied by using both the "shallow bed" and the "limited volume" techniques varying the granulometric composition of the resin fractions in the range of bead diameters from 0.42 to < 0.050 mm. It has been shown that the kinetics of Ca^{2+} release is far slower than that of F^- ions. The release of F^- ions from the resin mixtures of different compositions is essentially not affected by the presence of the cation exchanger in the Ca-form in the mixture. An opposite situation is observed for the release of Ca^{2+} ions, which appears to be far slower in the presence of the anion exchanger in the F-form in the resin mixtures. The results obtained are explained by different diffusivities of the ions under study. The formation of a microcrystalline CaF_2 layer on the surface of cation-exchanger beads has been shown to be responsible for the retardation of calcium ions release from the resin phase.

Author for correspondence. [1] On sabbatical leave from Lomonosov Moscow State University, Department of Physical Chemistry, 119899 Moscow, Russia; E-mail: dimitri@septsci.uab.es

INTRODUCTION

Ion-exchange materials are mainly used for removal and separation of ionic species from aqueous or non-aqueous solutions [1-5]. Demineralisation of water [6-8] and other non-electrolytes [3, 9, 10], removal of metal ions from industrial waste waters and effluents [11-13], separation of metal ion [14-16] and some other problems can be successfully solved by using ion-exchange materials of different types. The majority of industrial applications of ion exchangers are based on the "demineralisation" concept. Nevertheless, their ability to substitute (exchange) ions of one type for ions of another type quite logically suggests a possibility to use these materials for "remineralization" purposes. For example, application of ion-exchange materials as an easily regulated source of desired ionic species was effectively used for the preparation of artificial nutrient media for plants (ion-exchanger soils) [17]. For this purpose a cation- and anion-exchange resins were first loaded with ions of biogenic elements such as, K^+, Ca^{2+}, Mg^{2+}, NO_3^-, $H_2PO_4^-$ and some others and then mixed in the desired proportion corresponding to the physiological demands of plants [18]. A similar approach can be used to solve some other remineralization problems such as, for example, remineralization of mineralorganic (e.g., dental) tissues.

Tooth caries (both deep and surface) is known to result in demineralization of dental tissues due to bacterial activity leading to the formation of lactic acid and some other products of bacteria metabolism. This acid, being a relatively strong complexing agent [19], can interact with calcium containing tissues (such as, e.g.,

fluoroapatite) converting calcium component in the water soluble calcium lactate. This results, in turn, in the destruction of caries infected teeth due to their partial decalcination. A conventional treatment of deep caries is based on the use of calcium hydroxide containing materials. The prevention of caries is usually provided by using fluoride containing toothpastes, mouthrinses and varnishes [20, 21]. Several communications reported the use of ion-exchange resins in the Ca- and F-forms for the anti-carious treatment of dental tissues [22-24]. Nevertheless, no data on the kinetics of Ca^{2+} and/or F^- release from ion-exchange resins under conditions imitating their *in vivo* application can be found in the literature.

The present work has been undertaken 1) to study the kinetics of Ca^{2+} – (K^+ + Na^+) and F^- – Cl^- exchanges on weakly acidic and weakly basic ion-exchange resins in contact with solution of artificial saliva; 2) to evaluate the mechanism of the ion-exchange reactions under consideration through identification of the process rate-controlling step, and 3) to study the kinetics of both Ca^{2+} and F^- release from the mixtures of powdered resins of different compositions.

EXPERIMENTAL

Reagents, Ion exchangers and Apparatus

Calcium chloride, sodium fluoride, sodium chloride, potassium chloride, potassium hydroxide and acetic acid of analytical grade were purchased from Panreac (PA, Barcelona, Spain). Carboxylic resin, Lewatit S8528, and a weak base resin, Lewatit MP62, were kindly supplied by Bayer Hispania Industrial,

TABLE 1. MAIN CHARACTERISTICS OF ION-EXCHANGE RESINS

Type	Lewatit S8528	Lewatit MP62
Functional group	Carboxylic	Tertiary amine
Capacity (mmol/g)	3.55±0.03	2.91±0.04
Color	Yellow	Beige
Density (g/cm^3)	1.18	1.03
Apparent density (g/cm^3)	0.75 – 0.85	0.60 – 0.70
Working pH range	< 4	≤ 8

S.A. The main properties of the resins are collected in Table 1. Seamless cellulose dialysis tubing was purchased from Sigma Chemical CO. (St. Louis, USA). Doubly distilled water was used in all experiments. Prior to experiments the resins were additionally conditioned by following a standard procedure [25]. The conversion of the resins to the desired ionic form was carried out under dynamic conditions in ion-exchange columns by passing 0.3 M $CaCl_2$ or 0.9 M NaF solutions through the resin beds. The cation and anion exchanger were preliminary converted to the K- and the Ac-form, respectively, to simplify their final conversion to the desired ionic form (Ca^{2+} or F). After complete loading of the resins with respective counter-ion the resin phase was rinsed with water to remove the excess of electrolyte solution. Then the resins were quantitatively removed from the columns, filtered and air-dried. Samples of the air-dry resins in different ionic forms were sieved by using a standard set of stainless steal sieves (CISA, Spain) to collect the narrow granulometric fractions with bead diameters of 0.42, 0.335, 0.205 and 0.105 mm. To fulfil this condition, only the beads stuck in the holes of the respective sieve were collected. A portion of each resin was

also powdered by using a mechanical agate mortar (Retsch RMO, Germany) followed by sieving to obtain resin fractions with particle diameter of <0.05 mm. The concentration of calcium ions was controlled either by the ICP technique using an ARL Model 3410 spectrometer with minitorch (emission line of 422.67 nm) or by a 9300BN Orion selective electrode and a 3010 Easi Ag/AgCl reference electrode. The concentration of fluoride ions was followed by using a 9609BN Orion combined fluoride selective electrode. The release of ions under batch experiments was followed up by PC controlled ion-selective electrodes. Glass columns (of 1.0 and 1.5 cm i.d) with a porous polymeric bed support at the bottom and translucent end fittings (Bio-Rad, USA) were used for carrying out the ion-exchange equilibrium and kinetic experiments under dynamic experiments. Glass cells (of 5.5 cm i.d) connected with a thermostat (Grant KA, Spain) were used to study the ion-exchange kinetics at a given temperature under batch conditions.

Procedure

The experiments on the kinetics of ion exchange on resins of different granulation were carried out under dynamic conditions at 293 ± 1 K by using the "shallow bed" technique [see Ref. 25, p.94]. A small portion of each resin (0.1-0.5g) of known granulation was placed in an ion-exchange column. A solution of artificial saliva (0.5 g/dm^3 NaCl and 1 g/dm^3 KCl) was passed through the column at a high flow rate (35 ml/min). The resulting eluate was collected in portions followed by determination of either Ca^{2+} or F^- concentration in all samples

collected. Then the resins were rinsed with water to remove the excess of electrolyte solution followed by stripping of the residual Ca^{2+} or F^- ions with either 0.5 mol/dm^3 HCl (for cation-exchange resin) or 0.5 mol/dm^3 $NaNO_3$ (for anion-exchange resin). The stripping solution was collected and analysed to determine either Ca^{2+} or F^- content. Determination of the rate-controlling step was carried out by using the "interruption test" technique described elsewhere [see Ref. 25, p. 87].

The experiments on the kinetics of ion-exchange on finely powdered ion-exchangers (bead diameter <0.05mm) were carried out under batch conditions at 310 ± 0.5 K by using the "limited volume" technique [26]. A small portion (0.050 g) of the resin or resins mixture of different composition was introduced into a 6 cm dialysis tube. In experiments on evaluation of the rate of Ca^{2+} and F^- diffusion through the dialysis membrane (blank-experiments), the tube was loaded with an aliquot of 2 ml containing the same amount of respective ion as the resin portions used. The tube was closed hermetically and placed on a stainless steel net support rigidly fixed at the bottom of the thermostatic cell containing 50ml of artificial saliva pre-equilibrated at 310 K. The liquid phase in the cell was vigorously agitated by using a magnetic stirrer. The moment when the net was introduced in the cell was counted as zero time for kinetic experiments. The data obtained in dynamic experiments were used to determine the degree of resin conversion, F, expressed as follows:

$$F = \frac{\sum_{i=1}^{j} C_i v_i}{q_\infty} \qquad (1)$$

where v_i is the volume of the eluate sample number i; c_i is the concentration of ion under displacement (Ca^{2+} or F) in i sample, and q_∞ is the total capacity of the resin, which was determined from the results of kinetic and stripping experiments as follows:

$$q_\infty = \sum c_i v_i + V_{str} C_{str} \tag{2}$$

where V_{str} is the volume of the stripping solution collected, and C_{str} is the concentration of ion under interest in this solution.

The results of kinetic experiments obtained under batch conditions were used to calculate F values by using the following equation:

$$F = \frac{V_{as}\, c(t_i)}{q_\infty} \tag{3}$$

where V_{as} is the volume of artificial saliva in the cell; $c(t_i)$ is the concentration of ion under study in the cell corresponding to the period of time t_i, and $q_\infty = mq_s$ is the total capacity of the resin sample of mass m (g) with specific capacity of q_s (meq/g).

Experimental results obtained in kinetic experiments under dynamic conditions were presented in the form of respective kinetic curves (F versus time plots) followed by their treatment with the use of the following equations describing the kinetics of ion exchange controlled by intraparticle diffusion mechanism:

Model 1 [26]:

$$F = 1.08\,(Bt)^{1/2} \tag{4}$$

where t is the time, and parameter B is the effective diffusion rate defined as follows:

$$B = \frac{D\pi^2}{r^2} \tag{5}$$

Here D is the diffusion coefficient of ion under consideration in the resin phase, and r is the radius of the resin beads.

Model 2 (Vermeulen approximation) [27, 28]:

$$-\ln(1 - F^2) = \frac{D\pi^2}{r^2}\,t = B\,t \tag{6}$$

Model 1 (equation 4) is known to be applicable at $F < 0.05$ while the range of applicability of Model 2 (equation 6) covers the interval of all possible F values from 0 to 1.

RESULTS AND DISCUSSION

The ion-exchange reactions, which proceed in systems involving the resins under study and solution of artificial saliva (AS) can be written as follows:

Lewatit S8528 – AS system

$$(R\text{-}COO^-)_2\,Ca + 2Na^+ \rightarrow 2R\text{-}COO^-\,Na^+ + Ca^{2+} \tag{7}$$

$$(R\text{-}COO^-)_2\,Ca + 2K^+ \rightarrow 2R\text{-}COO^-\,K^+ + Ca^{2+} \tag{8}$$

Lewatit MP62 – AS system

$$R\text{-}(R')_2HN^+ F^- + Cl^- \rightarrow R\text{-}(R')_2HN^+ Cl^- + F^- \quad (9)$$

After adding equations (7) and (8) one obtains the following equation describing the overall cation-exchange process proceeding in Lewatit S8528 – AS system:

$$(R\text{-}COO^-)_2 Ca + (Na^+ + K^+) \rightarrow (R\text{-}COO^-)_2 Na^+K^+ + Ca^{2+} \quad (10)$$

Equation (10) permits to reduce the tricomponent cation-exchange system under consideration to a pseudo-bicomponent one. The validity of this approximation follows from the far higher selectivity of the carboxylic resin towards Ca^{2+} in comparison with that for alkali metal ions such as, Na^+ and K^+ [29-31]. Indeed, the far lower affinity of the resin towards unicharged ions and their higher diffusivity in the resin phase (in comparison with Ca^{2+} [see Ref. 25, p.90]) allows one to neglect their interference with each other. The ion-exchange reaction (10) can be considered to proceed "against" the selectivity of the resin and must be characterised by slow kinetics. The ion-exchange reaction (9) must proceed far faster than reaction (10) as in this case the sorbability sequence of exchanging ions is the opposite, i.e. a stronger sorbed ion (Cl^-) displaces a weaker sorbed one (F^-).

The typical concentration-time histories (kinetic curves) of $Ca^{2+} - (Na^+ + K^+)$ and $F^- - Cl^-$ exchanges on Lewatit S8528 and Lewatit MP62 resin samples of different granulation are shown in Fig.1a and 1b, respectively. As follows from

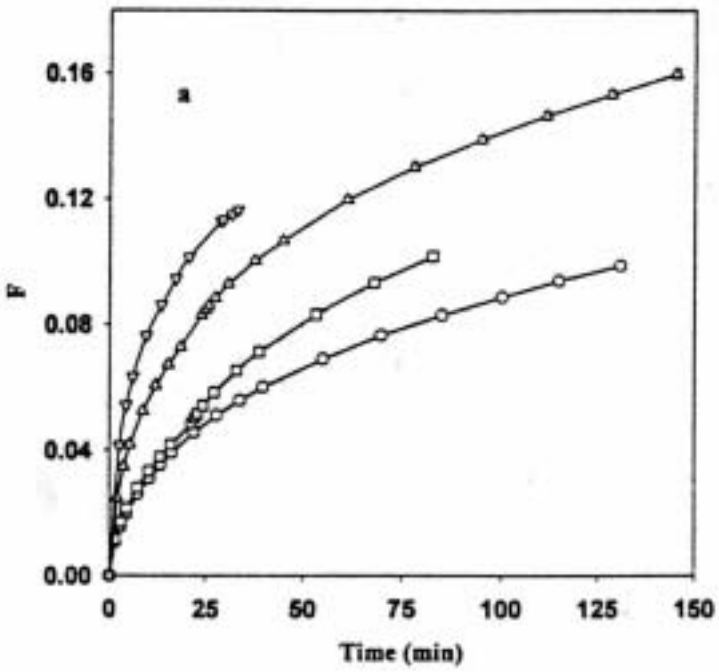

FIGURE 1. Concentration-time histories of Ca^{2+} – Na^{+}/K^{+} (a) and F^{-} – Cl^{-} (b) exchanges on Lewatit S8528 (a) and Lewatit MP62 (b) resin samples of different granulation at 293 K: 0.42 mm (circles), 0.335 mm (squares); 0.205 mm (triangles); 0.105 mm (inverse triangles).

the comparison of the kinetic curves shown in Fig. 1a with those presented in Fig. 1b, the rate of F^{-} ions release is far higher than that of Ca^{2+} ions, which confirms the above predictions. The kinetics of ion exchange in both systems depends on the size of resin beads indicating that intraparticle diffusion is the rate-controlling step of both processes. This conclusion is confirmed by the results obtained by determination of the rate-determining step of the ion-exchange reactions under study, shown in Fig. 2. As seen, the rate of exchange on both cation- (see Fig. 2a) and anion-exchange resin (see Fig. 2b) substantially increases after a temporary

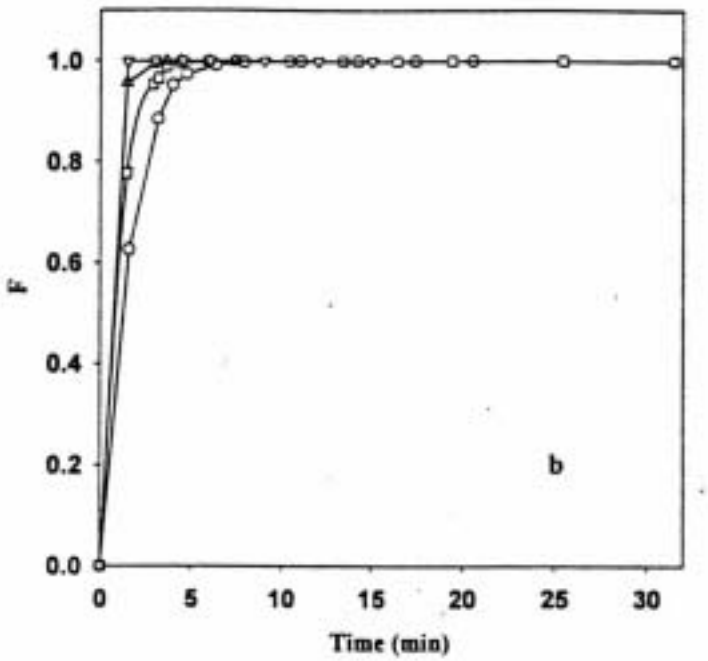

FIG. 1. Continued.

isolation of the resin from the solution phase ("interruption test"). This result clearly indicats that the ion-exchange process in both cases is controlled by the intraparticle diffusion mechanism [25]. An additional confirmation of this conclusion is provided by the data shown in Figs. 3 and 4 where the results of the treatment of kinetic curves shown in Fig. 1 are treated by using equation 4 (see Figs. 3a and 4a) and equation 6 (see Figs. 3b and 4b). As seen, both F vs $t^{1/2}$ and $-\ln(1 - F^2)$ vs t dependencies are well approximated by straight lines, which provides additional confirmation of the above conclusion about intraparticle diffusion control of the ion-exchange processes under study. Note that similar linear dependencies were obtained by the treatment of other experimental data on

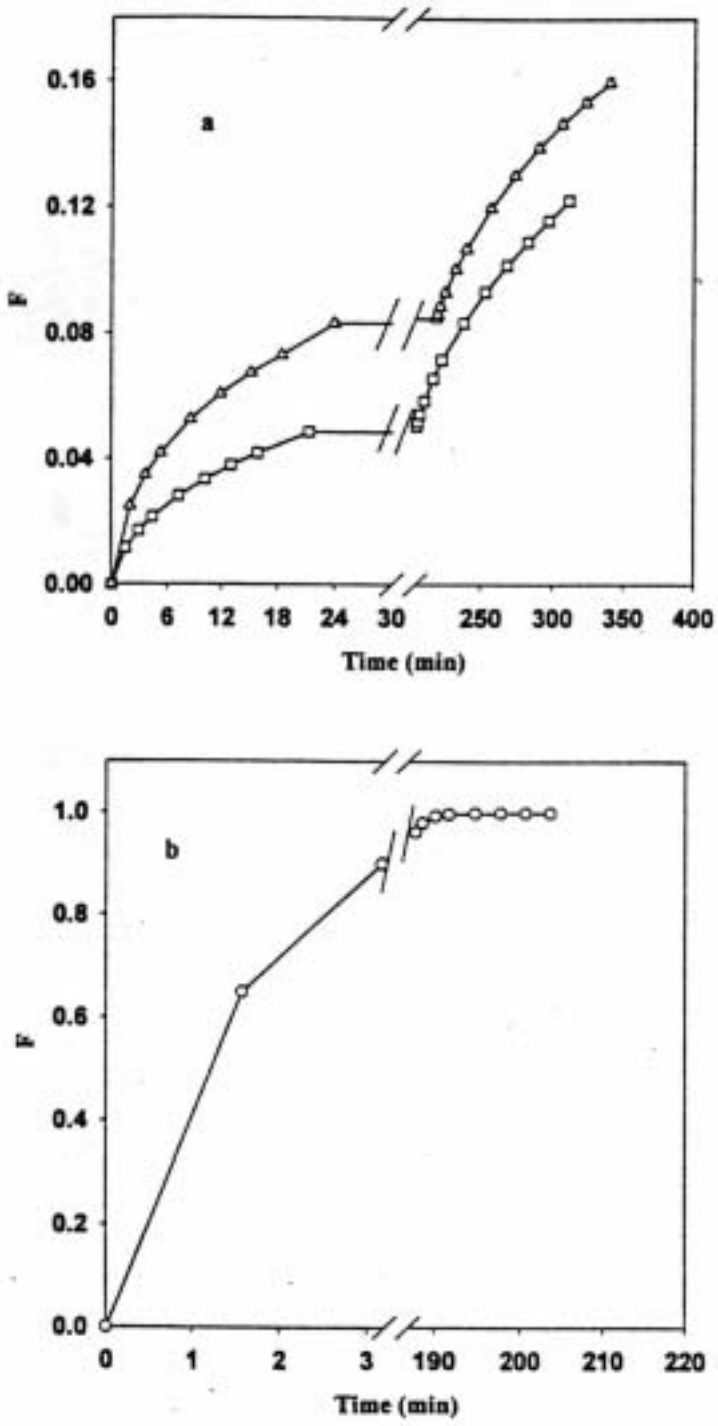

FIGURE 2. Kinetic curves of Ca – Na/K (a) and F – Cl (b) exchanges obtained in "interruption test" experiments on resin samples of different granulation: 0.42 mm (circles); 0.335 mm (squares); 0.205 (triangles).

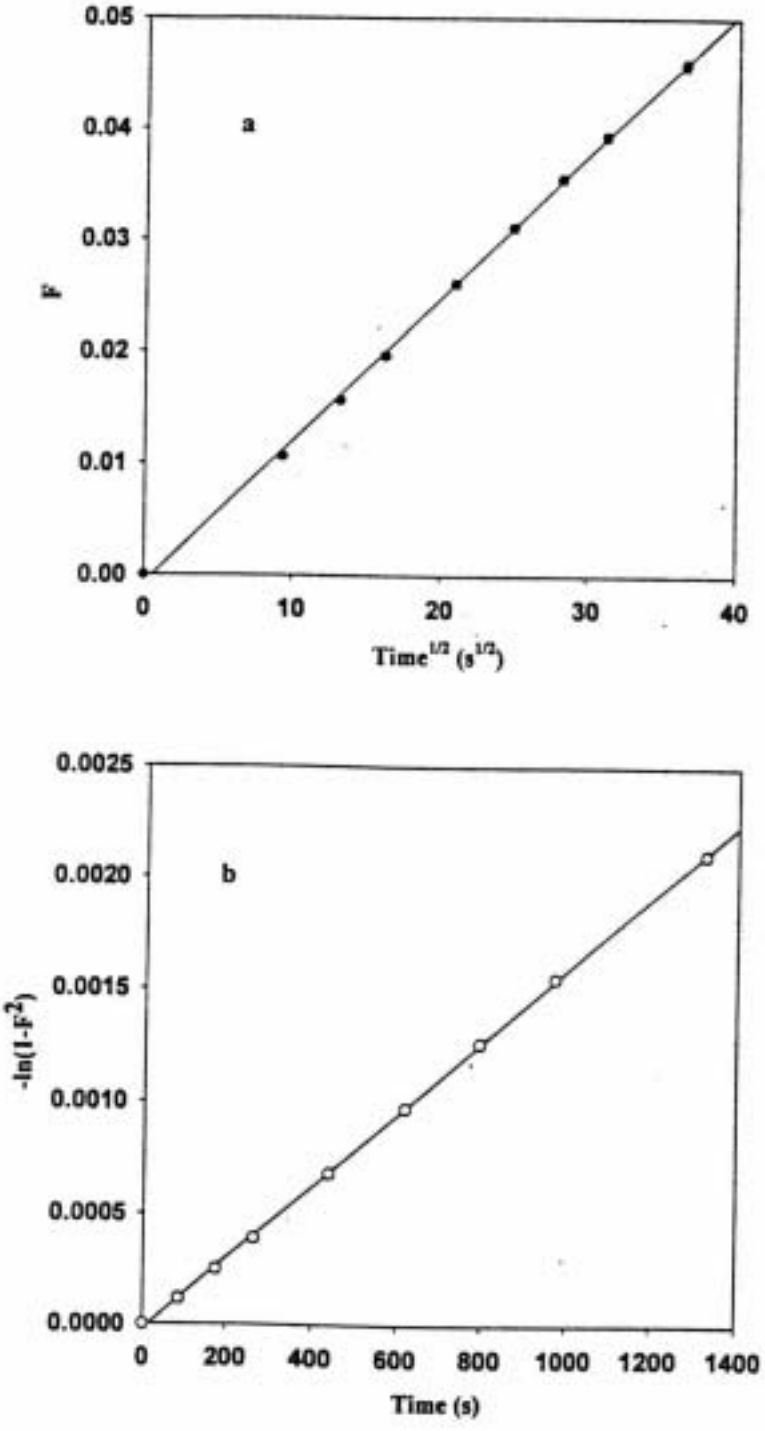

FIGURE 3. Results obtained by treatment of kinetic curves of Ca^{2+} – Na^{+}/K^{+} exchange on Lewatit S8528 resin sample of 0.42 mm by Model 1 (a) and Model 2 (b).

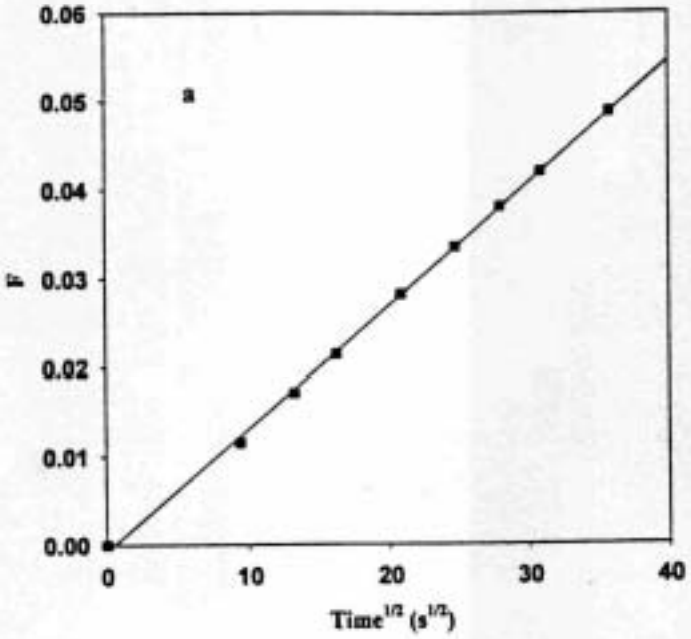

FIGURE 4. Results obtained by treatment of kinetic curves of Ca^{2+} – Na^{+}/K^{+} exchange on Lewatit S8528 resin sample of 0.335 mm by Model 1 (a) and Model 2 (b).

kinetics of both cation- and anion-exchange with Model 1 and Model 2. The results of these calculations are collected in Table 2 where the values of effective diffusion rate (B values, see equations 4 and 6) of Ca^{2+} and F^{-} ions in the respective resin phases are shown. As seen from Table 2, the effective diffusion rates of both Ca^{2+} and F^{-} ions substantially increase, as might be expected, with the decrease of diameter of resin beads. The data of Table 2 quantitatively illustrate the difference in diffusivities of Ca^{2+} and F^{-} ions in the corresponding resin phases, which can also be characterised by the values of the effective diffusion coefficients, D, of Ca^{2+} and F^{-} ions. The $D(Ca^{2+})$ and $D(F^{-})$ values calculated by using equations 4 and 6 are collected in Table 3.

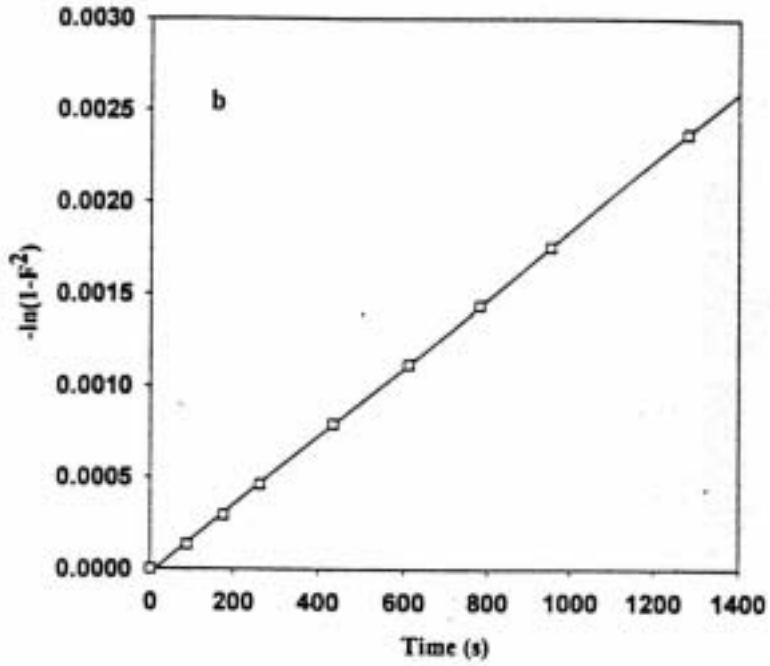

FIG. 4. Continued.

As follows from Table 3, although the $D(Ca^{2+})$ values calculated by both equation 4 and 6 are in a good agreement with each other, the use of Model 1 (equation 4) provides a better accuracy of D determination. The absolute $D(Ca^{2+})$ and $D(F^-)$ values differ from each other by four orders of magnitude. This reflects the influence of the selectivity parameters in the systems under consideration on the kinetics of the respective ion-exchange processes. The data shown in Table 2 also permit to estimate the B values corresponding to the resin fractions of small particle sizes (resin powders), which can be used as an active caries preventive component of toothpaste, varnishes, etc. This estimation is of particular importance as a very high hydrodynamic resistance of the powdered resin bed

TABLE. 2. EFFECTIVE DIFFUSION RATES, B, OF Ca^{2+} AND F^- IONS IN RESIN PHASE.

	B (s^{-1})		
	B (Ca^{2+}) x 10^6		B(F^-) x 10^3
Particle diameter (mm)	Model 1	Model 2	Model 2
0.42	1.4	2	8.8
0.335	1.7	2	14
0.205	4.9	5	25
0.105	9.3	7	72
0.05*	13	9	85

* Estimated from – log (B) vs particle size dependencies shown in Fig.5 (see text).

TABLE. 3. EFFECTIVE DIFFUSION COEFFICIENTS, D, OF Ca^{2+} AND F^- IONS IN RESIN PHASE.

	Effective diffusion coefficient (m^2s^{-1})		
	D (Ca^{2+}) x 10^{13}		D (F^-) x 10^{11}
Particle diameter (mm)	Model 1	Model 2	Model 2
0.42-0.105	5.5 ± 1.2	5.5 ± 2.0	3.7 ± 0.9

complicates the experimental determination of B values for resin powders under dynamic conditions (by using the "shallow bed" technique). Fig. 5 shows -log B versus bead diameter, d, plots for both systems under study. As seen, in both cases -log B vs d dependencies can be satisfactorily approximated by a straight line and, hence, can be used to estimate B values corresponding to the resin fractions with small particle sizes. The results of this estimation are also shown in Table 2 for resin fractions of 0.05 mm.

The dramatic difference in Ca^{2+} and F^- ion diffusivities reported in Tables 2 and 3 must influence the rate of ion release from the powdered resin mixtures.

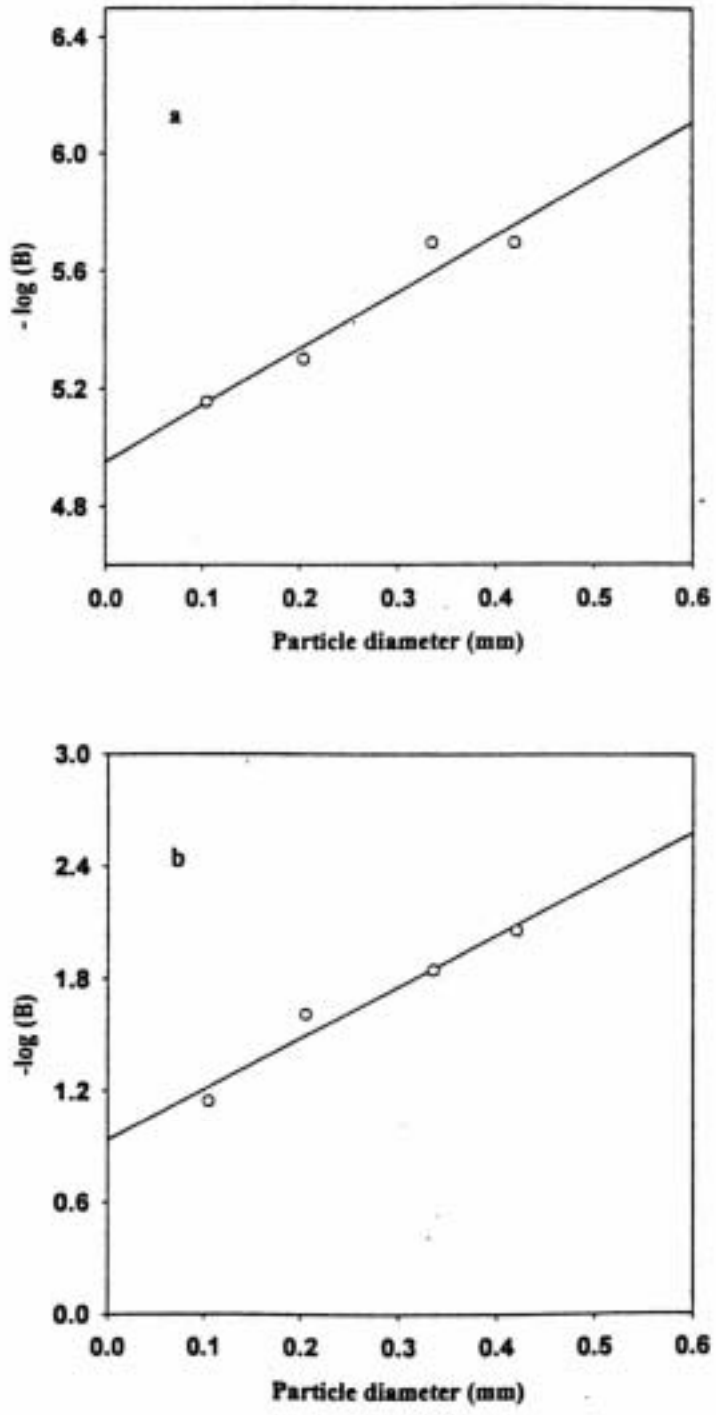

FIGURE 5. –log B versus particle diameter dependencies for Lewatit S8528 (a) and Lewatit MP62 (b) resins.

This hypothesis is based on the following equilibrium and kinetic features of the ion-exchange system involving a mixture of cation- and anion-exchange resins in the Ca- and F-forms and AS solution:

1. The ion-exchange reactions 9 and 10, proceeding simultaneously, are accompanied by interaction of Ca^{2+} and F^- ions leading to formation of low solubility calcium fluoride:

$$Ca + 2F \rightarrow CaF_2 \tag{11}$$

characterised by the solubility product, L:

$$L = [Ca^{2+}]\cdot[F^-]^2 = 2.7\times10^{-11} \tag{12}$$

It is easy to demonstrate that the ion-exchange equilibria in this systems can be described by the equilibrium constant K_{tot}, which is obtained by combining the equilibrium constants of reactions 9 and 10, K_1 and K_2, respectively, with equation 12 [32]:

$$K_{tot} \sim \frac{K_1 K_2}{L} \tag{13}$$

As seen from equation 13, the overall ion-exchange equilibrium in the system must be shifted to the right as $K_{tot} >> 1$. This means that both cation- and anion-exchange reactions in the system are coupled with each other due to subsequent reaction 11 proceeding between the ionic products of reactions 9 and 10. Formation of low solubility CaF_2 results in the decrease of concentration of both Ca^{2+} and F^- ions in the solution phase which leads, in turn, to the shift of both ion-

exchange equilibria to the right. Nevertheless, the shift of the equilibrium parameters of systems involving low solubility substances can be complicated by a substantial decrease of cation release.

2. The kinetics of ion exchange in a polyphase system including a cation exchanger, an anion-exchange resin and a crystallising substance is known to be complicated by the formation of a solid crystalline layer (solid core) of low solubility compound on the surface of the resin beads [33]. This layer can substantially decrease the rate of ion-exchange reaction (i.e., the rate of ion release) due to the partial blocking of the resin bead surface by a hardly penetrable (for exchanging ions) solid crystalline core [33]. The formation of the solid core preferentially proceeds on the surface of the ion exchanger that exhibits a slower kinetics (usually the cation exchanger) than the other ion-exchanger component of the system. For example, let us consider a batch system including a mixture of Lewatit S8528 and Lewatit MP62 resins in the Ca- and F-form, respectively, and some limited volume of AS. Under these conditions one can expect a relatively fast accumulation of F^- ions in the liquid phase in comparison with Ca^{2+} ions. In this situation the fluoride anions can be imagined as to be "awaiting" for the appearance of calcium cations from the cation exchanger to interact with them as in reaction 12. This interaction most probably proceeds at the surface of the Lewatit S8528 resin beads. Hence, the kinetics of Ca^{2+} release in the system under consideration must be slower in comparison with that of Ca^{2+} ions from the Lewatit S8528 resin alone measured under identical conditions. At the same time, the rate of F^- ion release in the resins mixture must be nearly identical to that from the Lewatit MP62 resin alone.

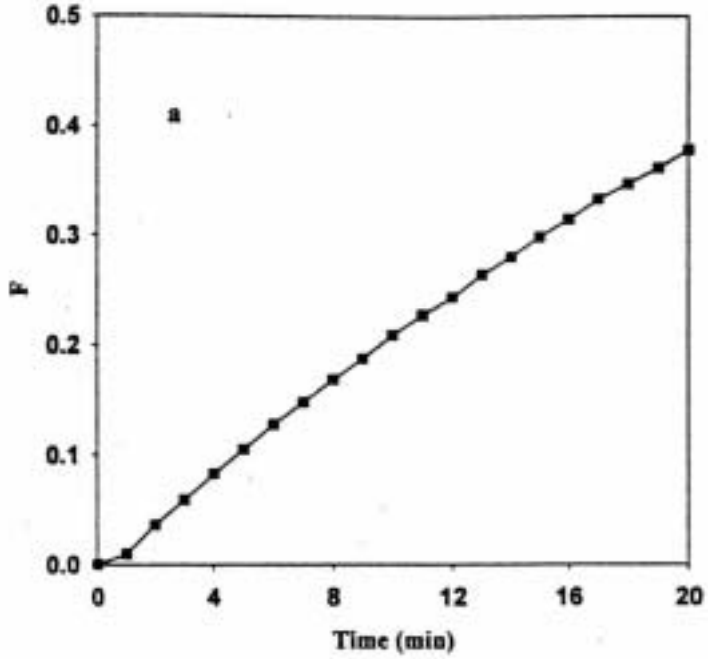

FIGURE 6. Concentration-time histories of fluoride release from powdered Lewatit MP62 resin (a) and mixtures of Lewatit MP62 and Lewatit S8528 resins in F- and Ca-form, respectively, of different compositions at 310 K. Lewatit MP62 : Lewatit S8528 ratio (in equivalents of functional groups) = 6:1 (circles); 4:1 (squares); 2:1 (triangles).

The confirmation of the above predictions is provided by the results of batch experiments carried out with monocomponent resin samples and resins mixtures of different compositions shown in Figs. 6 and 7[1]. Indeed, as seen in Fig. 6 the kinetics of F^- - Cl^- exchange is not significantly affected by the presence of a cation-exchanger in the Ca-form in the resin mixture (cf. Fig. 6a and 6b). On the

[1] The conditions of this series of experiments are dramatically different from those corresponding to dynamic kinetic studies. Therefore, the results cannot be compared with results shown in Fig.1.

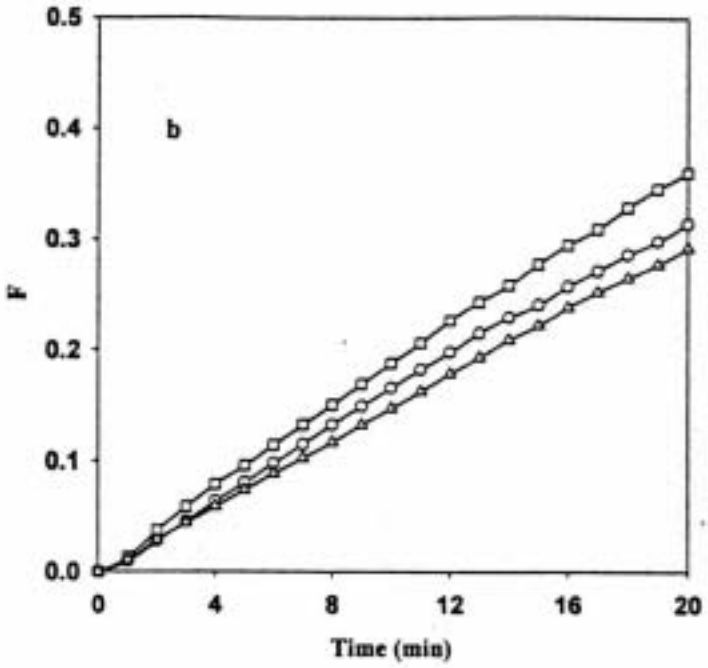

FIG. 6. Continued.

contrary, as clearly follows from Fig. 7, the release of Ca^{2+} ions from the resins mixture appears to be far slower than that from a monocomponent resin. As seen from Figs. 6 and 7, the composition of the mixture has only a very small effect on the rates of either Ca^{2+} or F^- ion releases. Note that the rate of both Ca^{2+} and F^- diffusion through the dialysis membrane is far higher than that of ions release from respective resins and can be disregarded.

The confirmation of the validity of the above hypothesis about the decrease of the rate of Ca^{2+} release in the presence of F^- ions in the solution phase due to formation of a solid CaF_2 core on the surface of the cation exchanger beads was obtained from the results of the following model experiment. Two small portions

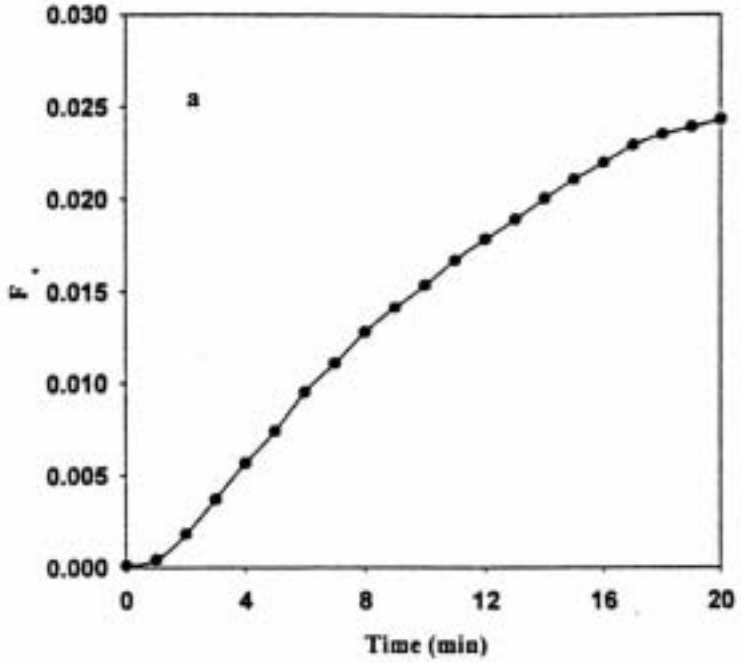

FIGURE 7. Concentration-time histories of calcium release from powdered Lewatit S8528 resin (a) and mixtures of Lewatit MP62 and Lewatit S8528 resins in F- and Ca-form, respectively, of different compositions at 310 K. Lewatit MP62 : Lewatit S8528 ratio (in equivalents of functional groups) = 1:6(circles); 1:4 (squares); 1:2 (triangles); 1:1 (inverse triangles).

of Lewatit S8528 resin (bead diameters of 0.42 and 0.105 mm) were placed in ion-exchange columns and treated under "shallow bed" conditions (see Experimental section) with a NaF solution having an F^- concentration equal to that of Cl^- ions in AS. The eluate was collected in portions in volumetric flasks containing a certain volume of 0.1 M NaEDTA to prevent the precipitation of CaF_2 in the solution collected. Then the eluate samples were analysed for Ca^{2+} content to plot the concentration-time histories shown in Fig.8. As seen, the

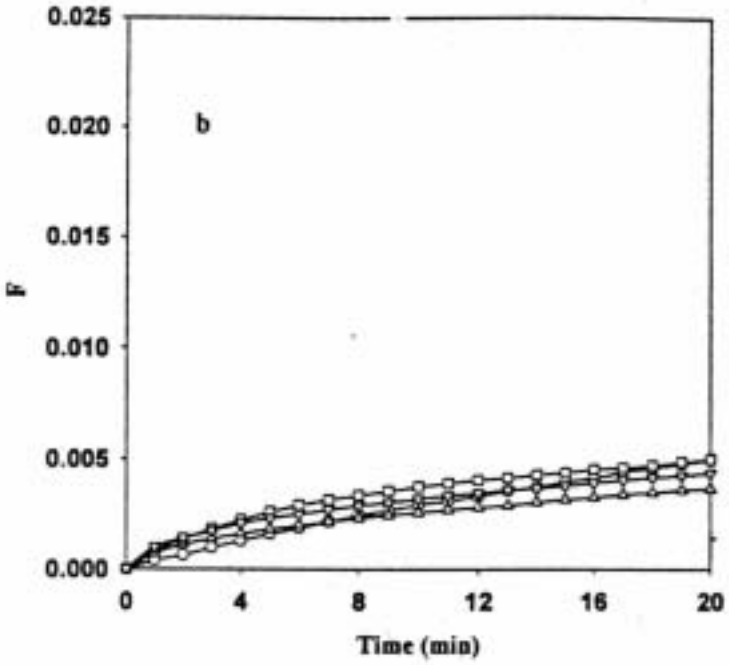

FIG. 7. Continued.

kinetics of Ca^{2+} - Na^{+} exchange in the presence of F^{-} ions appears to be far slower, as might be expected, than that of Ca^{2+} - (K^{+} + Na^{+}) exchange from AS.

The resin phase used in this experiment was removed from the columns followed by filtration from the solution phase and drying. Dry resin samples were analysed by SEM (scanning electron microscopy) technique by using a JSM-6300 microscope. The results of SEM analysis clearly indicated the formation of CaF_2 microcrystals on the surface of resin beads. Hence, the formation of solid CaF_2 core, by providing an additional diffusional resistance for the release of Ca^{2+} ions can be considered to be the main factor responsible for the decrease of the rate of Ca^{2+}– (K^{+} + Na^{+}) exchange in the system under study.

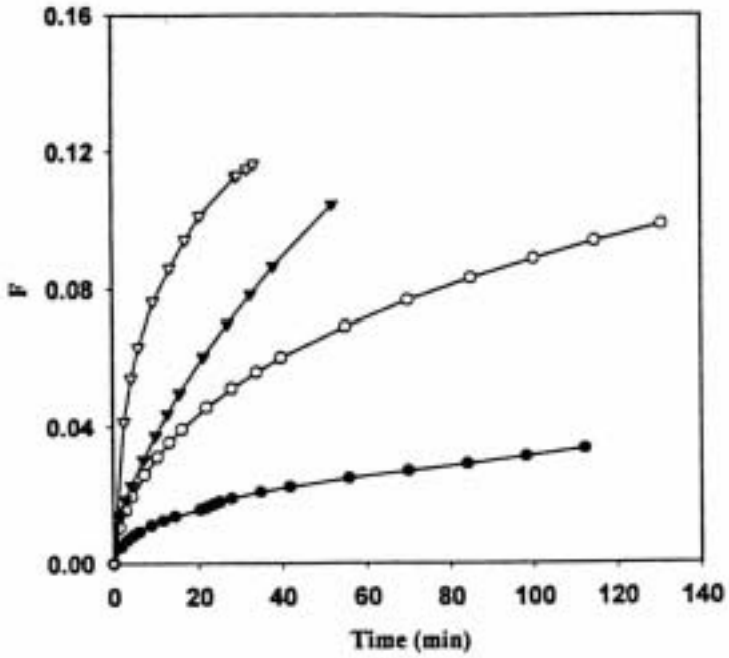

FIGURE 8. Concentration-time histories of calcium release from Lewatit S8528 resin of different granulation in Ca-form in contact with NaF (full symbols) and AS (empty symbols) solutions at 293 K (see text): 0.42 mm (circles); 0.105 mm (inverse triangles).

CONCLUSIONS

The results obtained in this study can be summarised as follows:

1. The kinetics of release of Ca^{2+} and F^- ions from the weak acid cation exchanger Lewatit S8528 and the weak base anion exchange resin Lewatit MP62 in contact with solution of artificial saliva is controlled by the intraparticle diffusion mechanism.
2. The rate of ion release from both ion-exchange resins studied can be quantitatively described in terms of effective diffusion rates (B values) of the

respective ions in the resin phase. The dependencies of –log B on the diameter of resin beads is satisfactorily approximated by straight lines and can be used to estimate B values for finely powdered resin fractions.

3. The rate of F^- ion release from the mixtures of resin powders of different compositions is not significantly affected by the presence of cation exchanger in the Ca-form, while the kinetics of Ca^{2+} release from resin mixtures substantially decreases in comparison with that from a monocomponent resin sample.
4. The difference in rates of Ca^{2+} and F^- ions release from the resin mixtures is attributed to the difference in their diffusivities in the respective resin phases leading to the accumulation of the faster diffusing F^- ions in the solution surrounding the beads of cation exchanger in the Ca-form. Interaction of Ca^{2+} and F^- ions accompanied by the formation of microcrystals of low solubility CaF_2 on the surface of cation exchanger beads results in a decrease of the rate of Ca^{2+} release from the resin phase.
5. The mixtures of powdered Lewatit S8528 and Lewatit MP62 resins in the Ca- and F-form, respectively, can be applied as an additive to toothpastes, tooth varnishes and other caries preventive materials as they combine a high rate of fluoride ion release with a sufficient release of calcium ions providing both anti-carious and remineralising activity.

ACKNOWLEDGEMENTS

AT is a recipient of a fellowship from CIRIT (Comissió de Recerca i Tecnologia de Catalunya). D.M. thanks the Catalonian Government for the

financial support of his visiting professorship at the Universitat Autónoma de Barcelona.

REFERENCES

1. R.Kh. Khamizov, D. Muraviev and A. Warshawsky, Recovery of Valuable Mineral Components from Seawater by Ion-Exchange and Sorption Methods, in Ion Exchange and Solvent Extraction, Vol. 12, J.A. Marinsky and Y. Marcus, Eds., Marcel Dekker, New York, 1995, pp.93-148.
2. F.L.D. Cloete and A.P. Marais, Ion Exchange Processes for the Recovery of Very Dilute Acetic and Related Acids, in Ion Exchange Developments and Applications, J.A. Greig, Ed., The Royal Society of Chemistry, Cambridge, 1996, pp.452-459.
3. V.I. Gorshkov, D. Muraviev and A. Warshawsky, Solv. Extr. Ion Exch., 16(1), 1-74 (1998).
4. V.I. Gorshkov, Yu.A. Kovalenko, D. Muraviev, G.A. Medvedev and N.B. Ferapontov, Study of Purification of Freon Compositions from Hydrochloric Acid Admixture, Lomonosov Moscow State University, Moscow 119289, VINITI-B-425095, 1974 (in Russian).
5. V.I. Gorshkov, Yu.A. Kovalenko, D. Muraviev and N.B. Ferapontov, Purification of Freon Compositions from Hydrohalogen Acid Impurities, Lomonosov Moscow State University, Moscow 119289, VINITI-B-518276, 1975 (in Russian).

6. T.V. Arden, Water Purification by Ion Exchange, Butterworths, London (1968).

7. T.V. Arden, Raw Water Treatment by Ion Exchange, in Ion Exchangers, K. Dorfner, Ed., Walter de Gruyter, Berlin, 1991, pp.717-790.

8. J.C. Bates, Ion Exchange Resins in Nuclear Power Stations, in Ion Exchange Developments and Applications, J.A. Greig, Ed., The Royal Society of Chemistry, Cambridge, 1996, pp.18-26.

9. I. Aoyama, Manufacture of High Purity Silica by Ion Exchange, Jap. Patent 61,270,209 (1986).

10. T. Miyagawa, H. Nawa and M. Sakurai, Manufacture of High Purity Hydrazine Hydrate Using Chelating Resins, Jap. Patent 63,218,505 (1988).

11. F. Martinola, Waste Water Treatment and Pollution Control by Ion Exchange, in Ion Exchangers, K. Dorfner Ed.,Walter de Gruyter, Berlin, 1991, pp.845-858.

12. T. Mitchenko, P. Stender and N. Makarova, Solv. Extr. Ion Exch., 16(1), 75-150 (1998).

13. W.H. Höll, Elimination of Heavy Metals from Waters by Means of Weakly Basic Anion Exchange Resins, in Ion Exchange Developments and Applications, J.A. Greig Ed.,The Royal Society of Chemistry, Cambridge, 1996, pp.404-411.

14. L. Chen, W. Xin, C. Dong, W. Wu and S. Yue, High-Pressure Ion-Exchange Separation of Rare Earths, in Ion Exchange and Solvent Extraction, Vol. 12, J.A. Marinsky and Y. Marcus Eds., Marcel Dekker, New York, 1995, pp.1-28.

15. D. Muraviev, J. Noguerol and M. Valiente, Reagentless Concentration of Copper from Acidic Mine Waters by the Dual-Temperature Ion Exchange Technique, in: Progress in ion exchange: Advances and Applications, A. Dyer, M.J. Hudson and P.A. Williams Eds.,The Royal Society of Chemistry, Cambridge, 1995, pp.349-356.

16. D. Muraviev, J. Noguerol and M. Valiente, Anal. Chem., 69, 4234-4241 (1997).

17. V.S. Soldatov and V.A. Bychkova, Ion Exchange Equilibria in Multicomponent Systems, Nauka i Tekhnika, Minsk (1988) (in Russian).

18. V.S. Soldatov, Ion Exchanger Mixtures Used as Artificial Nutrient Media for Plants, in Ion Exchange for Industry, M. Streat Ed., Ellis Horwood, Chichester, 1988, pp.652-658.

19 J.J. Christensen and R.M. Izatt, Handbook of Metal Ligand Heats and Related Thermodynamic Quantities, 3d Edn., Marcel Dekker, New York (1983), p.477.

20. B. Ögaard, J. Dent. Res., 69, 813-819 (1990).

21. L. Seppä and L. Pöllänen, Caries Res., 21, 375-379 (1987).

22. G. Naumann, G. Pieper and H-J. Rehberg, Dental Composition and Appliances Containing Anti-Carious Ion Exchange Resins, US Patent 3,978,206 (1976).

23. K.Kh. Urusov, T.V. Nikitina and G.N. Pakhomova, Periodontitis Stomatological Treatment, SU Patent 825,078 (1981).

24. D. Muraviev, L.V. Zvonnikova and L.A. Dmitrieva, Polymeric Composition, SU Patent 1826976 (1991).

25. K. Dorfner, Introduction to Ion Exchange and Ion Excangers, in Ion Exchangers, K. Dorfner Ed.,Walter de Gruyter, Berlin, 1991, pp.7-188.

26. F.G. Helfferich and Y-L. Hwang, Ion Exchange Kinetics, in Ion Exchangers, K. Dorfner Ed., Walter de Gruyter, Berlin, 1991, pp.1277-1310.

27. T. Vermeulen, G. Klein and N.K. Hiester, Adsorption and Ion Exchange, in R.H. Perry's Chemical Engineers' Handbook, Perry, D.W. Green and J.O. Maloney Eds.,6th edn., section 16, McGraw-Hill, New York (1984).

28. M. Streat and D. Naden, Ion Exchange in Uranium Extraction, in Ion Exchange and Sorption Processes in Hydrometallurgy. Critical Reports on Applied Chemistry, Vol.19, M. Streat and D. Naden Eds., John Wiley & Sons, Chichester, 1987, pp.1-55.

29. V.A. Ivanov, V.D. Timofeevskaya, V.I. Gorshkov and T.V. Eliseeva, High Purity Substances, 4, 309-315 (1991).

30. V.A. Ivanov, V.D. Timofeevskaya and V.I. Gorshkov, React. Polym., 17, 101-107 (1992).

31. D. Muraviev, J. Noguerol and M. Valiente, React.& Funct. Polym., 28, 111-126 (1996).

32. V.L. Bogatyrev, Ion Exchangers in Mixed Bed, Khimija, Leningrad (1968), p.45 (in Russian).

33. D. Muraviev, O.Yu. Sverchkova, N.M. Voskresensky and V.I. Gorshkov, React. Polym., 17, 75-88 (1992).

Received by Editor
August 24, 1999

ANNEX 2

KINETICS CHARACTERIZATION OF IONS RELEASE UNDER DYNAMIC AND BATCH CONDITIONS. I. WEAK ACID AND WEAK BASE TYPE RESINS.

A.Torrado and M. Valiente*

Departament de Química, Unitat Analítica, Centre GTS, Universitat Autònoma de Barcelona, Facultat de Ciències, Edifici Cn, E-08193, Bellaterra (Barcelona), Spain

Abstract

The aim of the present work concerns with a study on the kinetics of release of both Ca^{2+} and F^- from loaded ion exchange resins (weak acid and base character for Ca^{2+} and F^- respectively), using both dynamic and batch experimental conditions, with an artificial saliva solution as ion exchange media at 293 and 310 K. The influence of resins particle size and temperature were evaluated by the kinetics parameters effective rate of release (B) and diffusion coefficient (D). The rate of ions release increases with temperature and when particle size decreases. The experimental data were fitted by models based on intraparticle diffusion controlled processes. Under dynamic experimental conditions, the linear dependence of –log (B) with the diameter of resin particles can be applied for the estimation of B values when resins of very low particle size are considered. Under batch experimental conditions, only a linear relationship was attained for the case of slow ion exchange kinetics systems.

Keywords: ion exchange, kinetics release, macroporous ion exchanger, intraparticle diffusion, calcium, fluoride.

***Correspondence to:** Manuel Valiente, Departament de Química, Unitat Analítica, Centre GTS, Universitat Autònoma de Barcelona, Facultat de Ciències, Edifici Cn, E-08193 Bellaterra (Barcelona), Spain

Phone number. +34 93 581 2903

Fax number: +34 93 581 1985

E-mail: Manuel.Valiente@uab.es

1. Introduction

Calcium is a very abundant element in human body, 99% is found in bones and teeth whereas the 1% remaining is required for functions like blood clotting, nervous signals transmission and muscular contraction. Fluoride, on the other hand, is present in trace quantities but, ingested in appropriated quantities in water and food, and used topically in toothpastes, chewing gums, mouthrinses, etc, reduces the risk of dental caries and promotes enamel remineralization.[1] With this aim, new controlled release formulations based on ion exchange resins loaded with both ions immobilized have been developed.[2,3,4] The main advantage of including ion exchange resins in controlled release systems is the possibility of lowering the release rate of the active principle, thus increasing the long-lasting effect. On the other hand, these ion exchange resins act as regulators of the damaged tissues (e.g. teeth enamel) responding to their demand and providing, this way, an efficient remineralizing effect. The application of ion exchange materials has also additional advantages, in comparison with conventional chemical reagents. They do not introduce undesirable ions in the solution, the ions release is only due to the ion exchange reaction, they are characterized by pH values practically neutral and they can also adsorb bacteria on their surface. The majority of these resins are non toxic and are used not only in the pharmaceutical industry and medical applications,[5] but in the food industry as well.[6]

The aim of the present work has been to carry out a preliminary study on the kinetics of release of both Ca^{2+} and F^- from the corresponding ion exchange resins (weak acid and base character for Ca^{2+} and F^- respectively), using both dynamic and batch experimental conditions, with an artificial saliva solution as ion exchange media at 293 and 310 K. With fixed physicochemical parameters like porosity, crosslinkage, shape and ionic resins form, pH and ionic strength of the external solution, the influence of particle size and temperature were evaluated by kinetics parameters effective rate of release (B) and diffusion coefficient (D).

2. Experimental

2.1. Materials

Highly purified ion exchange resins, carboxylic type Lewatit S8528 and terciary amine type Lewatit MP62 with macroporous structures were kindly supplied by Bayer Hispania Industrial, S.A (Barcelona, Spain). $CaCl_2$ 1 M and 0.3 M, KCl 0.01 M, NaCl

0.008 M, NaF 0.9 M, $NaNO_3$ 0.3 M and, NaOH 2.2 M solutions were prepared from the corresponding Panreac (Barcelona, Spain) pro analysis quality solid salts. HCl 1 M and HAc 0.8 M solutions were prepared by dilution of the corresponding concentrated Panreac (Barcelona, Spain) pro analysis quality acids. In all cases, deionized water Milli-Q quality (Millipore, USA) was used.

2.2. Instrumentation

The release of Ca^{2+} and F^- under batch experimental conditions, was determined by corresponding ion selective electrodes system Orion (USA) controlled automatically by a PC, whereas under dynamic conditions, Ca^{2+} was determined spectrofotometrically by inductively coupled plasma atomic emission spectroscopy technique (ICP-OES) using an ARL model 3410 minitorch (USA). All the samples were analyzed with an uncertainty lower than 1.5 % and all the experiments were carried out by triplicate.

2.3. Resins loading

Resins were conditioned by following a standard procedure.[7] The conversion of the resins to the desired ionic form was carried out in ion exchange columns under dynamic conditions by passing aqueous solutions of the corresponding concentrations through the resin bed. After complete loading, the resin phase was successively washed with water to remove the excess of electrolyte solution, then quantitatively removed from the column and separated from water by filtration, followed by drying at the oven (60-70 ^oC). Resins in the different ionic forms were kept in hermetically sealed vials to avoid water absorption.

2.4. Resins capacity

Determination of the specific capacity of the different resins towards Ca^{2+} and F^- was carried out under dynamic conditions in columns by following a standard procedure.[8] A weighed portion of each loaded resin was introduced in a 10 cm column (8 mm Ø) and the counterion of interest was eluted with HCl in the case of the cationic resin and with $NaNO_3$ in the anionic one. Eluate was collected in volumetric flasks and analyzed. The results of the analysis were used to determine the specific capacity of the resins, q_s, according to the equation:

$$q_s = \frac{VC_i}{W_i} \quad (1)$$

where *V* is the total volume of eluted solution, *Ci* is the concentration of the solution containing the eluted ion *i* and *Wi* is the weight of resin loaded with this ion. The specific capacities determined experimentally are shown in Table 1.

2.5. Grinding and sieving

A fraction of each type of resin was ground in a mechanical agate mortar Retsch RMO (Germany) and sieved by using a set of standard stainless steel sieves in a mechanical siever, CISA (Spain). Thus, separate fractions of the resins were collected with particle sizes of diameter 0.42 mm, 0.5-0.42 mm, 0.42-0.25 mm, 0.25-0.16 mm, 0.16-0.05 mm, and <0.05 mm.

2.6. Ion exchange kinetics determination

2.6.1. Dynamic conditions

The study of ion exchange kinetics of the different samples was carried out under dynamic conditions using the "shallow bed" technique.[9] A small sample resin portion loaded with the specific target ion was introduced in a column connected to a thermostat and, a solution of artificial saliva (solution of concentration 1g/l KCl and 0.5g/l NaCl) was passed through the resin bed at high flow rate (~30 ml/min). Experiments were run at 310 K. All the resulting eluate was collected in volumetric flasks, analyzed and these analytical data transformed to the degree of conversion, *F*, by using the equation:

$$F = \frac{\sum_{t_i=1}^{t_n} c_i v_i}{q_\infty} \quad (2)$$

where *vi* corresponds to the volume of the eluate portion *i*, *Ci* to its concentration and q_∞ the total capacity of the resin, expressed as:

$$q_\infty = \sum c_i v_i + Vstr\ Cstr \quad (3)$$

where *Vstr* corresponds to the volume of an eluate sample obtained from an elution, with either acid or nitrate, carried out after the kinetics experiment and, *Cstr* to its concentration.

2.6.2. Batch conditions

The study of the kinetics of ions release under batch experimental conditions was carried out using the "limited volume" technique.[10] A small resin portion loaded with the corresponding target ion was introduced in a thermostated cell (at 293 or 310 K), containing 50 ml of artificial saliva vigorously agitated. The moment when the sample got into contact with the desorbing solution (artificial saliva) was considered as the starting time (time zero) for the kinetics experiment.

The experimental data obtained by ion selective electrodes were expressed in terms of degree of conversion values, *F*, of the resins by applying the equation:

$$F = \frac{V_{as} c(t_i)}{q_\infty} \tag{4}$$

where V_{as} is the volume of artificial saliva contained in the cell, *c(ti)* is the concentration of the target ion at the experiment time *ti* and, $q_\infty = mq_s$ is the total capacity of the resin (in mmols), being *m* the weight of resin portion and q_s (mmol/g) the specific capacity of the resin towards the corresponding ion determined as described in the section 2.4.

3. Results and discussion

3.1. Influence of particle size on the rate of Ca^{2+} and F^- release.

Kinetics release of Ca^{2+} and F^- from the different particle size fractions, either under dynamic or batch experimental conditions, are shown in Figures 1a-b and 2a-d. It can be observed that when resin particle size decreases the rate of ions release increases, because the contact surface between the solution and active functional groups of the polymeric matrix increases. Note that for fluoride ion this effect can be appreciated in shorter times because the rate of release is very fast. In previous studies,[11] it was shown that the rate of Ca^{2+} release is considerably lower than the corresponding of F^-, what can be explained by the higher affinity of Ca^{2+} towards the related polymeric matrix against the corresponding affinity of F^-.

Under batch conditions, resins characterized by a slow kinetics can rarely release all ions initially immobilized in the resin phase because of the attainment of the equilibrium with the media surrounding that will then contain the ion released as the ion exchange process proceeds. On the contrary, under dynamic conditions the desorbing

solution passing through the resin bed is free of counterions to be released, that's why higher degrees of conversion are obtained.

3.2. Influence of temperature on the rate of Ca^{2+} and F^- release

Temperature has a clear effect on ion exchange processes.[12] Figures 3a-d show that an increase in temperature results in an increase in the rate of ions release as a consequence of an increase in diffusion coefficients. This effect is reflected under both, dynamic and batch conditions.

3.3. kinetics characterization of the ion exchange process

3.3.1. Kinetics models description

Interruption tests carried out in a previous study[11] showed that the rate determining step of the ion exchange process under study was the intraparticle diffusion. So, results from the above Figures 1a-b and 2a-d were treated by specific kinetics models, valid for the description of ion exchange processes controlled by an intraparticle diffusion mechanism under dynamic and batch conditions.

3.3.1.1. Dynamic conditions

a) Model 1[13]

This model is valid for low degrees of conversion (F<0.05), so it will be applied only to the data obtained from the kinetics release of Ca^{2+} because F^- conversion degree gets unity in a few minutes. The model is based on the following equation:

$$F = 1.08(Bt)^{1/2} \tag{5}$$

where *B* is the effective rate of release which is related to the diffusion coefficient, *D*, by the expression:

$$B = \frac{D\pi^2}{r^2} \tag{6}$$

being *r* and *t* are the resin particle radius and time respectively.

b) Model 2[14]

The applicability rank of this model covers the whole range of degrees of conversion, *F*, from 0 to 1, and is based on the equation:

$$-ln(1-F^2) = 2\frac{D\pi^2}{r^2}t = 2Bt \qquad (7)$$

where *B* is the effective rate of release, *D* the diffusion coefficient, *r* the radius of the resin particle and *t* the respective time.

Lineal dependencies of *F* versus $t^{1/2}$ (Model 1) and $-ln\ (1-F^2)$ vs *t* (Model 2) verify that the mechanism through which the ion exchange process takes place is controlled by intraparticle diffusion. Some results of the treatment of the experimental data are shown in Figures 4a-c. Figures 4a and 4b correspond to the application of models 1 and 2 respectively to the data obtained of the release of Ca^{2+} whereas, results on Figure 4c corresponds to the application of model 2 on data of the release of F^-. In this latter case and as indicated before, only model 2 can be applied because F^- conversion degrees are considerably higher than 0.05.

Results obtained from data treatment with equations 5, 6 and 7, are shown in Table 2.

As can be appreciated in this table, the effective rates of release increase when particle size decreases.[15,13] It is also remarkable the great difference existing in the diffusivity of both ions in the respective resin phase. This difference can also be characterized in terms of the effective diffusion coefficient, $\overline{D}$, defined as the mean of diffusion coefficients of all particle sizes. The corresponding values are presented in Table 3.

The obtention of Ca^{2+} effective diffusion coefficients four orders of magnitude lower than the corresponding of F^-, makes evident the influence of the selectivity parameters of the ion exchange systems studied.

The application of both models to Ca^{2+} release data provides effective rates of release and effective diffusion coefficients that are in a good agreement between each other.

Results presented in Table 2 for Ca^{2+} at 310 K, together with those obtained at 293 K reported in a previous study,[11] are plotted as –log (B) versus particle size in Figures 5a-b. Note that for the results obtained from the application of both models at 293 K there is a lineal relationship with particle size. On the contrary, at 310 K the corresponding slope is considerably lower than the expected if it is compared with the results at 293 K. Only a good correlation of –log (B) versus particle size at both temperatures will allow predicting the behaviour of the ions release from resins of particle diameters different of

those studied in the present study. In the case of F^- (Figure 5c), there are no significantly differences between correlations obtained at 293 and 310 K. The high rate of release of the $F^- \leftrightarrow Cl^-$ exchange results in minimal variations in rate of F^- release from the corresponding polymeric matrix of different particle size.

Batch conditions are specially interesting for particle size resins lower than 100 microns due to the high hydrodynamic resistance existing when working under dynamic conditions using the "shallow bed" technique.

3.3.1.2. Batch conditions

T.R.E. Kressman and J. A. Kitchener[16] deduced an equation for ion exchange systems under batch experimental conditions:

$$\frac{Q_t}{Q_\infty} = \frac{6}{r}\frac{Q_0}{Q_0 - Q_\infty}\sqrt{\frac{Dt}{\pi}} \qquad (8)$$

where Q_0 is the total quantity of ions initially immobilized in the resin phase, Q_∞ is the quantity of ions released from the resin phase at equilibrium time, Q_t is the quantity of ions released from the resin phase till the moment t, r the resin particle radius, D the diffusion coefficient of the ion through the ion exchanger and, t time.

By plotting of Q_t/Q_∞ versus $t^{1/2}$, diffusion coefficients will be determined and, from equation 6 effective rates of release will be evaluated. In Figures 6a-h examples of the treatment of data presented in Figures 2a-d by the model described above are shown. The model fits all particle sizes correctly, however, two different behaviours can be distinguished mainly in fractions of bigger particle size. The initial release is slower due to a first step of swelling of the resin. Resins tend to absorb solvent from the media increasing the volume, thanks to an elastic gel structure; this behaviour was not appreciated in the study under dynamic experimental conditions discussed above since before each experiment the resin portion was kept in water for an hour. Once swelling has taken place an increase in the rate of release occurs. This phenomena is more relevant for higher particle sizes due to its smaller contact surface with external solution.

As it can be observed in Figures 6a-h, lineal dependencies of Q_t/Q_∞ versus t can be obtained. This verifies that the kinetics of the studied ion exchange processes under batch experimental conditions is controlled by intraparticle diffusion and, in the other

side, allows to calculate the kinetics parameters of interest for both ions. These values are presented in Tables 4 and 5.

Figures 7a-b show the dependence of the effective rate of Ca^{2+} and F^- release with particle size. As seen, the rate of Ca^{2+} release increases when particle size decreases. Note the exponential relation obtained for particle sizes under 100 microns. On the contrary, there is a direct relationship between the rate of release and temperature: when temperature increases the rate of release increases.

Correlation between *–log (B)* with particle sizes comprised between 0.42mm and <0.05mm is shown in Figure 8a. For Ca^{2+}, a linear correlation is obtained whereas, in the case of F^-, the variability in the effective rates of release of the different particle size fractions (Figure 7b) does not allow to establish any correlation (Figure 8b). F^- shows degrees of conversion considerably higher than that of Ca^{2+}, in fact, practically just when contacting the resin phase with artificial solution, full conversion is achieved. Thus, determining kinetics parameters with accuracy is very difficult.

Finally point out that under batch conditions, Ca^{2+} presents higher effective rates of release than F^-. This fact was explained in terms of the operation of the experimental system itself. In the case of high kinetics release resins, although ions are quickly released to the bulk solution and equilibrium is immediately achieved, the saturation of the solution in the releasing ion can delay the initial rate of release. Surprisingly, this effect affects mainly to F^-. Under dynamic conditions though, the desorbing solution passing through the resin bed is free of counterions to be released, so higher conversion degrees are obtained.

4. Conclusions

1- Differences in the rate of Ca^{2+} and F^- release from the corresponding weak type polymeric matrices can be explained in terms of relative affinity of the functional group immobilized in the resin phase towards the ions present in the solution.

2- The rate of ions release increases when temperature increases and particle size decreases.

3- Results from the study of the kinetics of release of Ca^{2+} and F^- under either dynamic or batch conditions are well interpreted by the models described valid for intraparticle diffusion controlled processes.

4- The rate of ions release from the ion exchange resins studied are quantitatively described in terms of effective rate of release (B) and effective diffusion coefficient ($\overline{D}$) of the respective ions in the resin phase. Under dynamic conditions, the linear dependence of –log (B) with the resin particles diameter can be used for the estimation of B values in very low particle resins. Under batch conditions, despite very low particle resins can be studied a linear relationship was only attained for the case of slow ion exchange kinetics systems.

Acknowledgements

A. T. acknowledges the Universitat Autònoma de Barcelona for the FI Research Grant to support her research studies. DCA, S.L. (Barcelona, Spain) is acknowledged for the financial support provided to this study.

REFERENCES

1 RIPA, L. *J. Public Health Dent.*, **1993**, 53(1), 17-44.

2 NAUMANN, G.; PIEPER G.; REHBERG, H-J. Dental Composition and Appliances Containing Anti-Carious Ion Exchange Resins, US Patent 3,978,206, 1976.

3 URUSOV, K. KH.; NIKITINA, T.V.; PAKHOMOV, G.N. *Periodontitis Stomatological Treatment*, SU Patent 825074, 1981.

4 VALIENTE, M; MURAVIEV, D; ZVONNIKOVA, L.V. *Material remineralizante de tejidos organominerales*, ES Patent 9700016, 1997.

5 PIROTTA, M.: *Ion Exchangers*, DORFNER, K. (ed.); Walter der Gruyter Publisher: Berlín, 1991, p.1073.

6 KUNIN, R.: *Ion Exchangers*, DORFNER, K. (ed.); Walter der Gruyter Publisher: Berlín, 1991, p.677.

7 DORFNER, K.: *Ion Exchangers*, DORFNER, K. (ed.); Walter der Gruyter Publisher: Berlín, 1991, p.128.

8 DORFNER, K.: *Ion Exchangers*, DORFNER, K. (ed.); Walter der Gruyter Publisher: Berlín, 1991, p.328.

9 DORFNER, K.: *Ion Exchangers*, DORFNER, K. (ed.); Walter der Gruyter Publisher: Berlín, 1991, p.94.

10 DORFNER, K.: *Ion Exchangers*, DORFNER, K. (ed.); Walter der Gruyter Publisher: Berlín, 1991, p.126.

11 MURAVIEV, D.; TORRADO, A.; VALIENTE, M. *Solv. Extr. & Ion Exch.*, **2000**, 18(2), 345-374.

12 MURAVIEV, D.; NOGUEROL, J.; VALIENTE, M. *React. & Funct. Polym.*, **1996**, 28, 111-126.

13 BOYD, G.E.; ADAMSON, A.W.; MYERS, L.S. Jr. *J. Am. Cem. Soc.*, **1947**, 69, 2836-2848.

14 STREAT, M.; NADEN, D.: *Ion Exchange and Sortion Processes in Hidrometallurgy. Critical Reports on Applied Chemistry*, Vol. 19; STREAT, M.; NADEN, D. (eds.); John Willey & Sons: Chichester, 1987, p.1.

15 IRWIN, W.J.; BELAID, K.A.; ALPAR, H.O. *Drug dev. Ind. Pharm.*, **1987**, 13 (9-11), 2047-2066.

16 KRESSMAN, T.R.E.; KITCHENER, J.A. *Disc. Faraday Soc.*, **1949**, 7, 90-104.

CAPTIONS AND LEGENDS

Table 1. Specific capacity of the resins towards Ca^{2+} and F^-.

Table 2. Effective rates of release, *B*, of Ca^{2+} and F^- in the resin phase, at 310K under dynamic conditions.

Table 3. Effective diffusion coefficients, $\overline{D}$, of Ca^{2+} and F^- in the resin phase at 310K under dynamic conditions.

Table 4. Effective rates of release, *B*, of Ca^{2+} and F^- in the resin phase under batch conditions.

Table 5. Effective diffusion coefficients, $\overline{D}$, of Ca^{2+} and F^- in the resin phase under batch conditions.

Figure 1 Kinetics release of resin samples of different particle size under dynamic conditions at 310K. **(a)** Lewatit S8528 in Ca^{2+}-form **(b)** Lewatit MP62 in F^--form.

Figure 2 Kinetics release of resin samples of different particle size under batch conditions. **(a)** Lewatit S8528 in Ca^{2+}-form, at 293K **(b)** Lewatit MP62 in F^--form, at 293K **(c)** Lewatit S8528 in Ca^{2+}-form, at 310K **(d)** Lewatit MP62 in F^--form, at 310K.

Figure 3 Kinetics release of resin samples of different particle size at 293 and 310K. **(a)** Lewatit S8528 in Ca^{2+}-form, under dynamic conditions **(b)** Lewatit MP62 in F^--form, under dynamic conditions **(c)** Lewatit S8528 in Ca^{2+}-form, under batch conditions **(d)** Lewatit MP62 in F^--form, under batch conditions.

Figure 4 Data treatment of resin samples of particle size 0.335mm at 310K with dynamic models **(a)** Ion exchange system $Ca^{2+} \leftrightarrow Na^+/K^+$: Lewatit S8528 in Ca^{2+}-form. Model 1 **(b)** Ion exchange system $Ca^{2+} \leftrightarrow Na^+/K^+$: Lewatit S8528 in Ca^{2+}-form. Model 2 **(c)** Ion exchange system $F^- \leftrightarrow Cl^-$: Lewatit MP62 in F^--form. Model 2.

Figure 5 Dependence of –log (B) with resins particle size under dynamic conditions at 293 and 310K. **(a)** Lewatit S8528 in Ca^{2+}-form. Treatment with model 1 **(b)** Lewatit S8528 in Ca^{2+}-form. Treatment with model 2 **(c)** Lewatit MP62 in F^--form. Treatment with model 2.

Figure 6 Data treatment of resin samples with batch model. **(a)** Ion exchange system $Ca^{2+} \leftrightarrow Na^{+}/K^{+}$: Lewatit S8528 in Ca^{2+}-form of particle size 0.42 mm at 293K **(b)** Ion exchange system $Ca^{2+} \leftrightarrow Na^{+}/K^{+}$: Lewatit S8528 in Ca^{2+}-form of particle size 0.42 mm at 310K **(c)** Ion exchange system $Ca^{2+} \leftrightarrow Na^{+}/K^{+}$: Lewatit S8528 in Ca^{2+}-form of particle size 0.105 mm at 293K **(d)** Ion exchange system $Ca^{2+} \leftrightarrow Na^{+}/K^{+}$: Lewatit S8528 in Ca^{2+}-form of particle size 0.105 mm at 310K **(e)** Ion exchange system $F^{-} \leftrightarrow Cl^{-}$: Lewatit MP62 in F^{-}-form of particle size 0.45mm at 293K **(f)** Ion exchange system $F^{-} \leftrightarrow Cl^{-}$: Lewatit MP62 in F^{-}-form of particle size 0.45mm at 310K **(g)** Ion exchange system $F^{-} \leftrightarrow Cl^{-}$: Lewatit MP62 in F^{-}-form of particle size 0.105mm at 293K **(h)** Ion exchange system $F^{-} \leftrightarrow Cl^{-}$: Lewatit MP62 in F^{-}-form of particle size 0.105mm at 310K.

Figure 7 Effective rate of release of resin samples of different particle size under batch conditions at 293 and 310K. **(a)** Lewatit S8528 in Ca^{2+}-form **(b)** Lewatit MP62 in F^{-}-form.

Figure 8 Dependence of –log (B) with resins particle size under batch conditions at 293 and 310K. **(a)** Lewatit S8528 in Ca^{2+}-form **(b)** Lewatit MP62 in F^{-}-form.

Table 1

	Capacity (mmol g^{-1})	
	Ca^{2+}	**F^-**
Lewatit S8528	3.11± 0.03	-
Lewatit MP62	-	2.91±0.04

Table 2

	B (s^{-1})		
	B (Ca^{2+}) x 10^6		**B (F^-) x 10^3**
∅ (mm)	**Model 1**	**Model 2**	**Model 2**
0.42 (Ca^{2+}) – 0.45 (F^-)	2.2	1.5	3.0
0.335	2.2	1.5	5.0
0.205	3.1	1.5	10.0
0.105	14	4.5	13.0

Table 3

	$\overline{D}$ ($m^2 s^{-1}$)		
	$\overline{D}$ (Ca^{2+}) x 10^{15}		$\overline{D}$ (F^-) x 10^{11}
∅ (mm)	**Model 1**	**Model 2**	**Model 2**
0.42/0.45 - 0.105	5.6 ± 3.0	3.5 ±2.5	1.0 ± 0.5

Table 4

	B (s^{-1})			
	T= 293K		T= 310K	
∅ (mm)	B (Ca^{2+}) x 10^5	B (F^-) x 10^6	B (Ca^{2+}) x 10^5	B (F^-) x 10^6
0.42 (Ca^{2+})- 0.45 (F^-)	4.2	621	1.0	249
0.335	3.6	5.4	3.6	6.1
0.205	3.7	1.6	12	7.8
0.105	23	297	38	586
<0.05	94	9.8	107	34

Table 5

	$\overline{D}$ ($m^2 s^{-1}$)			
	T= 293K		T= 310K	
∅ (mm)	$\overline{D}$ (Ca^{2+}) x 10^{14}	$\overline{D}$ (F^-) x 10^{13}	$\overline{D}$ (Ca^{2+}) x 10^{14}	$\overline{D}$ (F^-) x 10^{13}
0.42/0.45 - <0.05	11 ± 6	8 ± 16	9 ± 3	3 ± 6

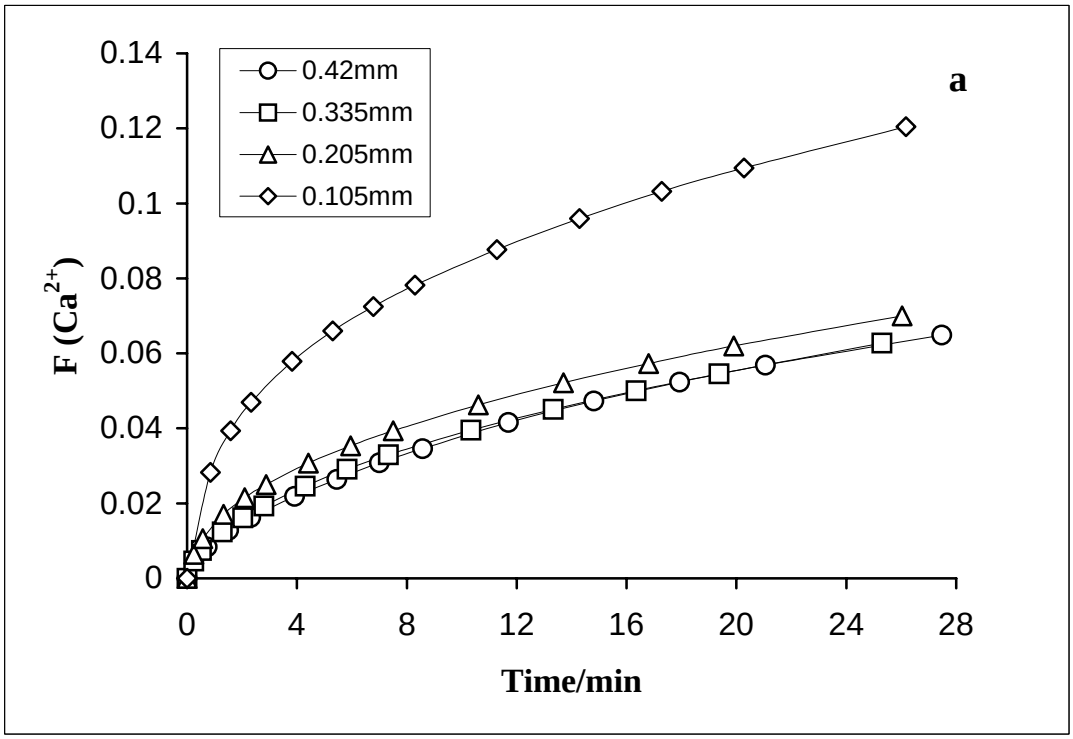
a
0.42mm
0.335mm
0.205mm
0.105mm
F (Ca2+)
0.14
0.12
0.1
0.08
0.06
0.04
0.02
0
0
4
8
12
16
20
24
28
Time/min

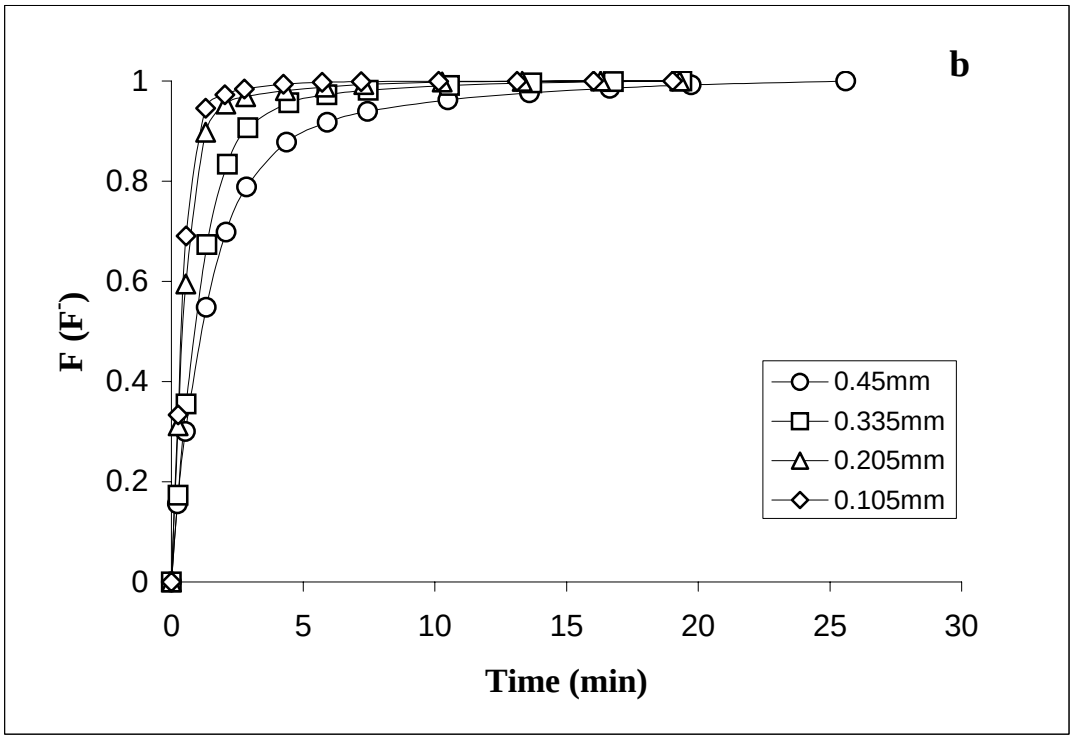
b
F (F-)
1
0.8
0.6
0.4
0.2
0
0
5
10
15
20
25
30
Time (min)
0.45mm
0.335mm
0.205mm
0.105mm

Figure 1

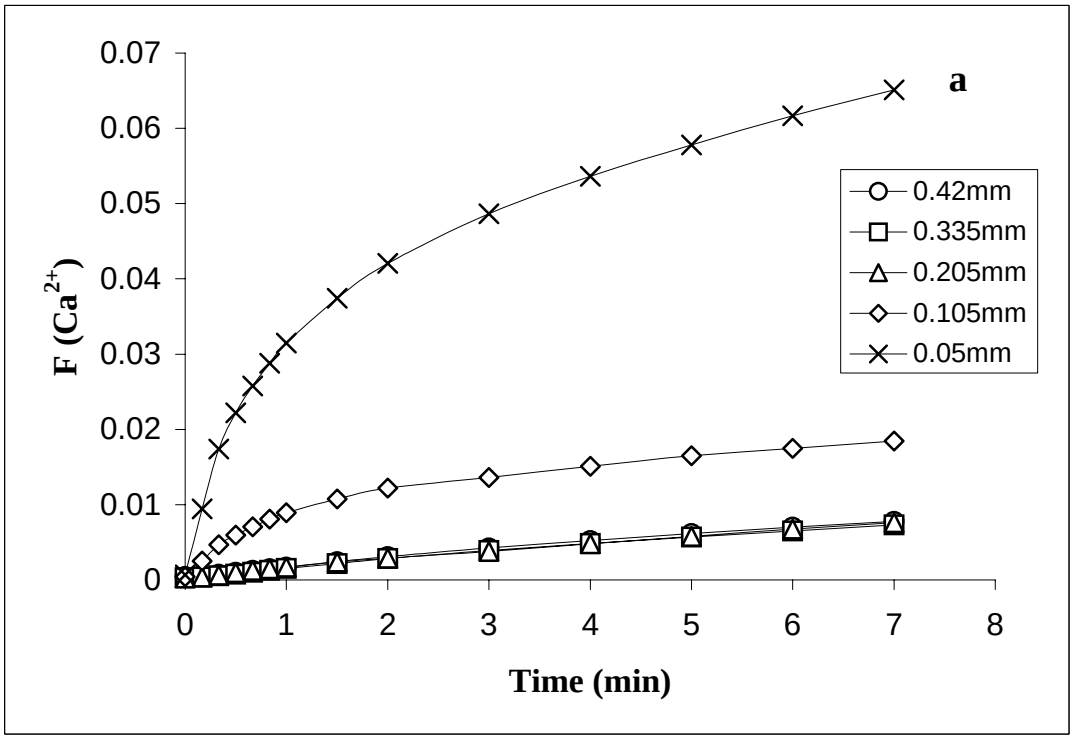
a
0.07
0.06
0.05
0.04
0.03
0.02
0.01
0
F (Ca2+)
0
1
2
3
4
5
6
7
8
Time (min)
0.42mm
0.335mm
0.205mm
0.105mm
0.05mm

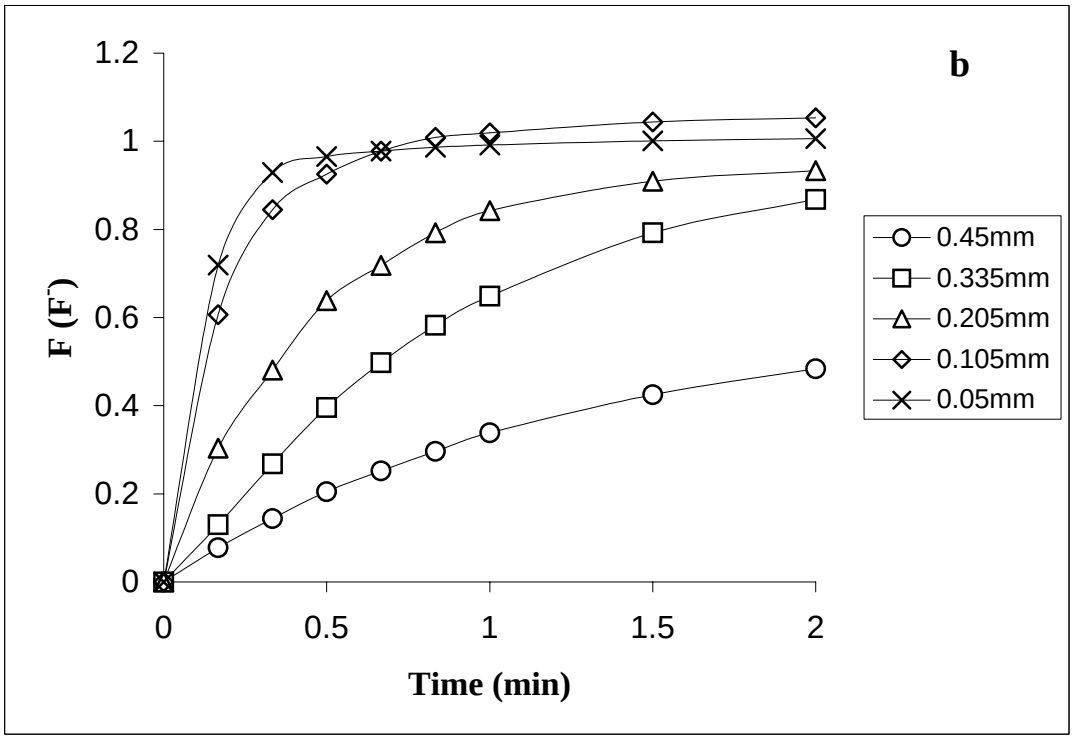
b
1.2
1
0.8
0.6
0.4
0.2
0
F (F-)
0
0.5
1
1.5
2
Time (min)
0.45mm
0.335mm
0.205mm
0.105mm
0.05mm

Figure 2

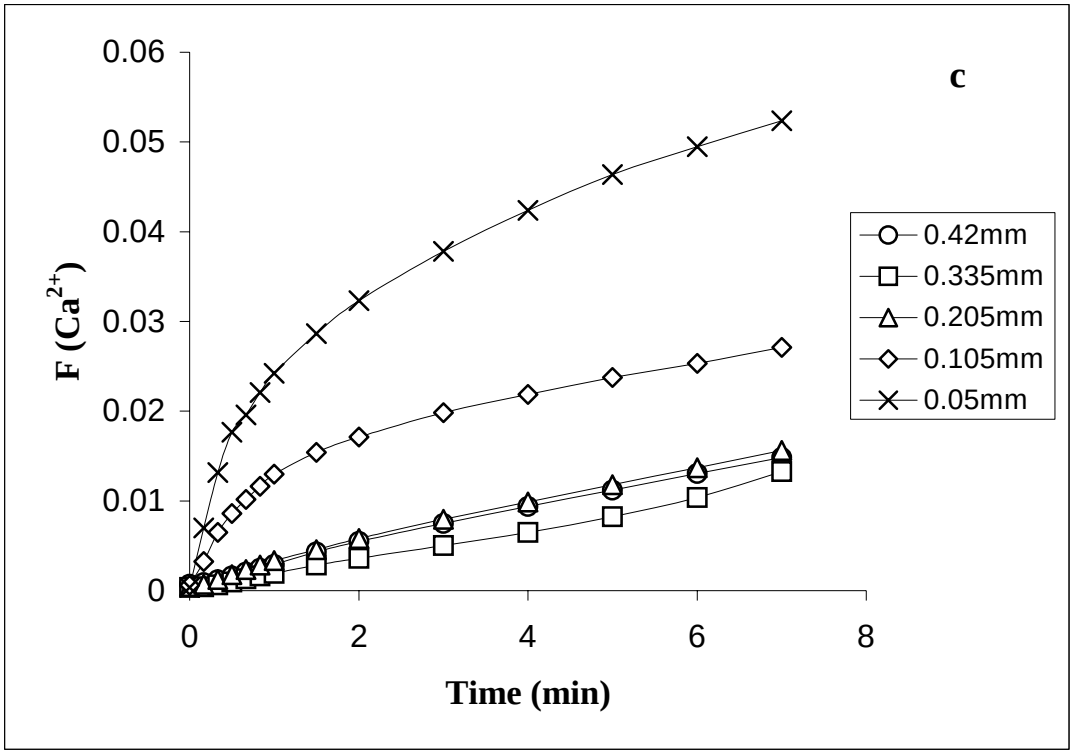
c
0.06
0.05
0.04
0.03
0.02
0.01
0
F (Ca2+)
0
2
4
6
8
Time (min)
0.42mm
0.335mm
0.205mm
0.105mm
0.05mm

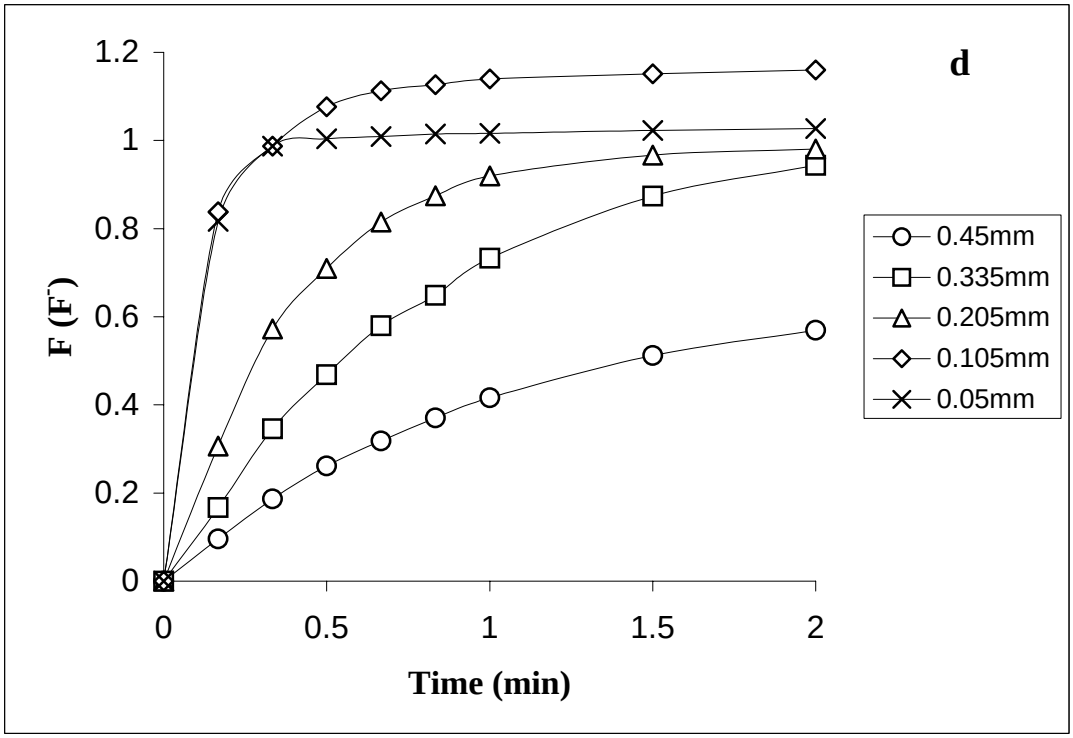
d
1.2
1
0.8
0.6
0.4
0.2
0
F (F-)
0
0.5
1
1.5
2
Time (min)
0.45mm
0.335mm
0.205mm
0.105mm
0.05mm

Figure 2

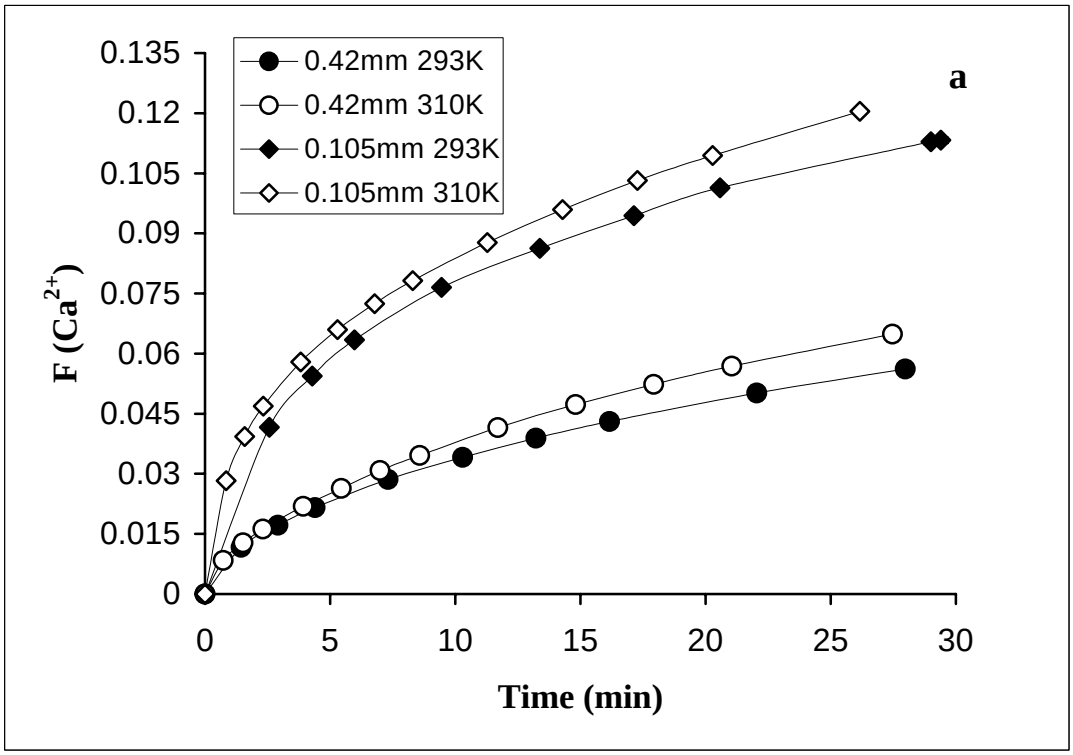
a
0.42mm 293K
0.42mm 310K
0.105mm 293K
0.105mm 310K
F (Ca2+)
0.135
0.12
0.105
0.09
0.075
0.06
0.045
0.03
0.015
0
0
5
10
15
20
25
30
Time (min)

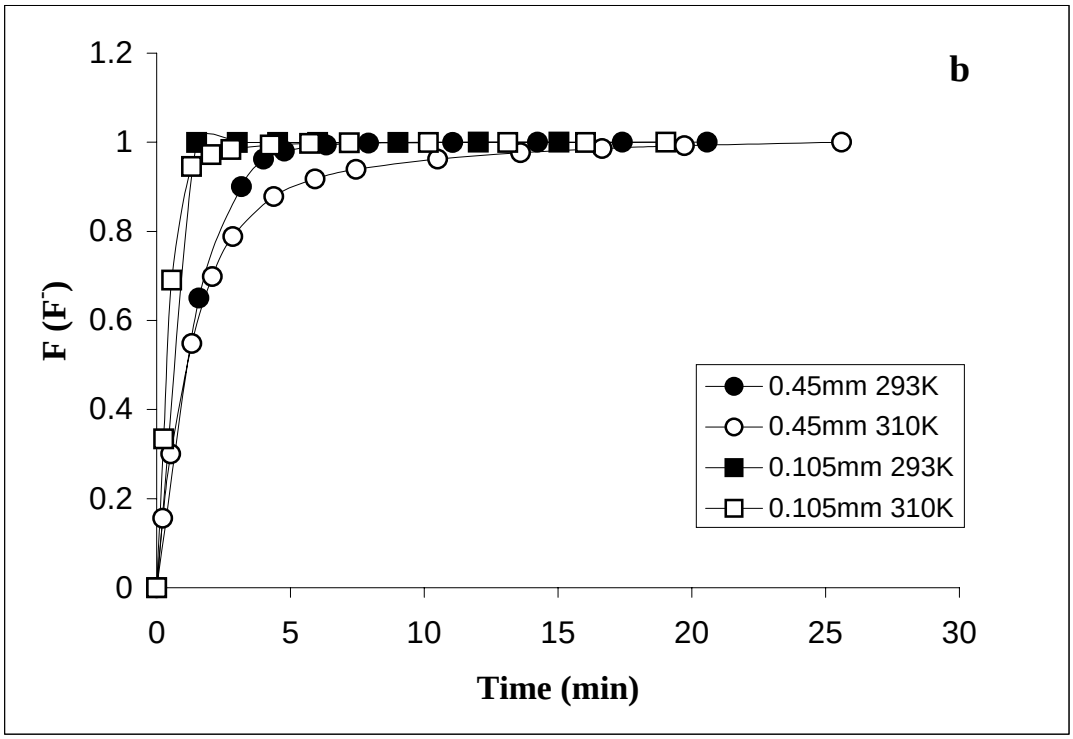
b
0.45mm 293K
0.45mm 310K
0.105mm 293K
0.105mm 310K
F (F-)
1.2
1
0.8
0.6
0.4
0.2
0
0
5
10
15
20
25
30
Time (min)

Figure 3

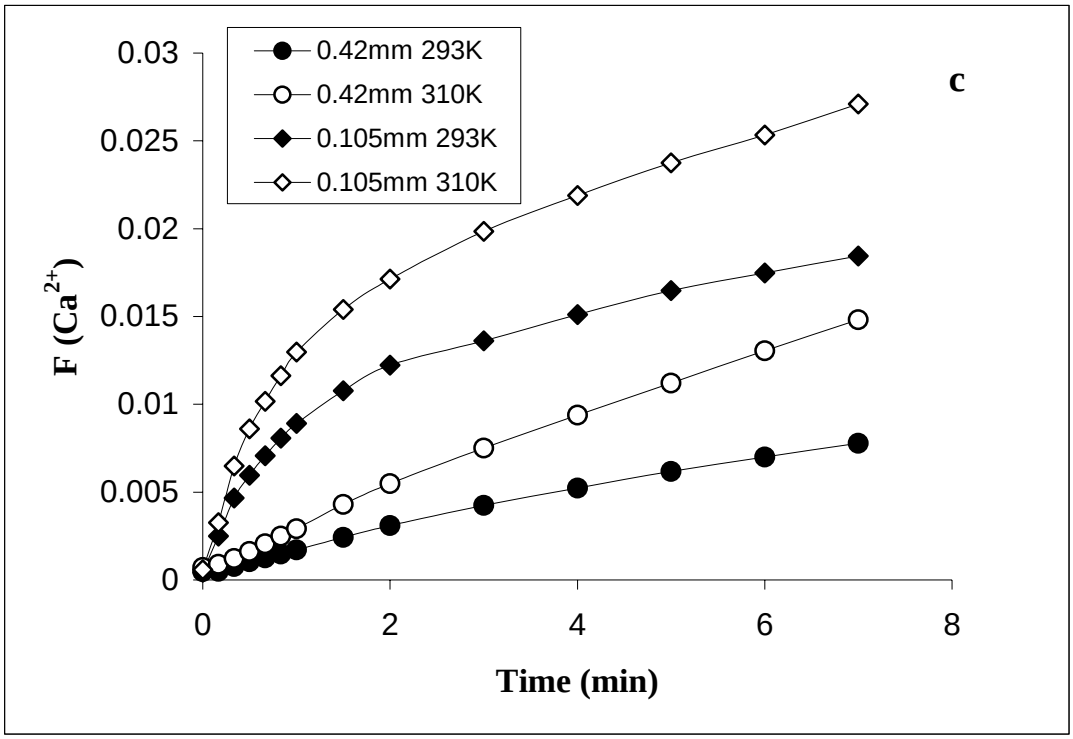
c
0.42mm 293K
0.42mm 310K
0.105mm 293K
0.105mm 310K
F (Ca2+)
0.03
0.025
0.02
0.015
0.01
0.005
0
0
2
4
6
8
Time (min)

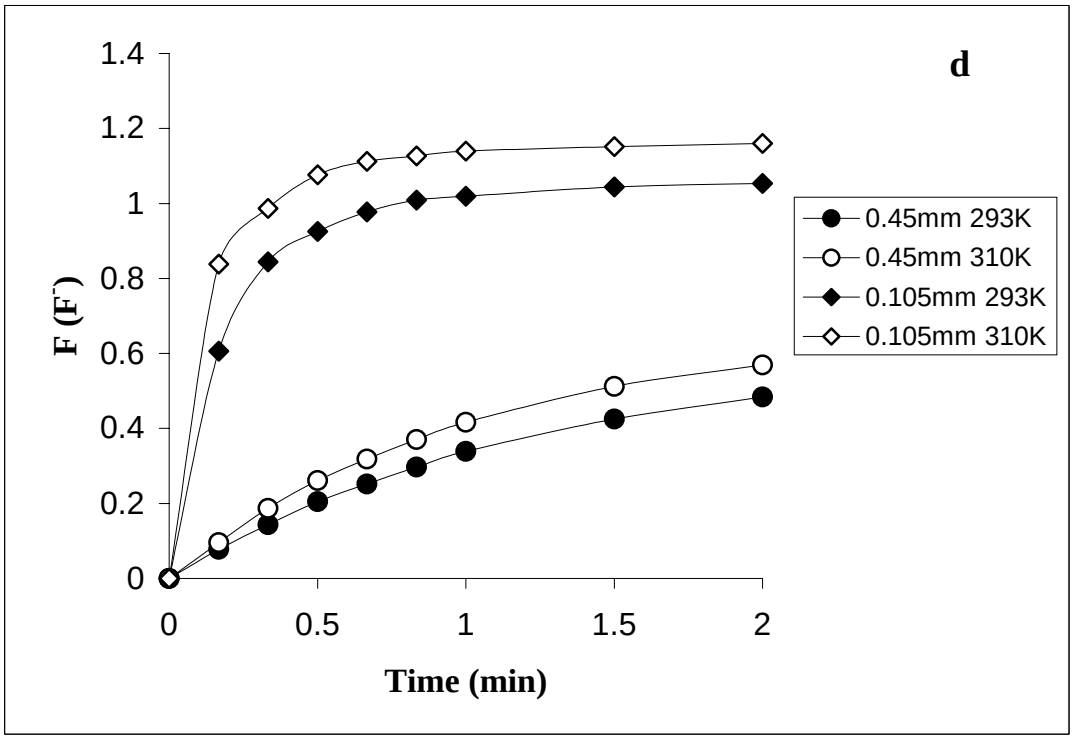
d
0.45mm 293K
0.45mm 310K
0.105mm 293K
0.105mm 310K
F (F-)
1.4
1.2
1
0.8
0.6
0.4
0.2
0
0
0.5
1
1.5
2
Time (min)

Figure 3

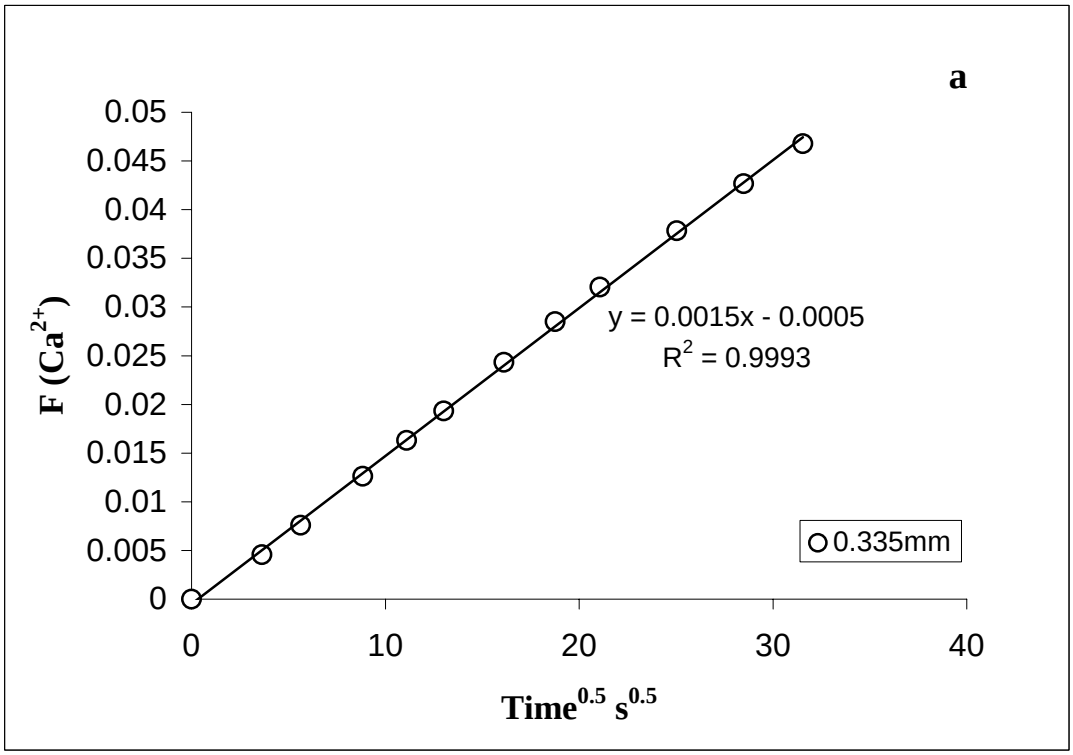
a
0.05
0.045
0.04
0.035
0.03
0.025
0.02
0.015
0.01
0.005
0
F (Ca2+)
y = 0.0015x - 0.0005
R2 = 0.9993
0.335mm
0
10
20
30
40
Time0.5 s0.5

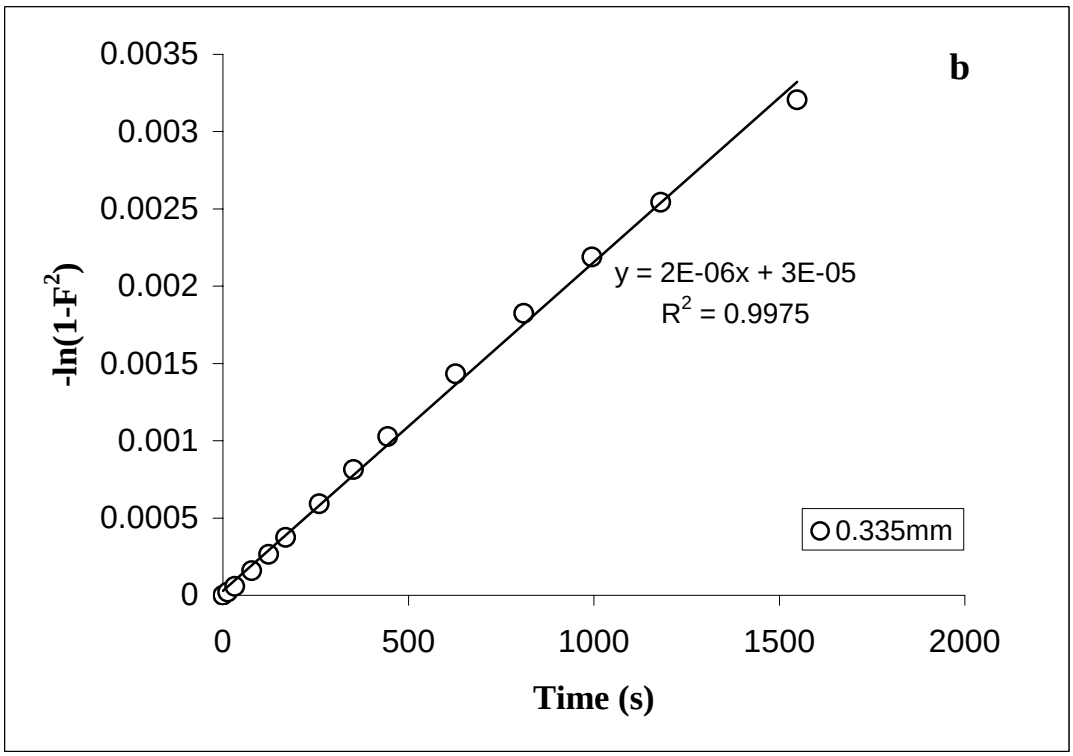
b
0.0035
0.003
0.0025
0.002
0.0015
0.001
0.0005
0
-ln(1-F2)
y = 2E-06x + 3E-05
R2 = 0.9975
0.335mm
0
500
1000
1500
2000
Time (s)

Figure 4

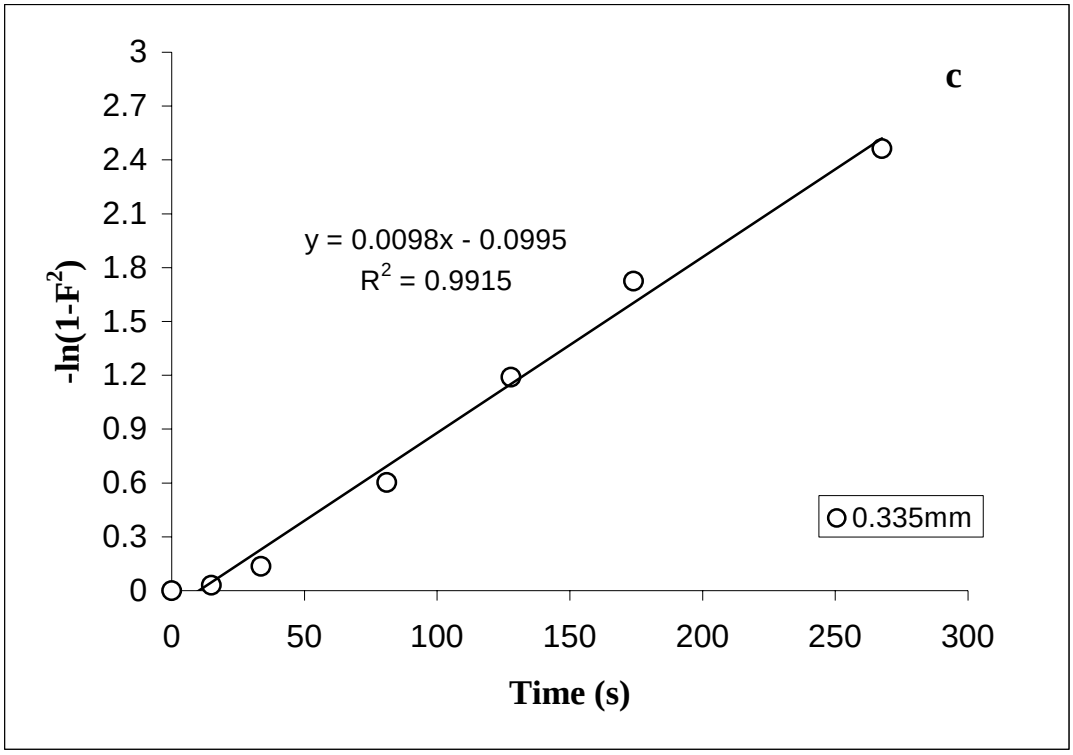
c
y = 0.0098x - 0.0995
R2 = 0.9915
0.335mm
-ln(1-F2)
Time (s)
0
0.3
0.6
0.9
1.2
1.5
1.8
2.1
2.4
2.7
3
0
50
100
150
200
250
300

Figure 4

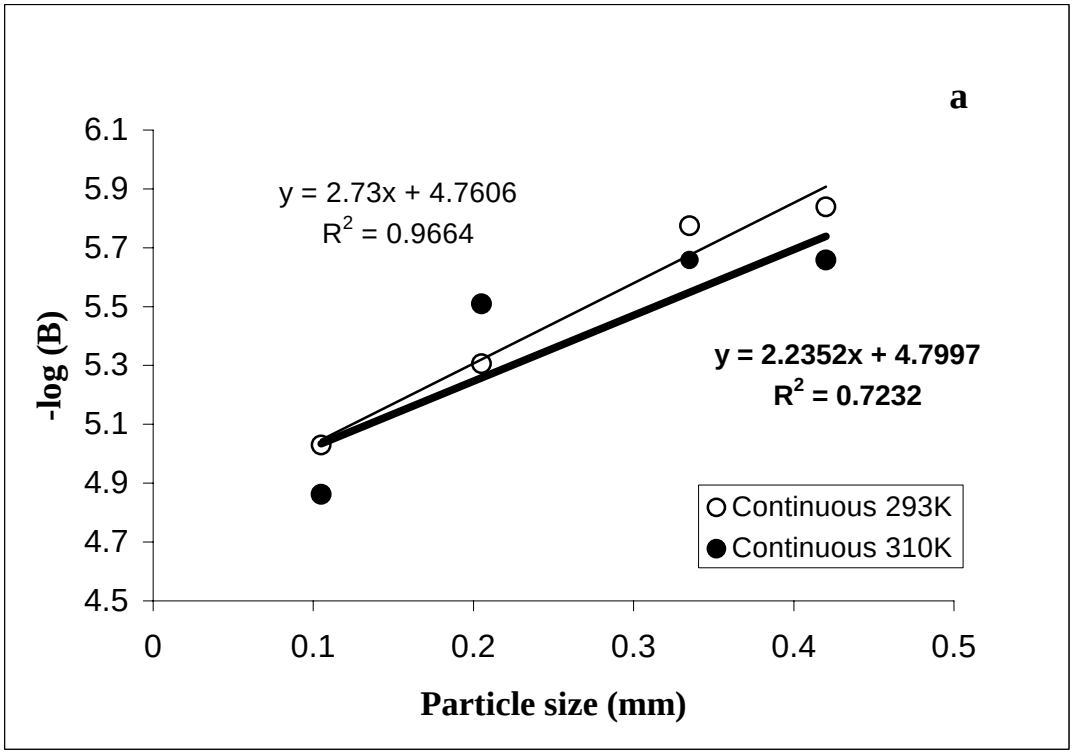
a
6.1
5.9
5.7
5.5
5.3
5.1
4.9
4.7
4.5
-log (B)
y = 2.73x + 4.7606
R2 = 0.9664
y = 2.2352x + 4.7997
R2 = 0.7232
Continuous 293K
Continuous 310K
0
0.1
0.2
0.3
0.4
0.5
Particle size (mm)

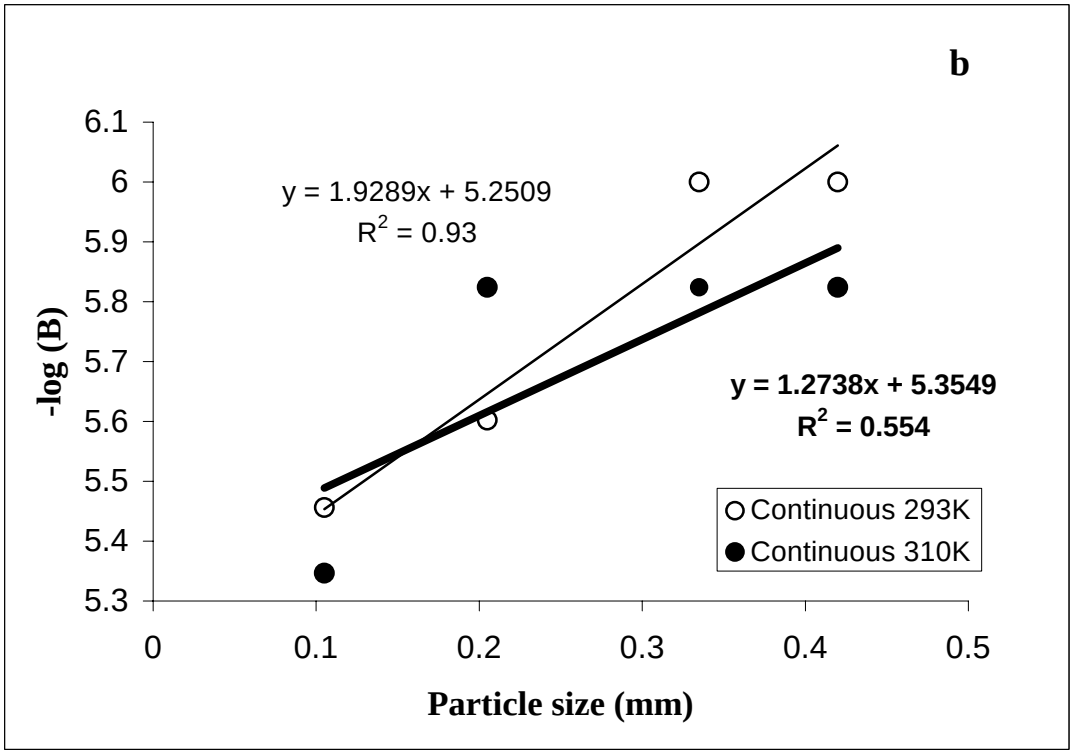
b
6.1
6
5.9
5.8
5.7
5.6
5.5
5.4
5.3
-log (B)
y = 1.9289x + 5.2509
R2 = 0.93
y = 1.2738x + 5.3549
R2 = 0.554
Continuous 293K
Continuous 310K
0
0.1
0.2
0.3
0.4
0.5
Particle size (mm)

Figure 5

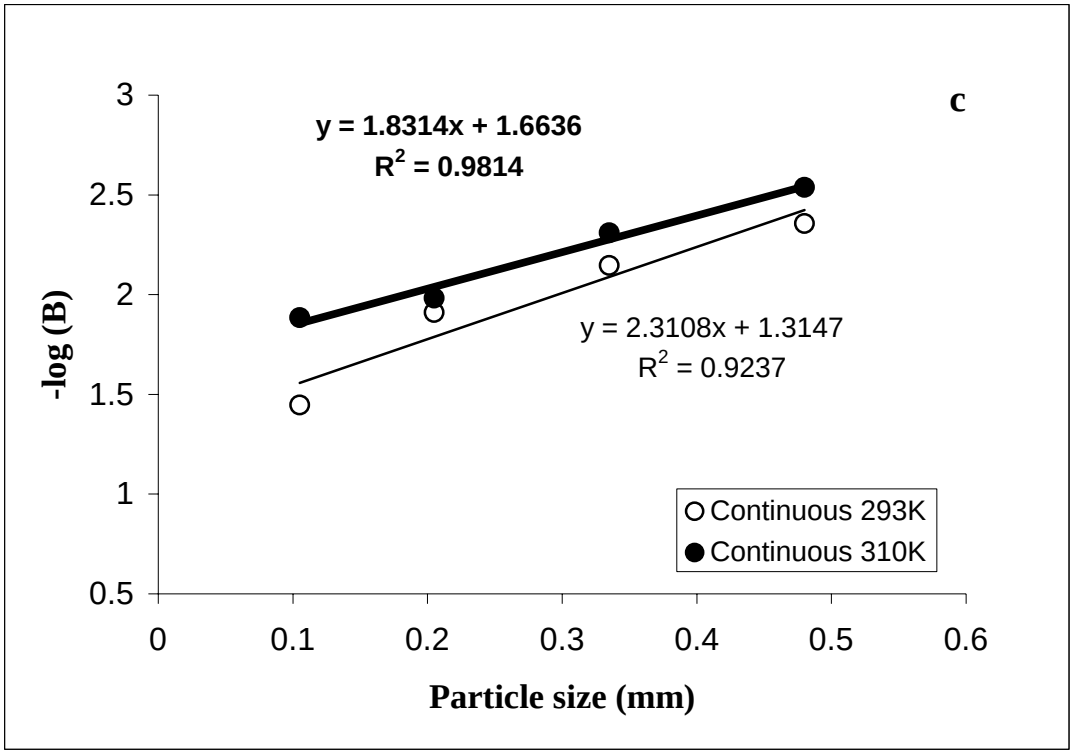
c
y = 1.8314x + 1.6636
R2 = 0.9814
y = 2.3108x + 1.3147
R2 = 0.9237
Continuous 293K
Continuous 310K
-log (B)
Particle size (mm)
3
2.5
2
1.5
1
0.5
0
0.1
0.2
0.3
0.4
0.5
0.6

Figure 5

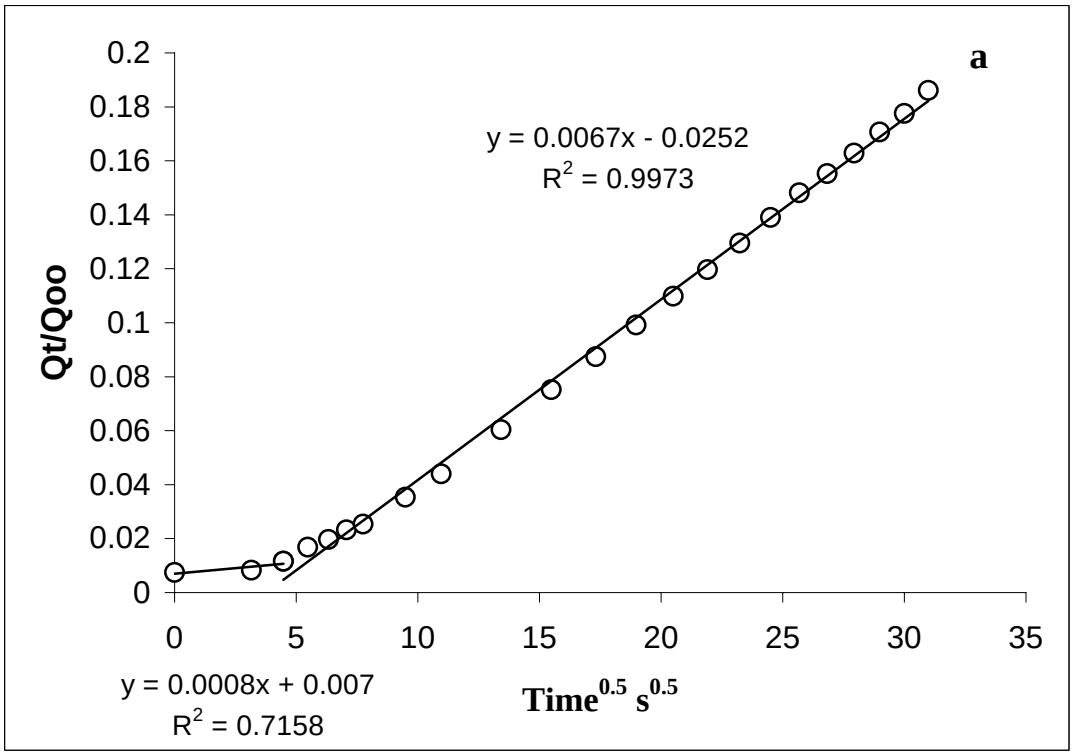
a
y = 0.0067x - 0.0252
R2 = 0.9973
Qt/Qoo
0.2
0.18
0.16
0.14
0.12
0.1
0.08
0.06
0.04
0.02
0
0
5
10
15
20
25
30
35
y = 0.0008x + 0.007
R2 = 0.7158
Time0.5 s0.5

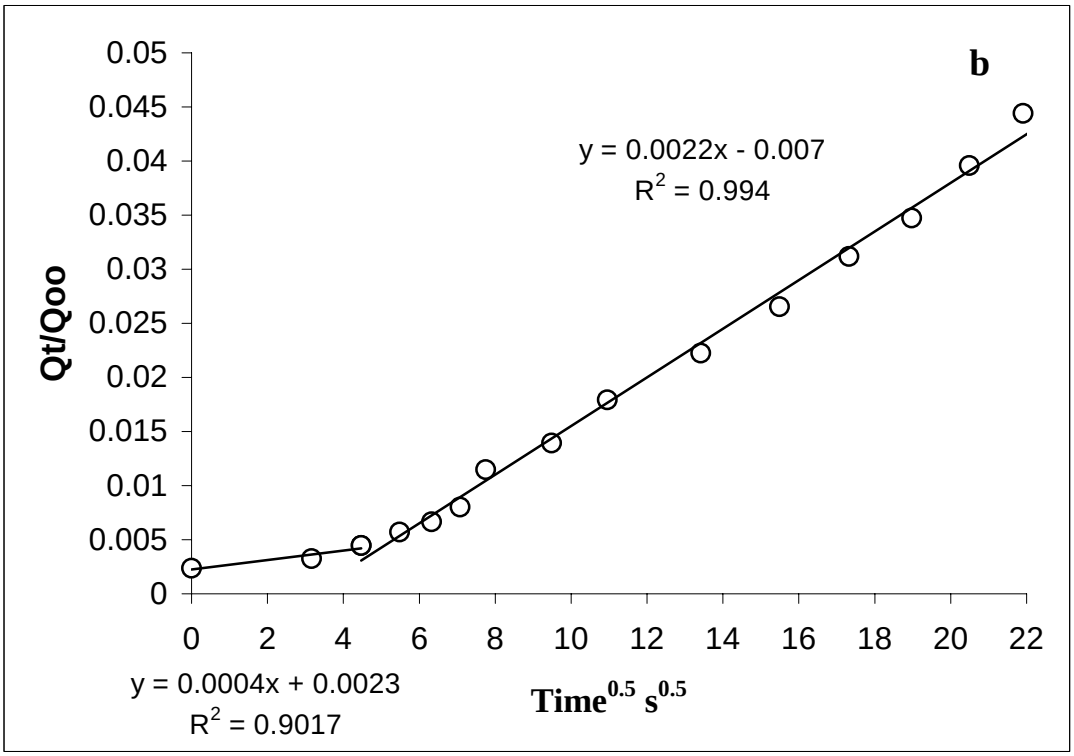
b
y = 0.0022x - 0.007
R2 = 0.994
Qt/Qoo
0.05
0.045
0.04
0.035
0.03
0.025
0.02
0.015
0.01
0.005
0
0
2
4
6
8
10
12
14
16
18
20
22
y = 0.0004x + 0.0023
R2 = 0.9017
Time0.5 s0.5

Figure 6

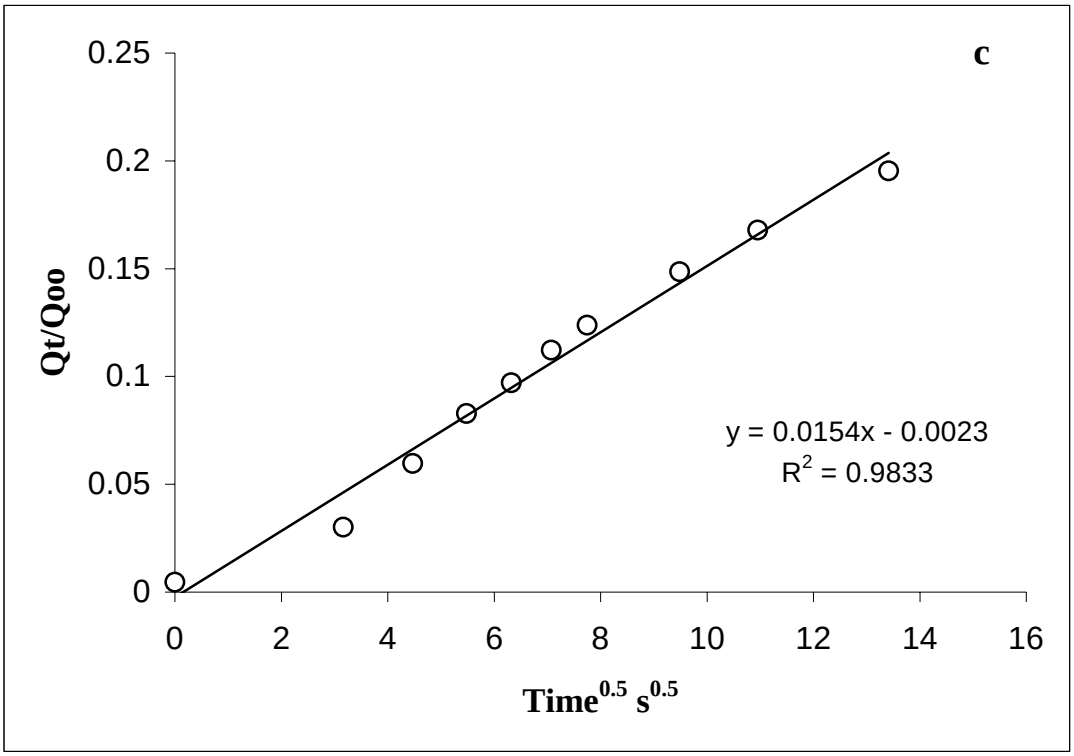
c
0.25
0.2
0.15
0.1
0.05
0
Qt/Qoo
y = 0.0154x - 0.0023
R2 = 0.9833
0
2
4
6
8
10
12
14
16
Time0.5 s0.5

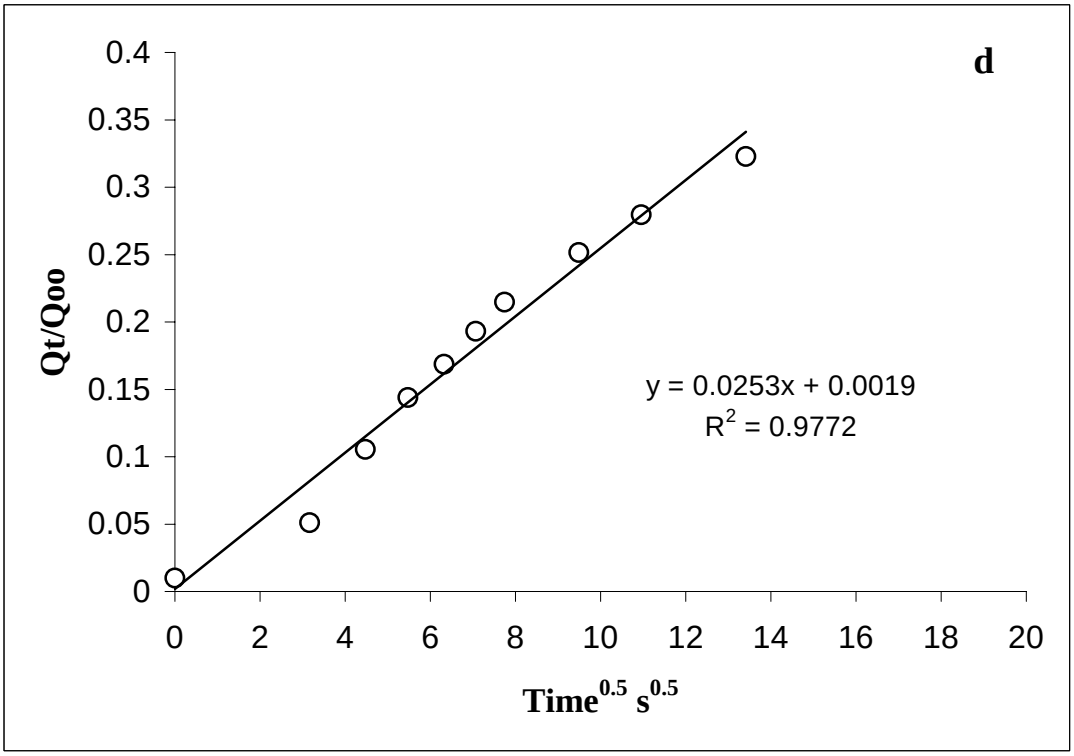
d
0.4
0.35
0.3
0.25
0.2
0.15
0.1
0.05
0
Qt/Qoo
y = 0.0253x + 0.0019
R2 = 0.9772
0
2
4
6
8
10
12
14
16
18
20
Time0.5 s0.5

Figure 6

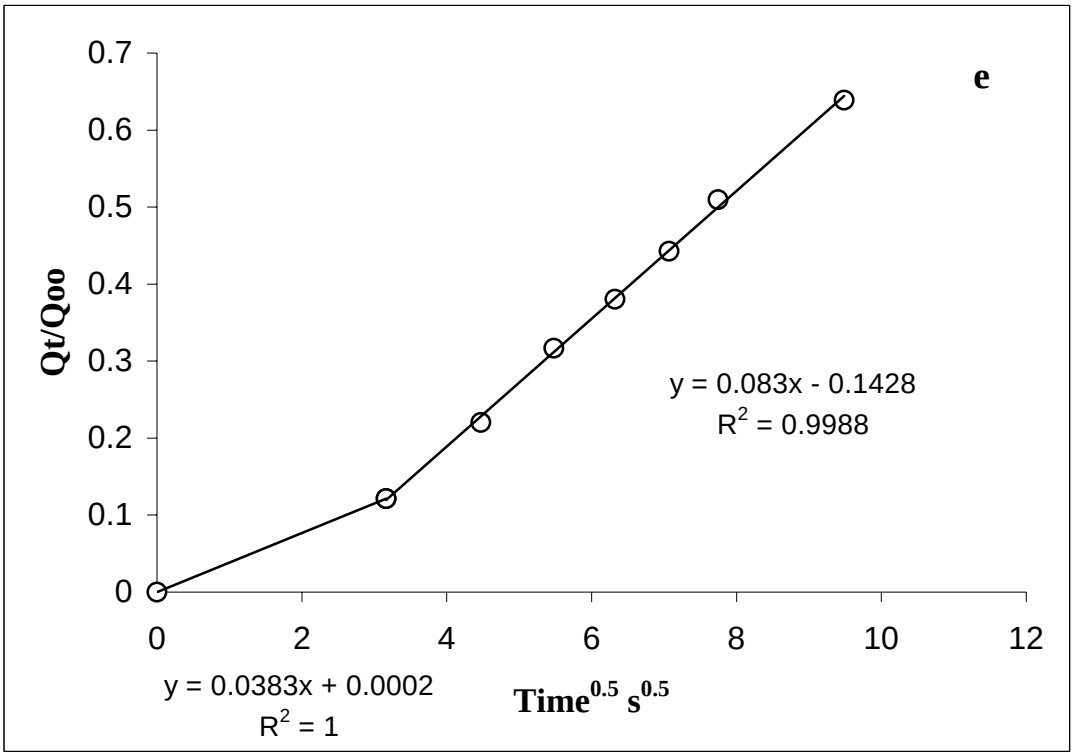
e
0.7
0.6
0.5
0.4
0.3
0.2
0.1
0
Qt/Qoo
y = 0.083x - 0.1428
R2 = 0.9988
0
2
4
6
8
10
12
y = 0.0383x + 0.0002
R2 = 1
Time0.5 s0.5

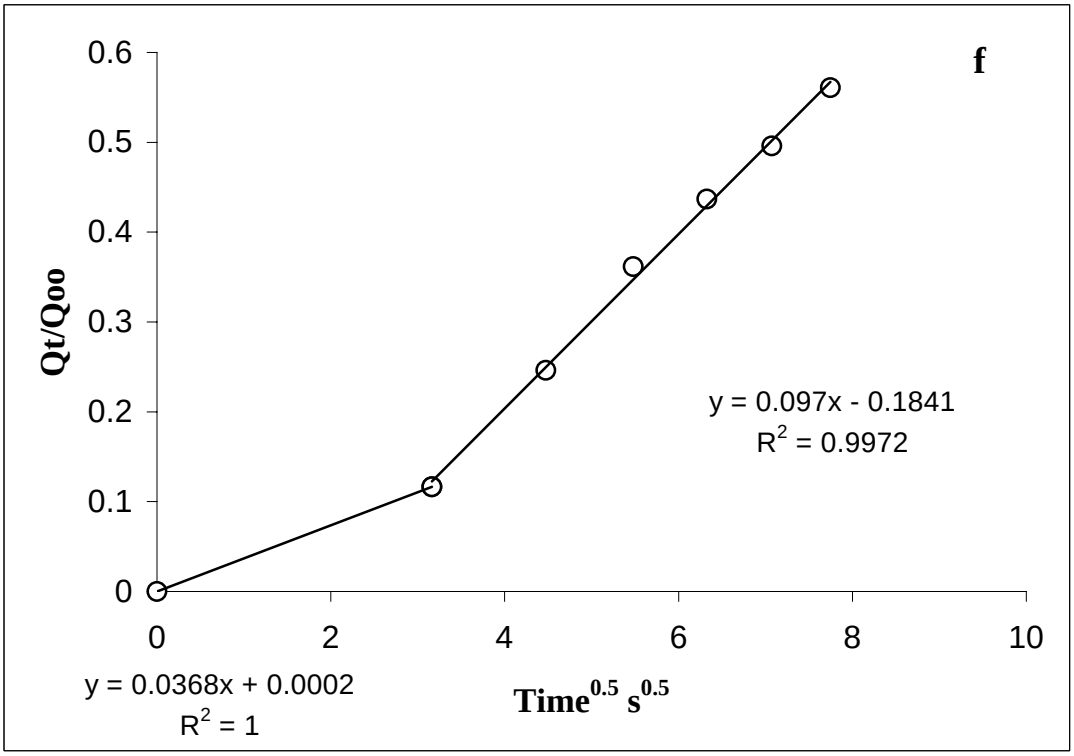
f
0.6
0.5
0.4
0.3
0.2
0.1
0
Qt/Qoo
y = 0.097x - 0.1841
R2 = 0.9972
0
2
4
6
8
10
y = 0.0368x + 0.0002
R2 = 1
Time0.5 s0.5

Figure 6

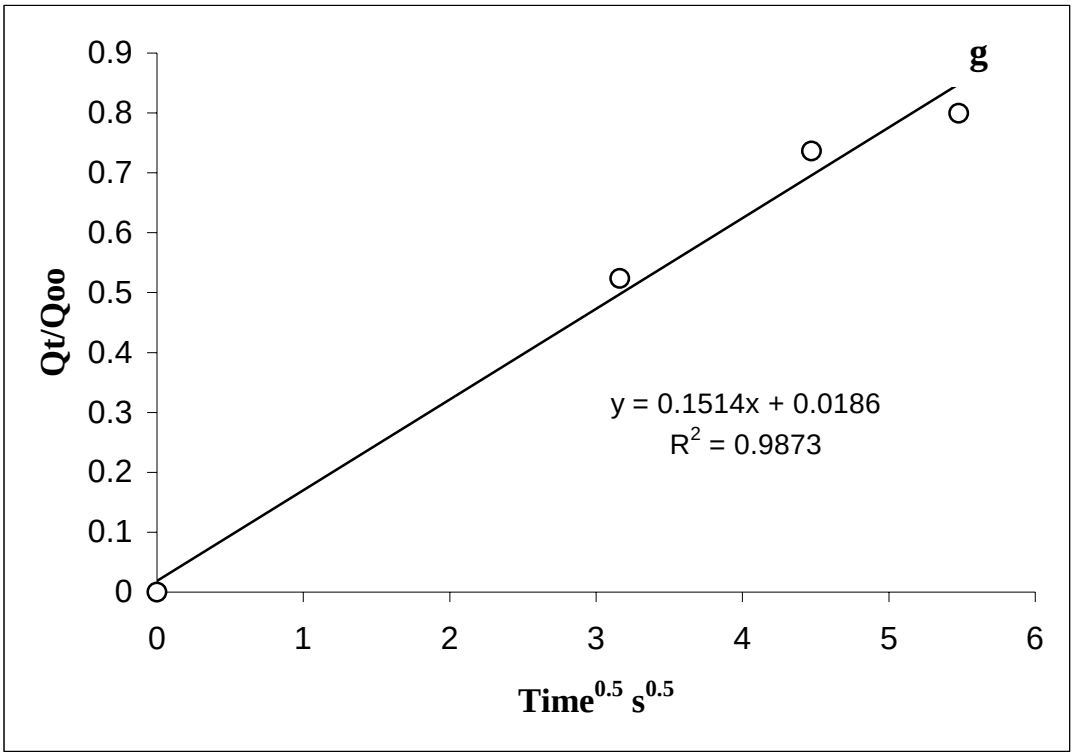
g
Qt/Qoo
0.9
0.8
0.7
0.6
0.5
0.4
0.3
0.2
0.1
0
0
1
2
3
4
5
6
y = 0.1514x + 0.0186
R2 = 0.9873
Time0.5 s0.5

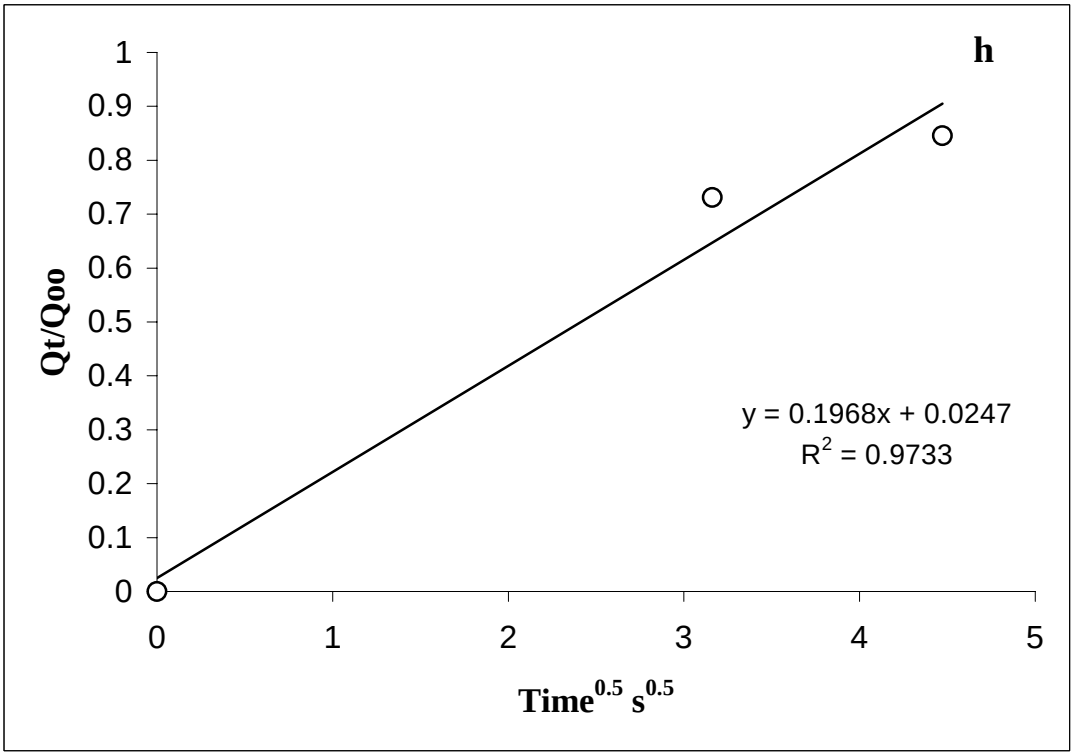
h
Qt/Qoo
1
0.9
0.8
0.7
0.6
0.5
0.4
0.3
0.2
0.1
0
0
1
2
3
4
5
y = 0.1968x + 0.0247
R2 = 0.9733
Time0.5 s0.5

Figure 6

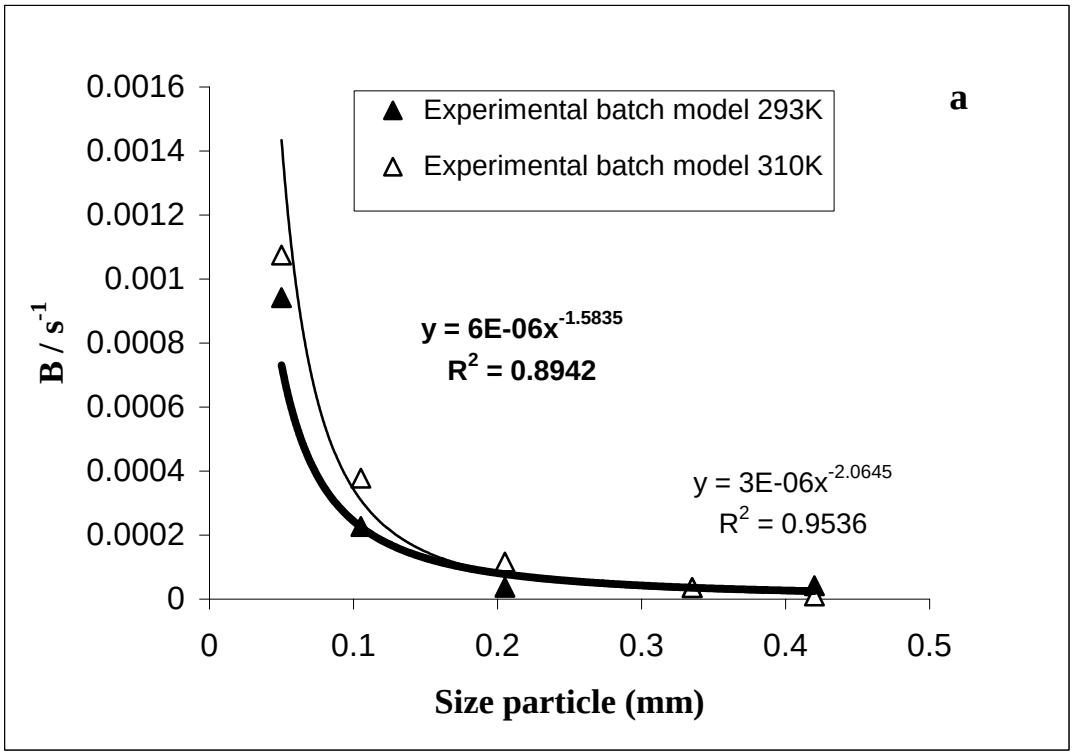
a
Experimental batch model 293K
Experimental batch model 310K
y = 6E-06x-1.5835
R2 = 0.8942
y = 3E-06x-2.0645
R2 = 0.9536
B / s-1
Size particle (mm)
0.0016
0.0014
0.0012
0.001
0.0008
0.0006
0.0004
0.0002
0
0
0.1
0.2
0.3
0.4
0.5

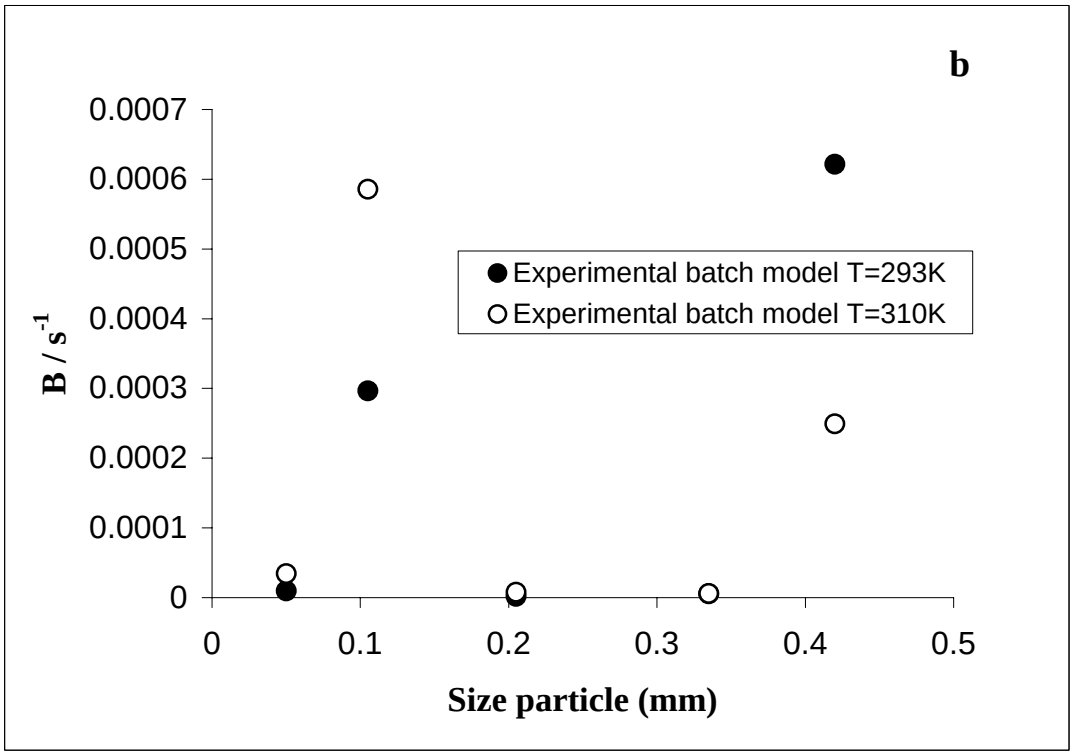
b
Experimental batch model T=293K
Experimental batch model T=310K
B / s-1
Size particle (mm)
0.0007
0.0006
0.0005
0.0004
0.0003
0.0002
0.0001
0
0
0.1
0.2
0.3
0.4
0.5

Figure 7

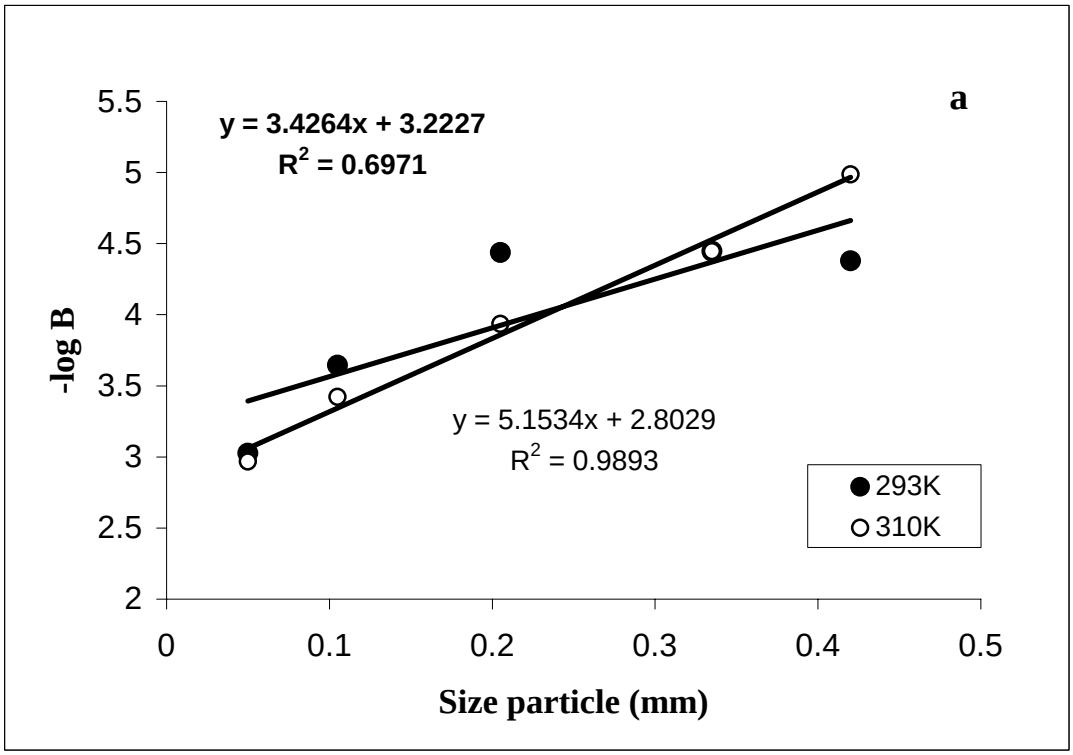
a
y = 3.4264x + 3.2227
R2 = 0.6971
y = 5.1534x + 2.8029
R2 = 0.9893
293K
310K
-log B
Size particle (mm)
5.5
5
4.5
4
3.5
3
2.5
2
0
0.1
0.2
0.3
0.4
0.5

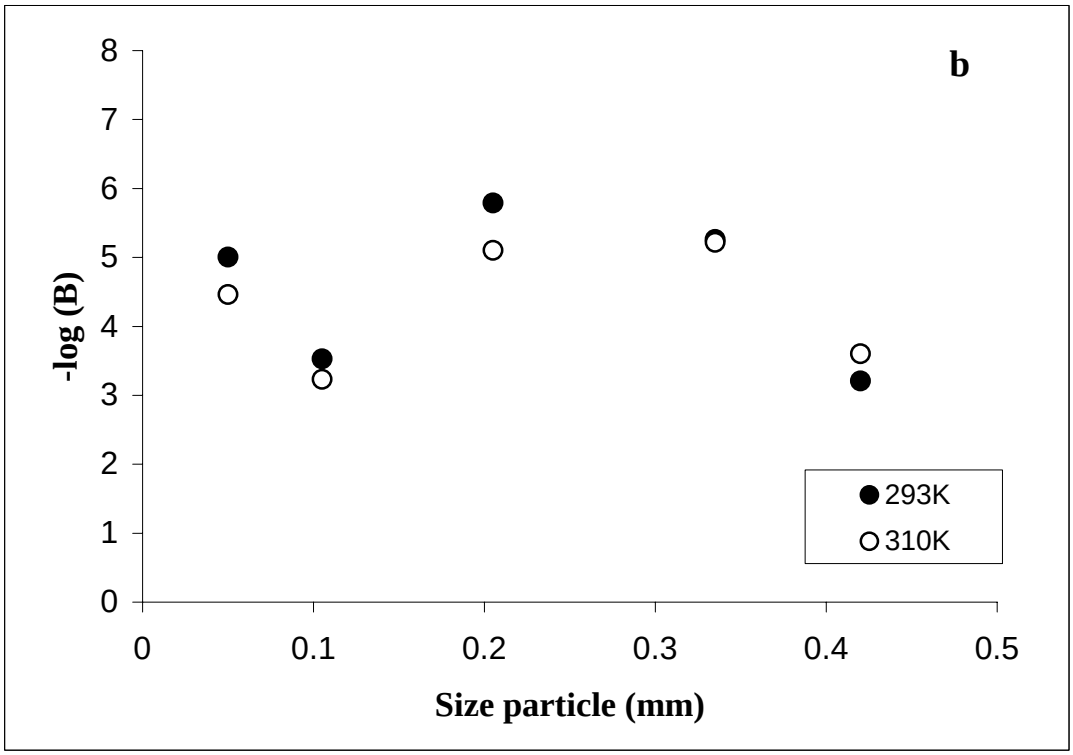
b
293K
310K
-log (B)
Size particle (mm)
8
7
6
5
4
3
2
1
0
0
0.1
0.2
0.3
0.4
0.5

Figure 8

ANNEX 3

KINETICS CHARACTERIZATION OF IONS RELEASE UNDER DYNAMIC AND BATCH CONDITIONS. II. STRONG ACID AND STRONG BASE TYPE ION EXCHANGE RESINS.

A.Torrado and M. Valiente*

Departament de Química, Unitat Analítica, Centre GTS, Universitat Autònoma de Barcelona, Facultat de Ciències, Edifici Cn, E-08193, Bellaterra (Barcelona), Spain

Abstract

The purpose of this study has been to investigate the influence of key parameters (i.e., the structure of the resin organic polymer and its particle size, as well as the temperature of the process) on the release of calcium and fluoride ions from cationic and anionic ion exchange resins of strong character, in order to develop a formulation for a controlled release of the mentioned ions, that are present in organomineral tissues. Kinetics parameters were evaluated under dynamic and batch conditions. It has been observed that the rate of Ca^{2+} and F^- release increases when temperature increases and particle size decreases. Because of the larger pore volumes that provide a greater effective surface area, macroporous ion exchangers observe a higher rate of ions release than those of gel nature. Results obtained in this study are well interpreted by the models based on intraparticle diffusion as rate controlling step of the ion exchange process. The effective rate of release, B (obtained from the application of mentioned models), of the respective ions in the resin phase describes quantitatively the kinetic process. Linear dependences of –log (B) with the resin particles diameters can be applied to the estimation of B values for very low particle size resins, materials commonly used in the development of controlled release formulations.

Keywords: ion exchange, kinetics release, gel ion exchanger, macroporous ion exchanger, intraparticle diffusion, calcium, fluoride.

***Correspondence to:** Manuel Valiente, Departament de Química, Unitat Analítica, Centre GTS, Universitat Autònoma de Barcelona, Facultat de Ciències, Edifici Cn, E-08193 Bellaterra (Barcelona), Spain

Phone number. +34 93 581 2903

Fax number: +34 93 581 1985

E-mail: Manuel.Valiente@uab.es

1. Introduction

Since the first ion-exchange resin was synthesized for the use in the isolation and purification of products from solutions, investigations carried out using this system have led to a considerable increase in the number of possible applications. This is especially true in the field of pharmacy where their use for sustained release of orally administered drugs was proposed some 40 years ago,[1,2] and quickly gained popularity.

Synthetic organic resins are the most widely used ion exchange materials. They are water-insoluble polymers possessing acidic or basic functional groups which are covalently bound to the hydrophobic matrix and associated with oppositely charged mobile counterions which enable the resin to undergo ion exchange.[3]

Among the advantages of including drugs in ion-exchange resins, so that they can be used as new drug delivery systems, we can mention the following: (i) a delay in the release of the drug that will permit a longer duration of its effects; a variety of drug delivery systems in the form of microspheres,[4] microcapsules,[5] nanoparticles,[6] and liposomes[7] have been developed for this purpose, (ii) an increase in its stability and (iii) the masking of possible unpleasant tasting drugs.[8]

Out of many methods for the preparation of sustained release formulations, the use of ion exchange resins has occupied an important place due to its well controllable properties like particle size, shape, and internal pore structure. The release of any substance that possesses an ionic site from a resin particle, can be controlled by intraparticle diffusion or by the resistance of the film surrounding the particle (film diffusion).[9] Several equations have been proposed in the literature.[10,11] In this concern, the essential objective is to determine the mechanism controlling the release. Normally, intraparticle diffusion control is expected for the release of species from a resin and hence the experimental data are tested for this type of mechanism.

Cationic and anionic ion exchange resins are suitable for the design of preparations with prolonged action.[12,13] Selection of the matrix quality (IX groups, capacity, particle size, cross-linking), external conditions (e.g. ionic strength, pH, temperature and choice of the release salt in the medium), and the properties of the releasable substance (charge, lipophilicity and molecular weight), can be manipulated to control the kinetics release of the active principle from the ion exchange system.[14,15]

The present study aims to investigate the influence of key parameters (i.e., the structure of the resin polymer and its particle size, as well as the temperature of the process) on

the release of calcium and fluoride ions from cationic and anionic ion exchange resins of strong character (strong acid and strong base) to develop a controlled release formulation for the possible applications to remineralization of dental tissues, which are known to be formed by carbonated calcium hydroxyapatite. In the presence of fluoride, after a remineralization process the new mineral will contain calcium hydroxyapatite and fluoroapatite ($Ca_5(PO_4)_3F$), both of which are less soluble than the original carbonated calcium hydroxyapatite, what will protect the teeth from further acid attacks. Kinetics parameters of the release of target ions calcium and fluoride were evaluated under dynamic and batch experimental conditions.

2. Experimental

2.1. Materials

Ion exchange sulphonic resins Lewatit S100 (gelular structure) and SP112WS (macroporous structure) and quaternary amine resins Lewatit M600 (gelular structure) and MP600 (macroporous structure) were kindly supplied by Bayer Hispania Industrial, S.A (Barcelona, Spain). $CaCl_2$ 0.5 M, KCl 0.01 M, NaCl 0.008 M, NaF 0.8 M, and $NaNO_3$ 0.5 M solutions were prepared from the corresponding pro analysis quality solid salts Panreac (Barcelona, Spain). HCl 0.5 M solution was prepared by dilution of the corresponding concentrated pro analysis quality acid Panreac (Barcelona, Spain). In all cases, deionized water Milli-Q quality (Millipore, USA) was used.

2.2. Instrumentation

The release of Ca^{2+} and F^- under batch experimental conditions, was determined by ion selective electrodes Orion (USA) controlled automatically by a PC, whereas under dynamic conditions, Ca^{2+} was measured spectrofotometrically by inductively coupled plasma atomic emission spectroscopy technique (ICP-OES) using an ARL model 3410 minitorch (USA). All the samples were analyzed with an uncertainty lower than 1.5 % and all the experiments were carried out by triplicate.

2.3. Resins loading

Resins were conditioned by following a standard procedure.[16] The conversion of the resins to the desired ionic form was carried out in ion exchange columns under dynamic conditions by flowing aqueous solutions of the corresponding reagents through the resin

bed. After complete loading, the resin phase was successively washed with water to remove the excess of electrolyte solution, quantitatively removed from the column and separated from water by filtration, followed by drying at the oven (60-70 ºC). Resins in the different ionic forms were kept in hermetically sealed vials to avoid water absorption.

2.4. Resins capacity

Determination of the specific capacity of the different resins towards Ca^{2+} and F^- was carried out under dynamic conditions in columns by following a standard procedure.[17] A weighed portion of each resin was introduced in a 10 cm column (8 mm Ø) and the counterion of interest was eluted with HCl in the case of the cationic resin and with $NaNO_3$ in the anionic one. Eluate was collected in volumetric flasks and analyzed. The results of the analysis were used to determine the specific capacity of the resins, q_s, according to the equation:

$$q_s = \frac{VC_i}{W_i} \quad (1)$$

where *V* is the total volume of eluted solution, *Ci* is the concentration of the solution containing the eluted ion *i*, and *Wi* is the weight of resin loaded with this ion. The specific capacities determined experimentally are shown in Table 1.

2.5. Grinding and sieving

A fraction of each type of resin was ground in a mechanical agate mortar Retsch RMO (Germany) and sieved by using a set of standard stainless steel sieves in a mechanical siever, CISA (Spain). Thus, separate fractions of the resins were collected with particle sizes of diameter 0.42 mm, 0.42-0.25 mm, 0.25-0.16 mm, 0.16-0.05 mm, and <0.05 mm.

2.6. Ion exchange kinetics

2.6.1. Dynamic conditions

The study of ion exchange kinetics of the different samples was carried out under dynamic conditions using the “shallow bed” technique.[18] A small resin portion loaded with the specific target ion was introduced in a column connected to a thermostat and, a

solution of artificial saliva (solution of concentration 1g/l KCl and 0.5g/l NaCl) was passed through the resin bed at high flow rate (~30 ml/min). Experiments were run at 293 and 310 K. All the resulting eluate was collected in volumetric flasks, analyzed and these analytical data transformed to the degree of conversion, *F*, by using the equation:

$$F = \frac{\sum_{t_i=1}^{t_n} c_i v_i}{q_\infty} \qquad (2)$$

where *vi* corresponds to the volume of the eluate portion *i*, *Ci* to its concentration and q_∞ the total capacity of the resin, expressed as:

$$q_\infty = \sum c_i v_i + Vstr\ Cstr \qquad (3)$$

where *Vstr* corresponds to the volume of an eluate sample obtained from an elution, with either acid or nitrate, carried out after the kinetics experiment and, *Cstr* to its concentration.

2.6.2. Batch conditions

The study of the kinetics of ions release under batch conditions was carried out by using the "limited volume" technique.[19] A small resin portion loaded with the corresponding target ion was introduced in a thermostated cell (at 293 or 310 K), containing 50ml of artificial saliva vigorously agitated. The moment when the sample got into contact with the desorbing solution (artificial saliva) was considered as the starting time (time zero) for the kinetics experiment.

The experimental data obtained by ion selective electrodes were expressed in terms of degree of conversion, *F*, of the resins by applying the equation:

$$F = \frac{V_{as}\ c(t_i)}{q_\infty} \qquad (4)$$

where V_{as} is the volume of artificial saliva contained in the cell, *c(ti)* is the concentration of the target ion at the time of the experiment *ti* and, $q_\infty = mq_s$ is the total capacity of the resin (in mmols), being *m* the weight of resin portion and q_s (mmol/g) the specific capacity of the resin towards the corresponding ion determined as described in the section 2.4.

3. Results and discussion

3.1. Influence of particle size on the rate of Ca^{2+} and F^- release

Kinetics release of Ca^{2+} and F^- from the different matrices and particles size fractions, either under dynamic or batch conditions, are shown in Figures 1a-d and 2a-d. It can be observed that the rate of ions release increases when resin particle size decreases. The rate of release depends significantly on the average size of the resin particles due to the greater diffusional path lengths in larger beds.[20] Note that for fluoride ion this effect must be appreciated in shorter times because the equilibrium is quickly achieved. As previously reported in the case of weak base and acid types of ion exchangers[21] this can be explained in terms of affinity of the ion exchanger matrix towards the ion of interest. Quaternary amine anionic ion exchangers have a higher selectivity for chloride ion present in the artificial saliva whereas, sulphonic cation exchangers have a higher affinity for calcium ion (ion initially fixed) than for Na^+ and K^+ present in the desorbing solution. In the first studies though, Ca^{2+} rate of release was even lower than the one obtained with the corresponding strong acid type matrix. In fact, calcium ions are known to adsorb stronger to carboxylic groups than to sulphonic ones.[22]

3.2. Influence of temperature on the rate of Ca^{2+} and F^- release

As observed in Figures 3a-d and 4a-d, temperature affects the ions rate of release due to its influence on the diffusion coefficients. The rise in temperature, under either dynamic or batch conditions, accelerates the rate of exchange.[23]

3.3. Kinetics characterization of the ion exchange process

To a proper characterization of ion exchange kinetics, it is essential to determine the mechanism of control release.

Boyd et al.[24] demonstrated that three possible control mechanisms may take place in an ion exchange process: (i) Diffusion in the resin boundary liquid (film diffusion rate determining step) (ii) Diffusion in the solid particle (intraparticle diffusion rate determining step) (iii) Diffusional resistances in both phases. Several factors will affect to proper ascertain the mechanism taking place in a given system.

Under batch conditions, if the rate of ions release increases with the stirring of the liquid, then either (i) or (iii) will be the rate controlling step, whereas for mechanism (ii)

the ions release should be independent of the power stirring. Experiments were carried out under controlled 450 and 780 rpm stirring conditions and are shown in Figures 5a-b and 6a-b. It can be appreciated, that the stirring conditions have no influence on the ion exchange rates. This fact together with the dependence of the degree of conversion with the exchanger bead diameter for both resins tested, gel and macroporous type, suggests an ion exchange mechanism controlled by intraparticle diffusion.[20]

Under dynamic conditions, the information provided by the interruption tests of previous studies,[25,21] establishes that the ion exchange mechanism is controlled by intraparticle diffusion.

Thus, results from the above Figures 1 and 2 were treated by specific kinetics models, valid for the description of ion exchange processes controlled by intraparticle diffusion.

3.3.1. Dynamic conditions

The model selected, developed by Vermeulen,[26] is applicable over the whole range of degrees of conversion, *F*, from 0 to 1, and is based on the equation:

$$-\ln(1-F^2) = 2\frac{D\pi^2}{r^2}t = 2Bt \qquad (5)$$

where *B* is the effective rate of release, *D* the diffusion coefficient, *r* the radius of the resin particle and *t* the respective experiment time.

Observed linear dependences of $-ln\ (1-F^2)$ versus time verify that the mechanism through which ion exchange process takes place, in both gel or macroporous type ion exchangers, is controlled by intraparticle diffusion. Some results of data treatment are shown in Figures 7a-d. Results obtained from experiments carried out at higher temperature (310 K) were also correspondingly treated. The effective rates of release, *B*, calculated according to equation 5 are presented in Tables 2 and 3. As can be appreciated in the collected data, the effective diffusion rates increase when particle size decreases, this is in accordance with the results shown in Figures 1a-d. Differences in diffusivity between both ions are also confirmed whatever polymeric structure is studied. On the other hand, differences between effective rates of the ions release and the polymeric matrix structure are not appreciated because the model only include data obtained at the beginning of the experiments. On the contrary, a comparison of the rate of Ca^{2+} and F^- release from gel and macroporous ion exchangers (Figures 8a-b) reveals some appreciable and advantageous difference towards macroporous matrix, mainly

when long periods of time are considered. A single macroporous ion exchange particle may be viewed as a cluster of tiny microgels with an interconnected network of pores which provide a greater effective surface area due to the larger pore volumes.[27] The same conclusions can be drawn at 310 K.

When comparing the results obtained from the –log (B) dependence with particle size at 273 and 310 K (Figures 9a-d), it is observed that at both temperatures there is a good linear correlation. This correlation will enable to predict the behaviour of Ca^{2+} and F^-, under the conditions studied, for resin fractions under 100 microns; otherwise discontinuous conditions (batch) should be applied. Batch conditions are especially interesting for particle size resins lower than 100 microns due to the high hydrodynamic resistance existing when working under dynamic conditions using the "shallow bed" technique. However, the small acceleration promoted by the increase of temperature can not be quantitatively appreciated with the model applied.

3.3.2. Batch conditions

T.R.E. Kressman and J. A. Kitchener[28] deduced the following equation for ion exchange processes under batch experimental conditions:

$$\frac{Q_t}{Q_\infty} = \frac{6}{r}\frac{Q_0}{Q_0 - Q_\infty}\sqrt{\frac{Dt}{\pi}} \qquad (6)$$

where Q_0 is the total quantity of ions initially immobilized in the resin phase, Q_∞ is the quantity of ions released from the resin phase at equilibrium time, Q_t is the quantity of ions released from the resin phase till the moment t, r the resin particle radius, D the diffusion coefficient of the ion through the ion exchanger and, t time. The diffusion coefficient can be related with the effective rate of release B, by the equation:

$$B = \frac{D\pi^2}{r^2} \qquad (7)$$

where r and t are the resin particle radius and time respectively.

By plotting Q_t/Q_∞ versus $t^{1/2}$, diffusion coefficients will be determined and effective rates of release calculated with equation 7. In Figures 10a-h examples of the treatment of data from Figures 2a-d by the model described above are shown. The model fits correctly the data from different particle sizes; however, two different behaviours can be distinguished mainly in fractions of higher diameter. Swelling of resin particles

produced at the beginning of the experiments causes this effect. A much higher surface/volume ratio in small particle sizes results in a faster hydration process. This different behaviour was not observed in the study under dynamic experimental conditions discussed above because, in this case, before each experiment the resin was kept in water for an hour to prevent the cracking of the column due to swelling effect. Once swelling has taken place, a considerable increase in the rate of release is appreciated.

Taking into account this last consideration, linearity attained with all particle sizes, temperatures and ion exchangers structures (plots with a correlation coefficient, r^2, always higher than 0.9), suggests that the ions diffusion is controlled by a intraparticle diffusion process.

Results obtained from data treatment with equations 6 and 7, are shown in Tables 4 and 5.

Similar conclusions to those obtained from the corresponding dynamic conditions can be drawn now. An inversely proportional relationship between particle size and the rate of ions release is once again reflected in the obtained results. Differences between effective rates of the ions release and the polymeric matrix structure are hardly appreciated in the case of Ca^{2+} whereas, for F^- there is more variability. This will affect the correlation of –log (B) versus particle size which is presented in Figures 11a-d. Indeed, only in the case of cationic ion exchangers, linear plots with a correlation coefficient r^2 higher than 0.9 are obtained. Again, the model described does not let to quantify neither the effect of temperature nor the differences between ion exchange structures, despite Figures 12a-b, show considerable higher rates of ions release for macroporous type ion exchangers.

Finally, it is remarkable that Ca^{2+} presents effective rates of release of the same order of magnitude for both dynamic and batch conditions. In the latter case Ca^{2+} shows higher rates of release than F^- that presented effective rates of release two orders of magnitude higher under the corresponding dynamic conditions. It has been reported[13] than when samples prepared for sustained release delivery system are loaded at higher temperatures, they show slower release profiles, this is probably due to the swelling of the resin particles as a result of both thermal and hydration effects produced as temperature increases. An increase in the pore diameter provides access to centers of ionic activity deep within the resin structure, and as temperature drops on cooling, resin

particles shrink and trap the drug within the matrix, leading to increased drug loading and reduced release profiles. After the loading process resins in fluoride form were not submitted to an excessively high temperature in the drying process, so this effect must be explained in terms of operation of the system itself. Under batch conditions with resins of low kinetics release, all ions initially immobilized in the resin phase can rarely be released from the polymeric matrix because an equilibrium situation with bulk solution surrounding the ion exchanger is achieved. In the case of high kinetics release resins, although ions are quickly released to the bulk solution and equilibrium is immediately achieved, saturation of the solution in the releasing ion can delay the initial rate of release. Under dynamic conditions though, the desorbing solution passing through the resin bed is free of counterions to be released, so higher conversion degrees are obtained.

4. Conclusions

1- Differences in the rate of Ca^{2+} and F^- release from the corresponding strong type polymeric matrices can be explained in terms of relative affinity of the functional group immobilized in the resin phase towards the ions present in the solution. Besides, the rate of ions release increases when temperature increases and when particle size decreases.

2- Macroporous ion exchangers show a higher rate of ions release than gel type resins due to the larger pore volumes resulting in a greater effective surface area.

3- Results from the study of the kinetics of release of Ca^{2+} and F^- under either dynamic or batch conditions are explained by the models described valid for intraparticle diffusion controlled processes.

4- The rate of ions release from the strong ion exchange resins studied are quantitatively described in terms of effective rate of release (B) of the respective ions in the resin phase. Under dynamic conditions, the linear dependence of –log (B) with the resin particles diameter can be used for the estimation of B values in powdered resins. Under batch conditions, despite powdered resins can be studied a linear relationship was also obtained. However, differences observed in kinetics release curves due to the type of polymeric matrix and temperature effects are not reflected in the corresponding effective rates of release.

Acknowledgements

A. T. acknowledges the Universitat Autònoma de Barcelona for the FI Research Grant to support her research studies. DCA, S.L. (Barcelona, Spain) is acknowledged for the financial support provided to this study.

REFERENCES

1 CHAUDHRY, N.C.; SAUNDERS, L. *J. Pharm. Pharmacol.*, **1956**, 8, 975-986.

2 SCHLICHTING, D.A. *J. Pharm. Sci*., **1962**, 51, 134-136.

3 DORFNER, K.: *Ion Exchangers*, DORFNER, K. (ed.); Walter der Gruyter Publisher: Berlín, 1991, p.1-5.

4 ISHIZAKA, T.; ENDO, K.; KOISHI, M. *J. Pharm. Sci*., **1981**, 70, 358-363.

5 GARCÍA-ENCINA, G.; TORRES, D.; SEIJO, B.; VILA JATO, J.L. *J. Controlled Release*, **1993**, 23, 201-207.

6 SOPPIMATH, K. S. et al. *J. Controlled Release*, **2001**, 70, 1-20.

7 PESCHKA, R.; DENNEHY, C.; SZOKA, F.C. Jr. *J. Controlled Release*, **1998**, 56, 41-51.

8 BORODKIN, S.; SUNDBERG, D. P. *J. Pharm. Sci.*, **1971**, 60, 1523-1527.

9 HELFFERICH, F. *Ion Exchange*, Dover Publications, Inc., New York, 1995, p.250-322.

10 BHASKAR, R.; MURTHY, R.S.R.; MIGLANI, B.D.; VISWANATHAN, K. *Int. J. Pharm.*, **1986**, 28, 59-66.

11 PETRUZZELLI, D.; HELFFERICH, F.G.; LIBERTI, L.; MILLAR, J.R.; PASSINO, R. *React. Polym.*, **1987**, **7**, 1-13.

12 PLAIZIER-VERCAMMEN, J.A. *Int. J. Pharm.*, **1992**, 87, 31-36.

13 MOHAMED, F.A. *S.T.P. Pharm. Sci.*, **1996**, 6(6), 410-416.

14 JASKARI, T. et al. *J. Controlled Release*, **2001**, 70, 219-229.

15 CONAGHEY, O.M.; CORISH, J.; CORRIGAN, O.I. *Int. J Pharm.*, **1998**, 170, 215-224.

16 DORFNER, K.: *Ion Exchangers*, DORFNER, K. (ed.); Walter der Gruyter Publisher: Berlín, 1991, p.128.

17 DORFNER, K.: *Ion Exchangers*, DORFNER, K. (ed.); Walter der Gruyter Publisher: Berlín, 1991, p.328.

18 DORFNER, K.: *Ion Exchangers*, DORFNER, K. (ed.); Walter der Gruyter Publisher: Berlín, 1991, p.94.

19 DORFNER, K.: *Ion Exchangers*, DORFNER, K. (ed.); Walter der Gruyter Publisher: Berlín, 1991, p.126.

20 OANCEA, A.M.S.; PINCOVSCHI, E. *Solv. Extr. & Ion Exch.*, **2000**, 18(5), 981-1000.

21 MURAVIEV, D.; TORRADO, A.; VALIENTE, M. *Solv. Extr. & Ion Exch.*, **2000**, 18(2), 345-374.

22 JASKARI, T. et al. *J Controlled Release*, **2001**, 70, 219-229.

23 BRICCIO, O.; COCCA, J.; SASTRE, H. *Solv. Extr. & Ion Exch.*, **1992**, 10(2), 381-401.

24 BOYD, G.E.; ADAMSON, A.W.; MYERS, L.S. Jr. *J. Am. Chem. Soc.*, **1947**, 69, 2836-2848.

25 LI, P.; SENGUPTA, A.K. *React. & Func. Polym.*, **2000**, 44, 273-287.

26 STREAT, M.; NADEN, D.: *Ion Exchange and Sortion Processes in Hidrometallurgy. Critical Reports on Applied Chemistry*, Vol. 19; STREAT, M.; NADEN, D. (eds.); John Willey & Sons: Chichester, 1987, p.1.

27 DELAYETTE-MILLS, M et al. *An. Chim. Acta*, **1981**, 124, 365-372.

28 KRESSMAN, T.R.E.; KITCHENER, J.A. *Disc. Faraday Soc.*, **1949**, 7, 90-104.

CAPTIONS AND LEGENDS

Table 1. Specific capacity of the resins towards Ca^{2+} and F^-.

Table 2. Effective rates of release of Ca^{2+} and F^- in the macroporous type resin phase at 293K under dynamic conditions.

Table 3. Effective rates of release of Ca^{2+} and F^- in the gel type resin phase at 293K under dynamic conditions.

Table 4. Effective rates of release of Ca^{2+} and F^- in the macroporous type resin phase at 293K under batch conditions.

Table 5. Effective rates of release of Ca^{2+} and F^- in the gel type resin phase at 293K under batch conditions.

Figure 1 Kinetics release of resin samples of different particle size under dynamic conditions at 293K. **(a)** Lewatit SP112WS in Ca^{2+}-form **(b)** Lewatit MP600 in F^--form. **(c)** Lewatit S100 in Ca^{2+}-form **(d)** Lewatit M600 in F^--form.

Figure 2 Kinetics release of resin samples of different particle size under batch conditions at 293K **(a)** Lewatit SP112WS in Ca^{2+}-form **(b)** Lewatit MP600 in F^--form **(c)** Lewatit S100 in Ca^{2+}-form **(d)** Lewatit M600 in F^--form.

Figure 3 Kinetics release of resin samples of different particle size under dynamic conditions at 293 and 310K. **(a)** Lewatit SP112WS in Ca^{2+}-form **(b)** Lewatit MP600 in F^--form **(c)** Lewatit S100 in Ca^{2+}-form **(d)** Lewatit M600 in F^--form

Figure 4 Kinetics release of resin samples of different particle size under batch conditions at 293 and 310K **(a)** Lewatit SP112WS in Ca^{2+}-form **(b)** Lewatit MP600 in F^--form **(c)** Lewatit S100 in Ca^{2+}-form **(d)** Lewatit M600 in F^--form.

Figure 5 Agitation effect on the kinetics release of resin samples of different particle size under batch conditions at 293K. **(a)** Lewatit SP112WS in Ca^{2+}-form **(b)** Lewatit MP600 in F^--form.

Figure 6 Agitation effect on Kinetics release of resin samples of different particle size under batch conditions at 310K. **(a)** Lewatit S100 in Ca^{2+}-form **(b)** Lewatit M600 in F^--form.

Figure 7 Data treatment of resin samples of particle sizes 0.42 and 0.105 mm with dynamic model (293K). **(a)** Ion exchange system $Ca^{2+}\leftrightarrow Na^{+}/K^{+}$: Lewatit SP112WS **(b)** Ion exchange system $F^{-}\leftrightarrow Cl^{-}$: Lewatit MP600 in F^{-}-form **(c)** Ion exchange system $Ca^{2+}\leftrightarrow Na^{+}/K^{+}$: Lewatit S100 in Ca^{2+}-form **(d)** Ion exchange system $F^{-}\leftrightarrow Cl^{-}$: Lewatit M600 in F^{-}-form.

Figure 8 Kinetics release of resin samples of particle sizes of 0.42 and 0.105mm, under dynamic conditions at 293K **(a)** Lewatit SP112WS and S100 in Ca^{2+}-form **(b)** Lewatit MP600 and M600 in F^{-}-form.

Figure 9 Dependence of –log (B) with resin particle size under dynamic conditions at 293 and 310K. **(a)** Lewatit SP112WS in Ca^{2+}-form **(b)** Lewatit MP600 in F^{-}-form. **(c)** Lewatit S100 in Ca^{2+}-form **(d)** Lewatit M600 in F^{-}-form.

Figure 10 Data treatment of resin samples with batch model (293K and 310K). **(a)** Ion exchange system $Ca^{2+}\leftrightarrow Na^{+}/K^{+}$: Lewatit SP112WS in Ca^{2+}-form of particle size 0.42 mm **(b)** Ion exchange system $Ca^{2+}\leftrightarrow Na^{+}/K^{+}$: Lewatit SP112WS in Ca^{2+}-form of particle sizes 0.105 mm **(c)** Ion exchange system $F^{-}\leftrightarrow Cl^{-}$: Lewatit MP600 in F^{-}-form of particle size 0.42mm **(d)** Ion exchange system $F^{-}\leftrightarrow Cl^{-}$: Lewatit MP600 in F^{-}-form of particle size 0.105mm. **(e)** Ion exchange system $Ca^{2+}\leftrightarrow Na^{+}/K^{+}$: Lewatit S100 in Ca^{2+}-form of particle size 0.42 mm **(f)** Ion exchange system $Ca^{2+}\leftrightarrow Na^{+}/K^{+}$: Lewatit S100 in Ca^{2+}-form of particle size 0.105 mm **(g)** Ion exchange system $F^{-}\leftrightarrow Cl^{-}$: Lewatit M600 in F^{-}-form of particle size 0.42mm **(h)** Ion exchange system $F^{-}\leftrightarrow Cl^{-}$: Lewatit M600 in F^{-}-form of particle size 0.105mm.

Figure 11 Dependence of –log (B) with resin particle size in size under batch conditions at 293 and 310K. **(a)** Lewatit SP112WS in Ca^{2+}-form **(b)** Lewatit MP600 in F^{-}-form **(c)** Lewatit S100 in Ca^{2+}-form **(d)** Lewatit M600 in F^{-}-form.

Figure 12 Kinetics release of resin samples of particle sizes of 0.42 and 0.105mm under batch conditions at 293K. **(a)** Lewatit SP112WS and S100 in Ca^{2+}-form **(b)** Lewatit MP600 and M600 in F^{-}-form.

Table 1

	Capacity (mmol g^{-1})	
	Ca^{2+}	**F^-**
Lewatit S100	1.75± 0.03	-
Lewatit S112WS	1.47± 0.01	-
Lewatit M600	-	2.84±0.05
Lewatit MP600	-	2.33±0.08

Table 2

	B (s^{-1})	
Particle diameter (mm)	**B (Ca^{2+}) x 10^4**	**B (F^-) x 10^3**
0.42	1.0	3.3
0.335	1.0	7.1
0.205	2.5	13
0.105	4.0	17

Table 3

	B (s^{-1})	
Particle diameter (mm)	**B (Ca^{2+}) x 10^4**	**B (F^-) x 10^3**
0.42	0.5	5.7
0.335	1.0	6.9
0.205	2.0	12.5
0.105	3.5	12.0

Table 4

	B (s^{-1})	
Particle diameter (mm)	**B (Ca^{2+}) x 10^4**	**B (F^-) x 10^5**
0.42	6.7	0.6
0.335	9.9	0.9
0.205	35.0	19
0.105	49	28
<0.05	130	24

Table 5

	B (s^{-1})	
Particle diameter (mm)	**B (Ca^{2+}) x 10^4**	**B (F^-) x 10^5**
0.42	4.3	5.2
0.335	17	2.6
0.205	30	15
0.105	46	17
<0.05	80	35

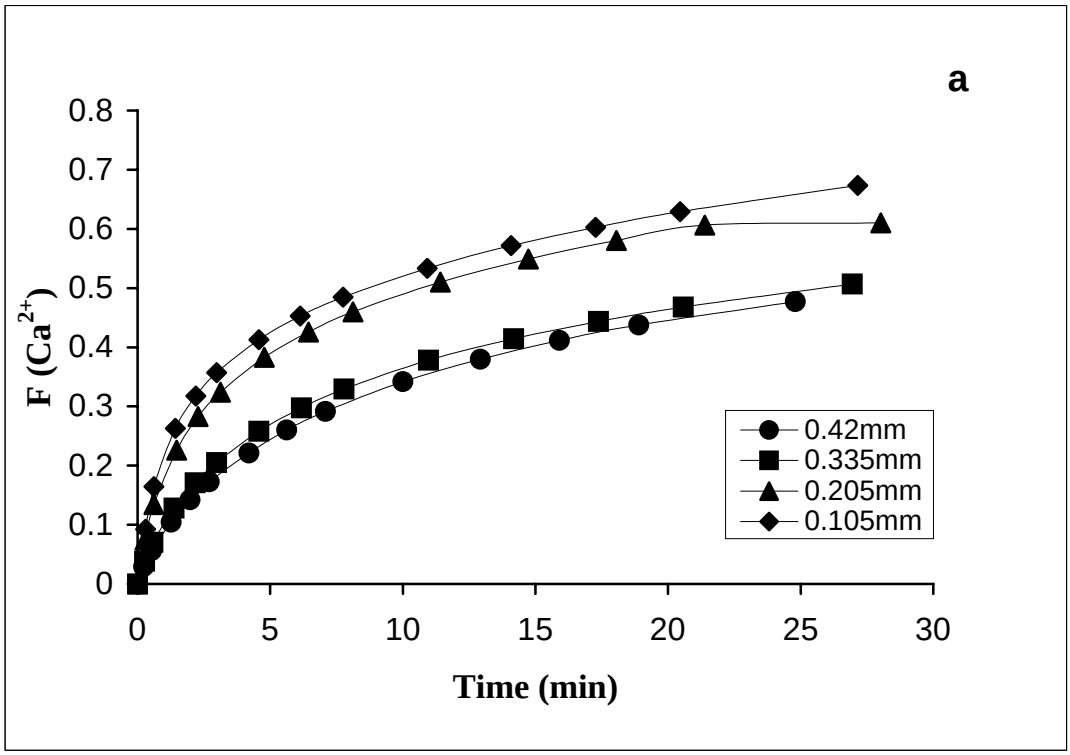
a
0.8
0.7
0.6
0.5
0.4
0.3
0.2
0.1
0
F (Ca2+)
0
5
10
15
20
25
30
Time (min)
0.42mm
0.335mm
0.205mm
0.105mm

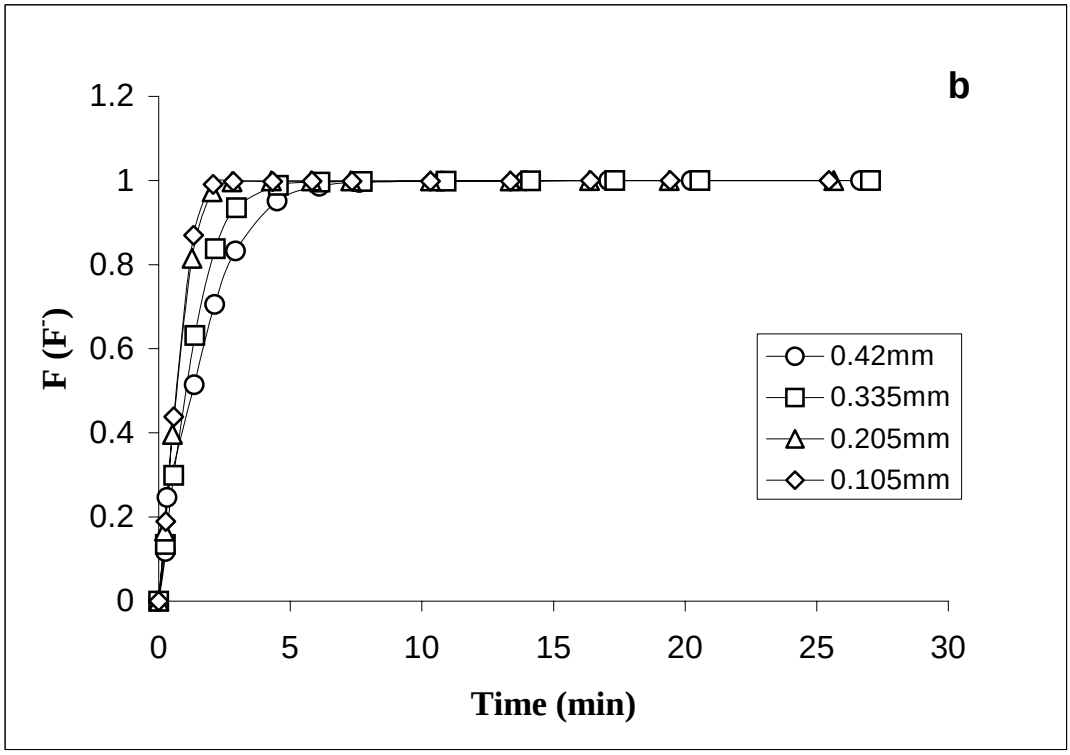
b
1.2
1
0.8
0.6
0.4
0.2
0
F (F-)
0
5
10
15
20
25
30
Time (min)
0.42mm
0.335mm
0.205mm
0.105mm

Figure 1

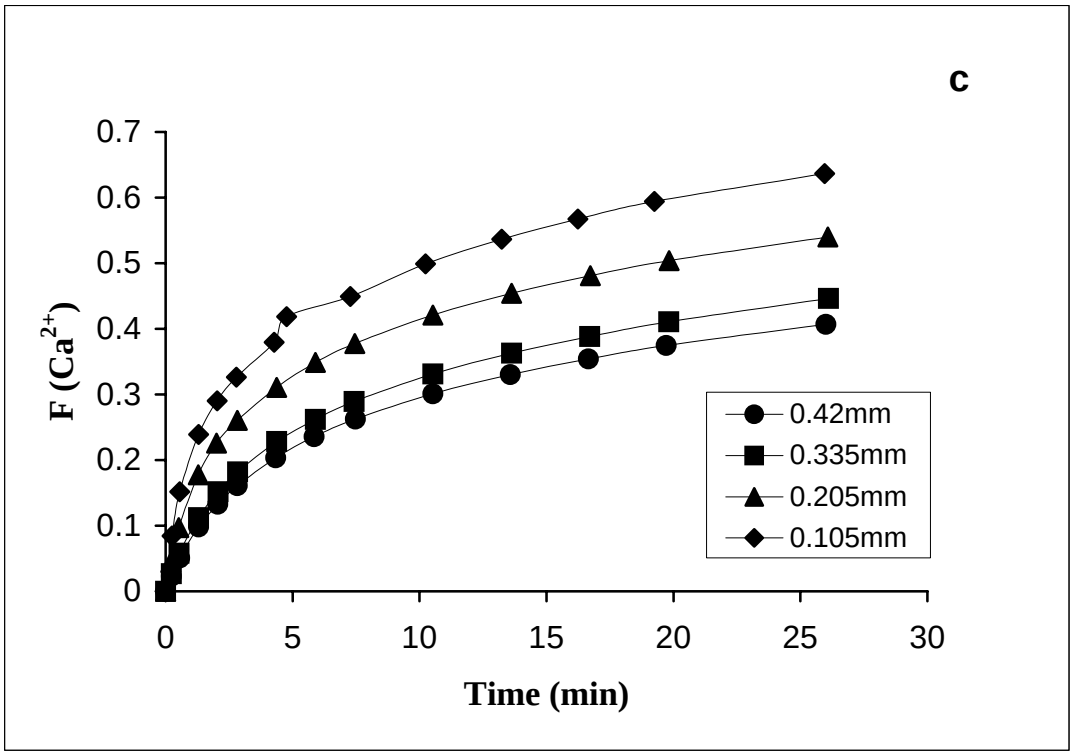
c
0.7
0.6
0.5
0.4
0.3
0.2
0.1
0
F (Ca2+)
0
5
10
15
20
25
30
Time (min)
0.42mm
0.335mm
0.205mm
0.105mm

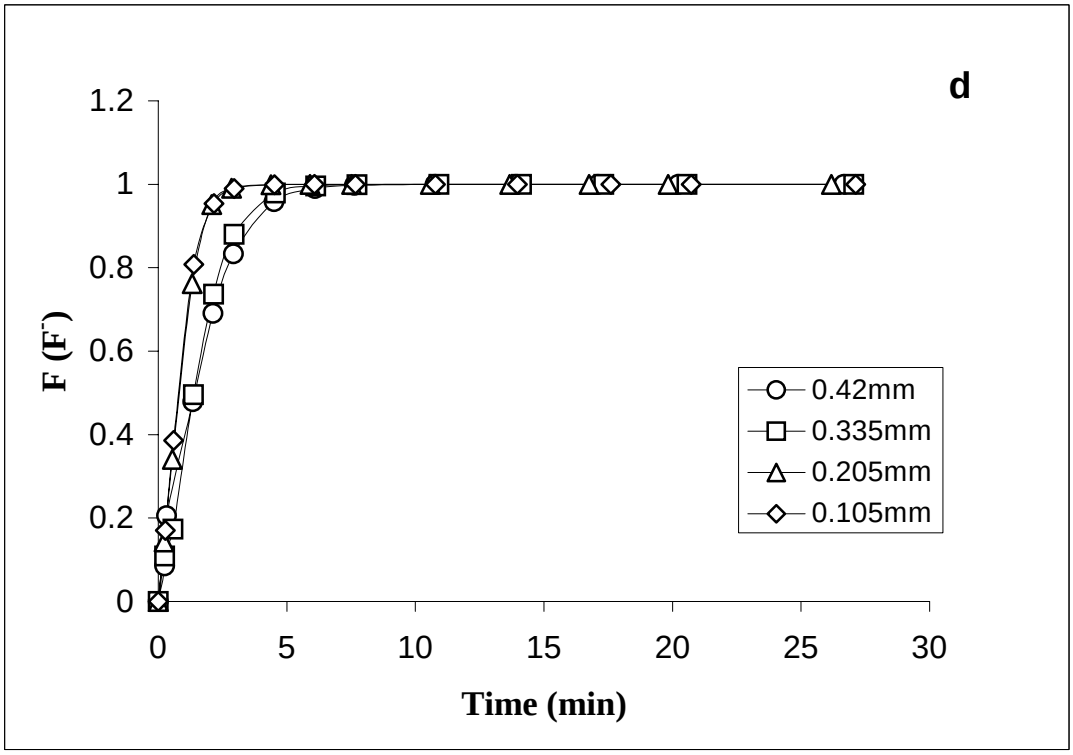
d
1.2
1
0.8
0.6
0.4
0.2
0
F (F-)
0
5
10
15
20
25
30
Time (min)
0.42mm
0.335mm
0.205mm
0.105mm

Figure 1

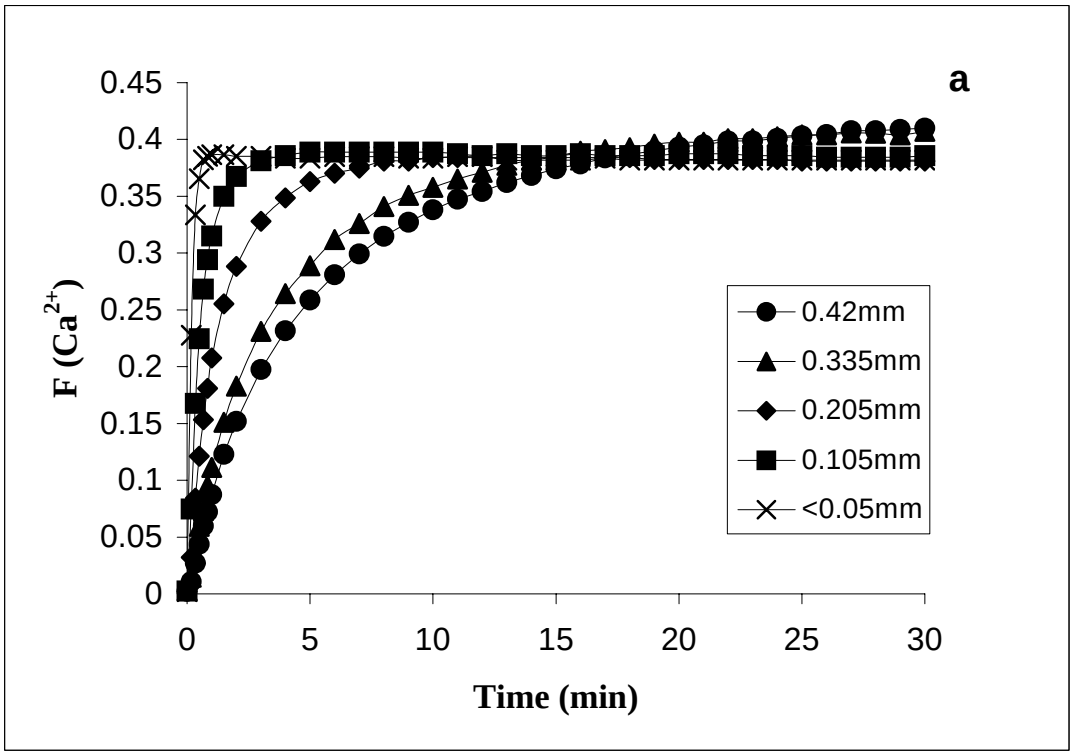
a
0.45
0.4
0.35
0.3
0.25
0.2
0.15
0.1
0.05
0
F (Ca2+)
0
5
10
15
20
25
30
Time (min)
0.42mm
0.335mm
0.205mm
0.105mm
<0.05mm

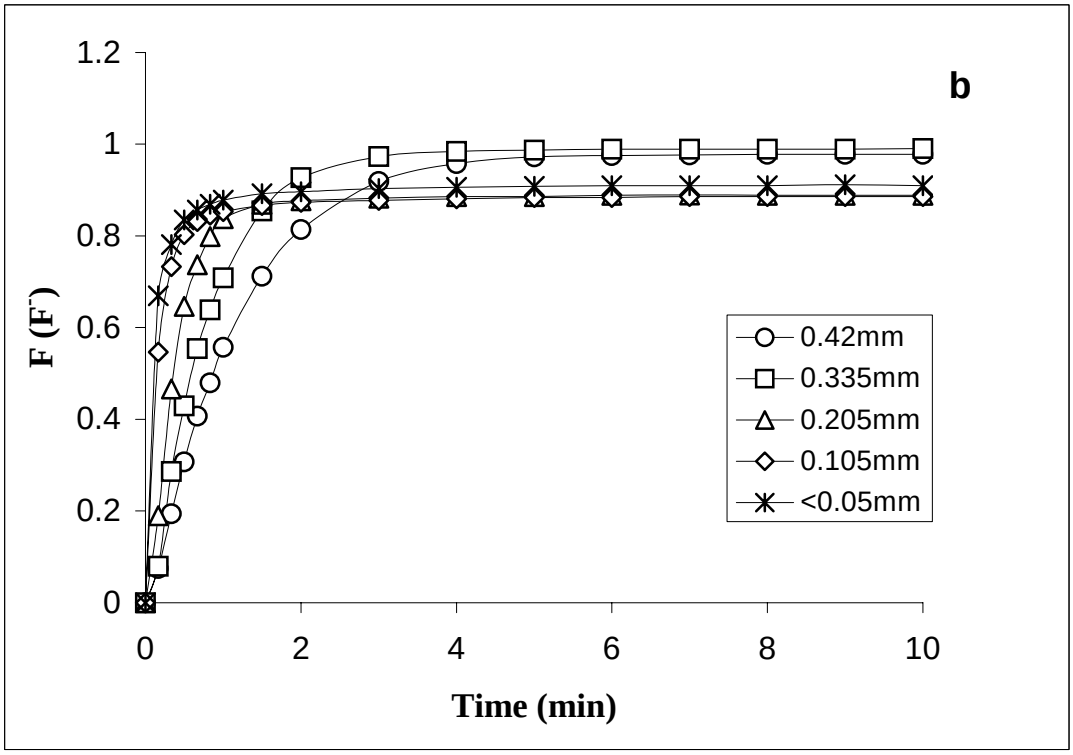
b
1.2
1
0.8
0.6
0.4
0.2
0
F (F-)
0
2
4
6
8
10
Time (min)
0.42mm
0.335mm
0.205mm
0.105mm
<0.05mm

Figure 2

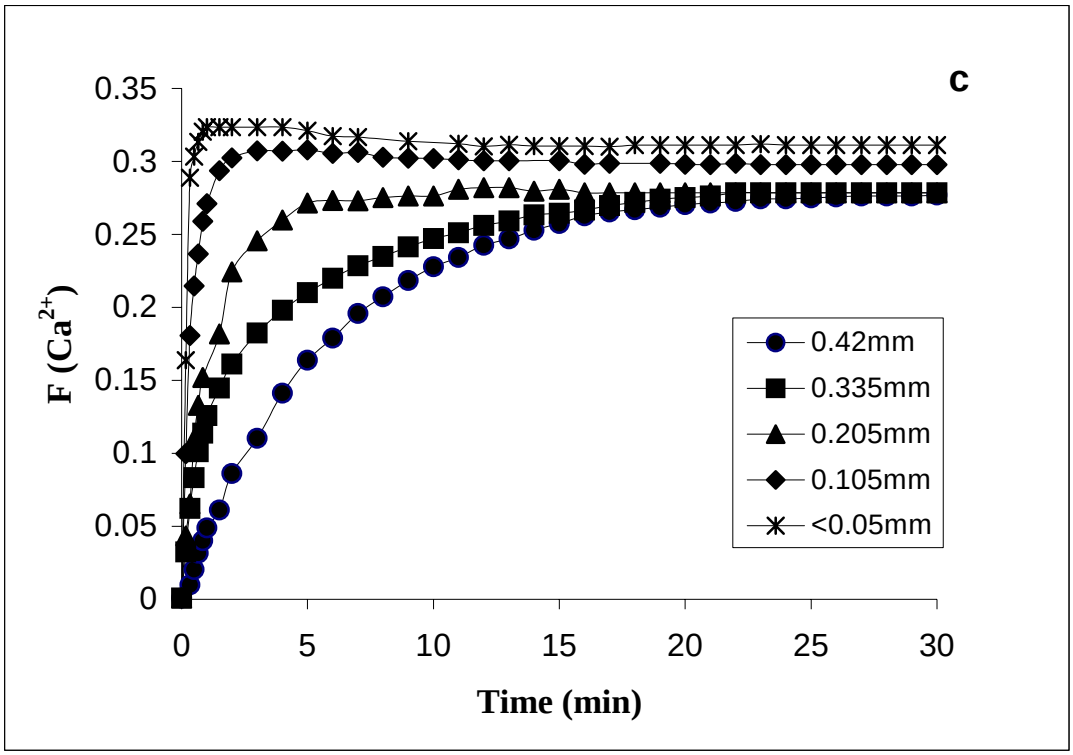
c
0.35
0.3
0.25
0.2
0.15
0.1
0.05
0
F (Ca2+)
0
5
10
15
20
25
30
Time (min)
0.42mm
0.335mm
0.205mm
0.105mm
<0.05mm

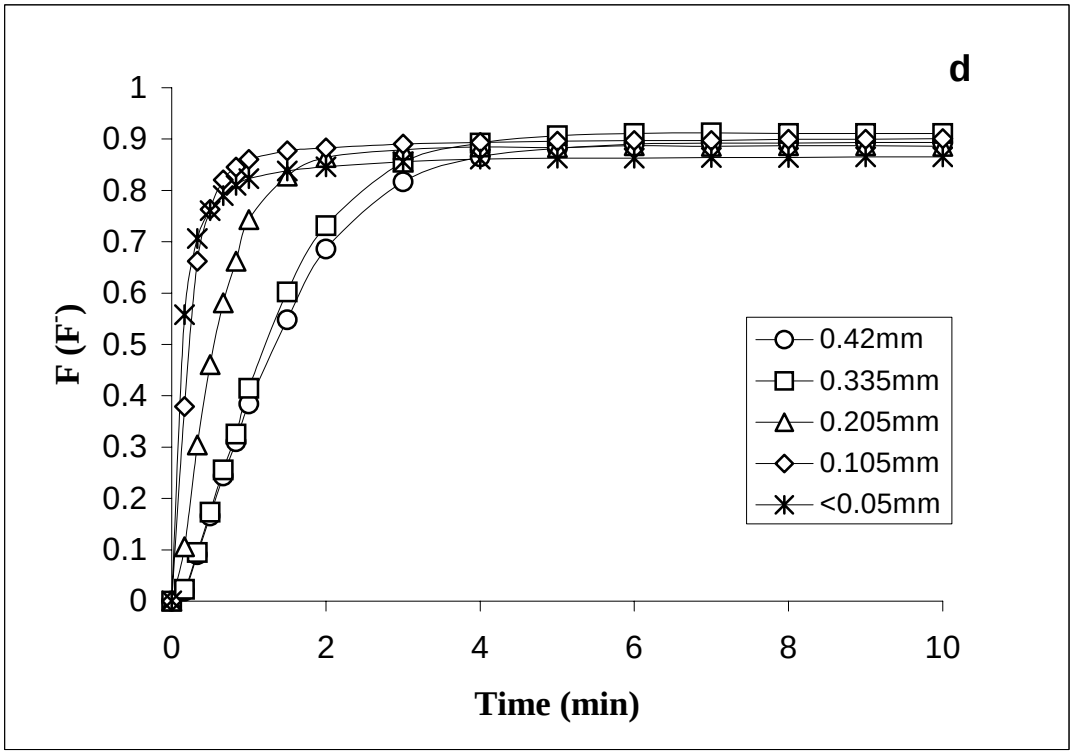
d
1
0.9
0.8
0.7
0.6
0.5
0.4
0.3
0.2
0.1
0
F (F-)
0
2
4
6
8
10
Time (min)
0.42mm
0.335mm
0.205mm
0.105mm
<0.05mm

Figure 2

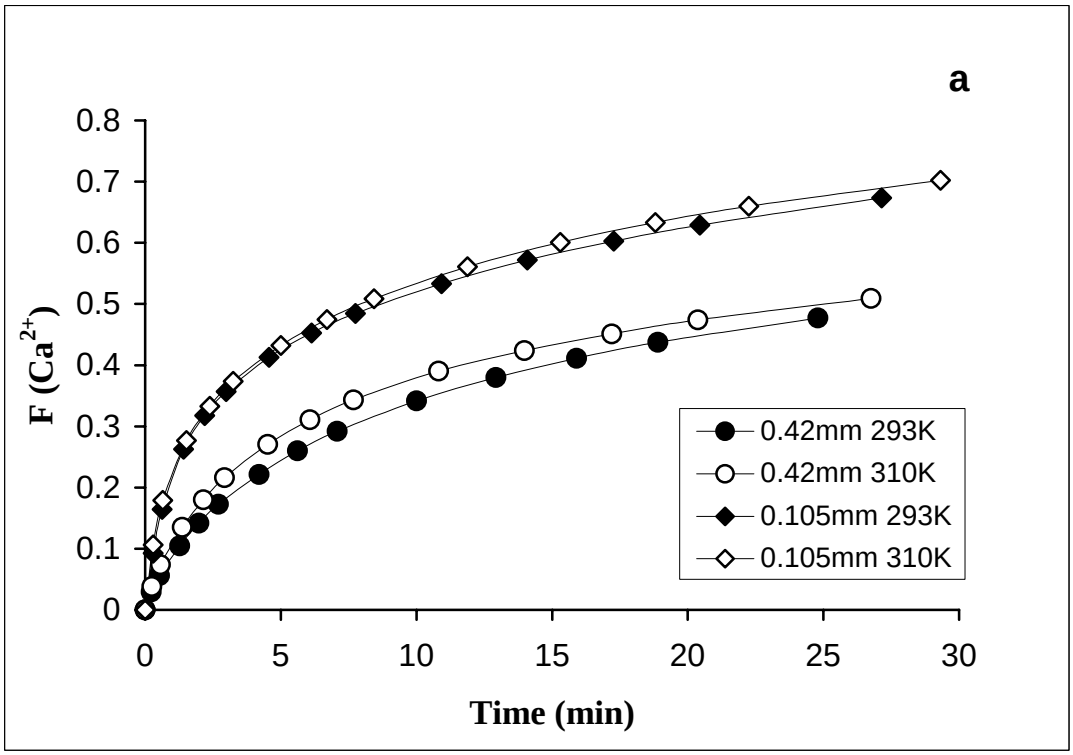
a
0.8
0.7
0.6
0.5
0.4
0.3
0.2
0.1
0
F (Ca2+)
0
5
10
15
20
25
30
Time (min)
0.42mm 293K
0.42mm 310K
0.105mm 293K
0.105mm 310K

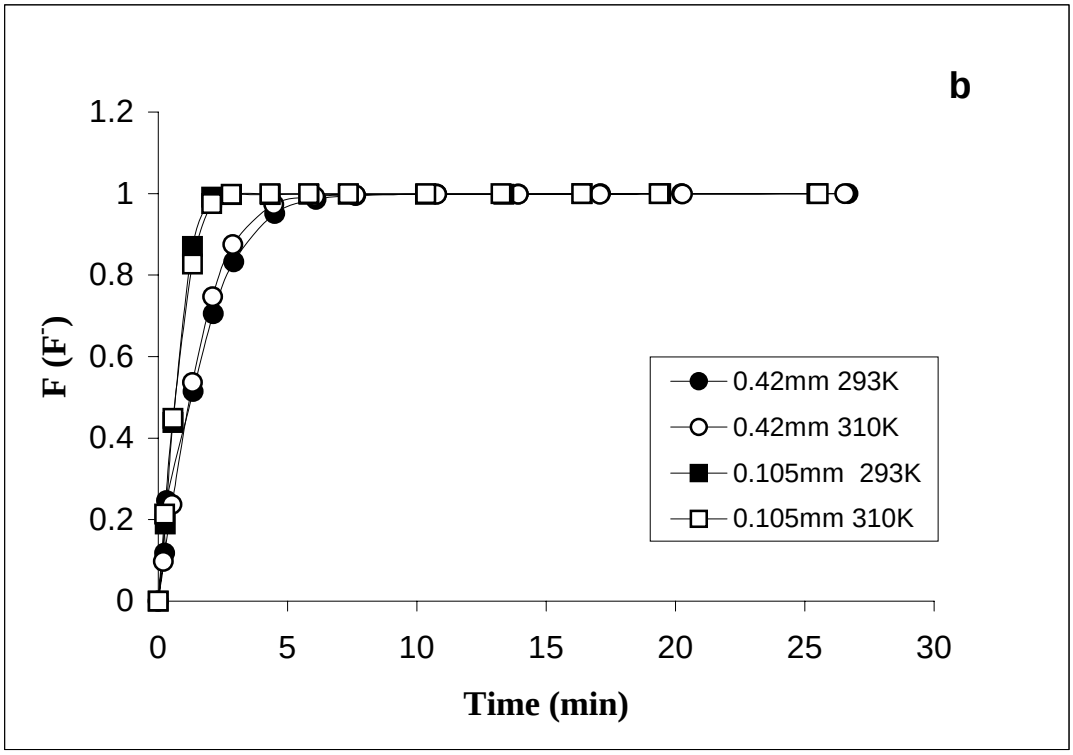
b
1.2
1
0.8
0.6
0.4
0.2
0
F (F-)
0
5
10
15
20
25
30
Time (min)
0.42mm 293K
0.42mm 310K
0.105mm 293K
0.105mm 310K

Figure 3

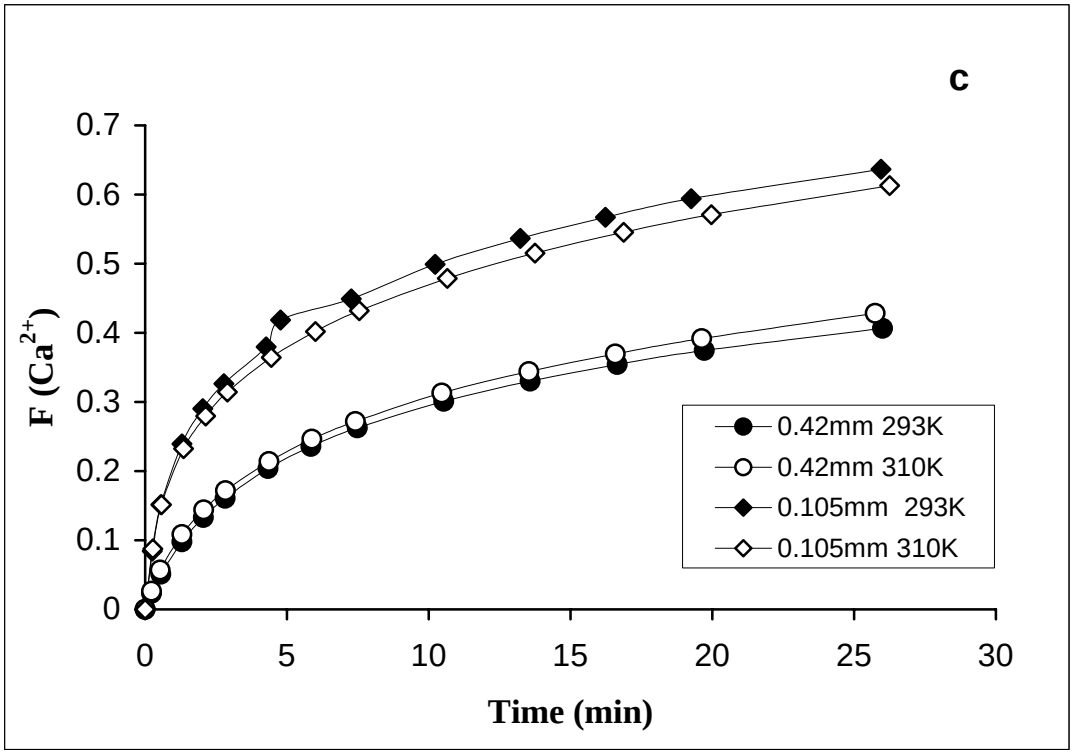
c
0.7
0.6
0.5
0.4
0.3
0.2
0.1
0
F (Ca2+)
0
5
10
15
20
25
30
Time (min)
0.42mm 293K
0.42mm 310K
0.105mm 293K
0.105mm 310K

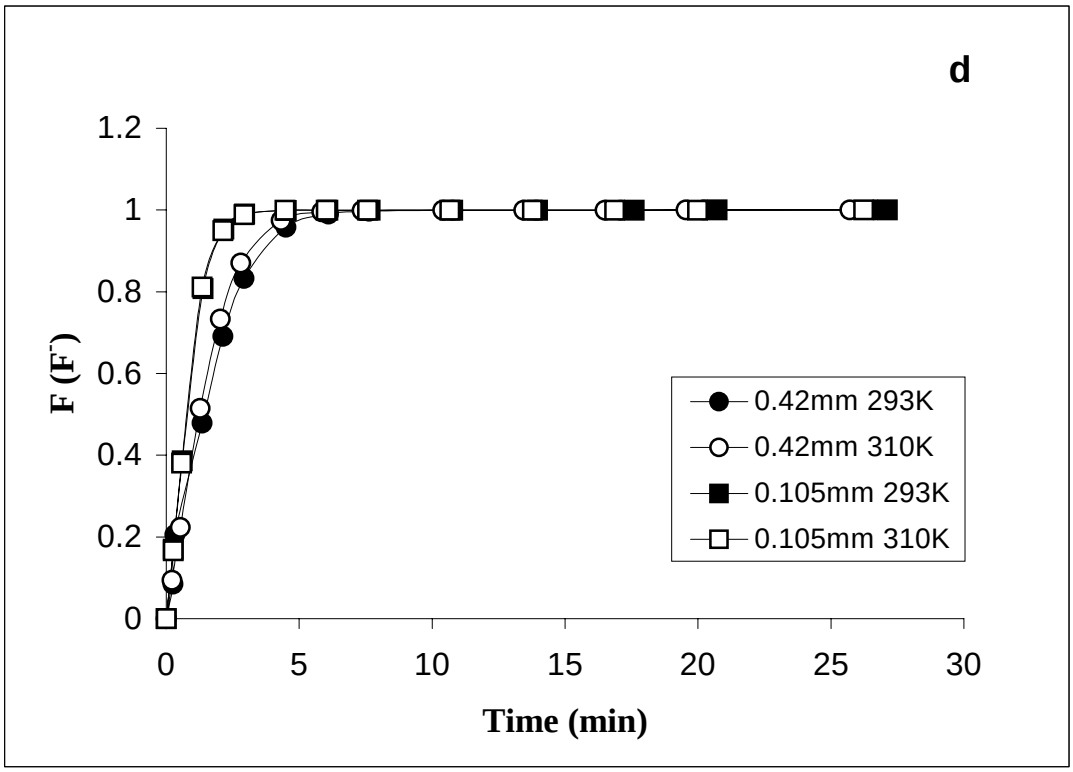
d
1.2
1
0.8
0.6
0.4
0.2
0
F (F-)
0
5
10
15
20
25
30
Time (min)
0.42mm 293K
0.42mm 310K
0.105mm 293K
0.105mm 310K

Figure 3

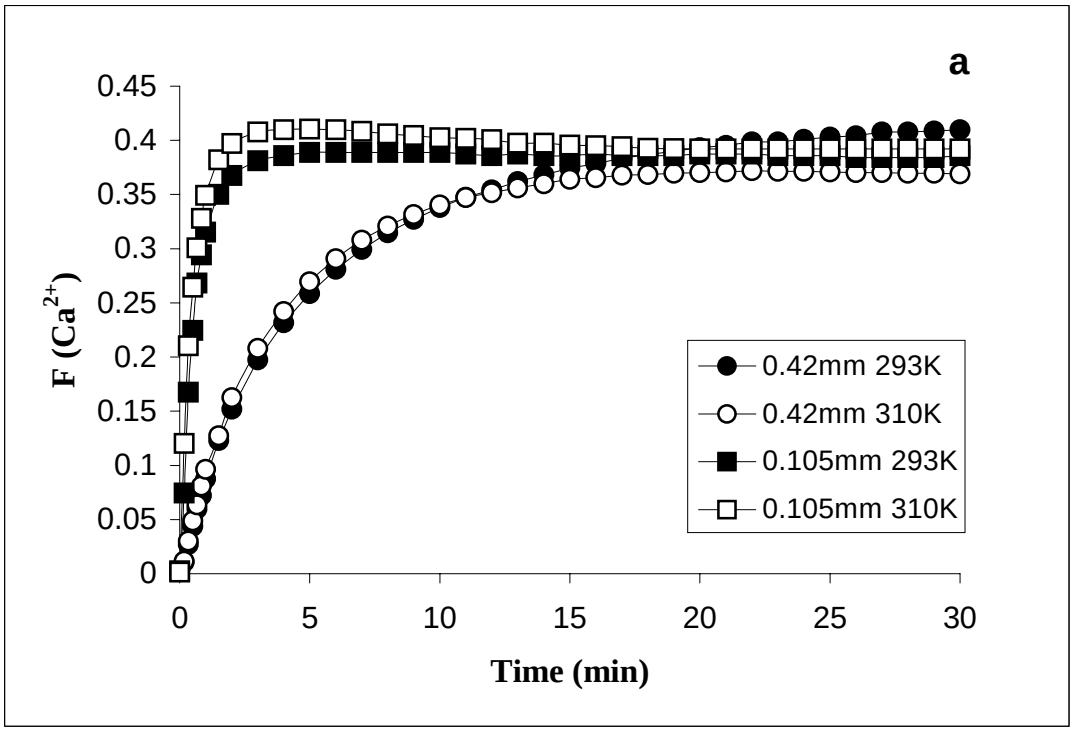
a
0.45
0.4
0.35
0.3
0.25
0.2
0.15
0.1
0.05
0
F (Ca2+)
0
5
10
15
20
25
30
Time (min)
0.42mm 293K
0.42mm 310K
0.105mm 293K
0.105mm 310K

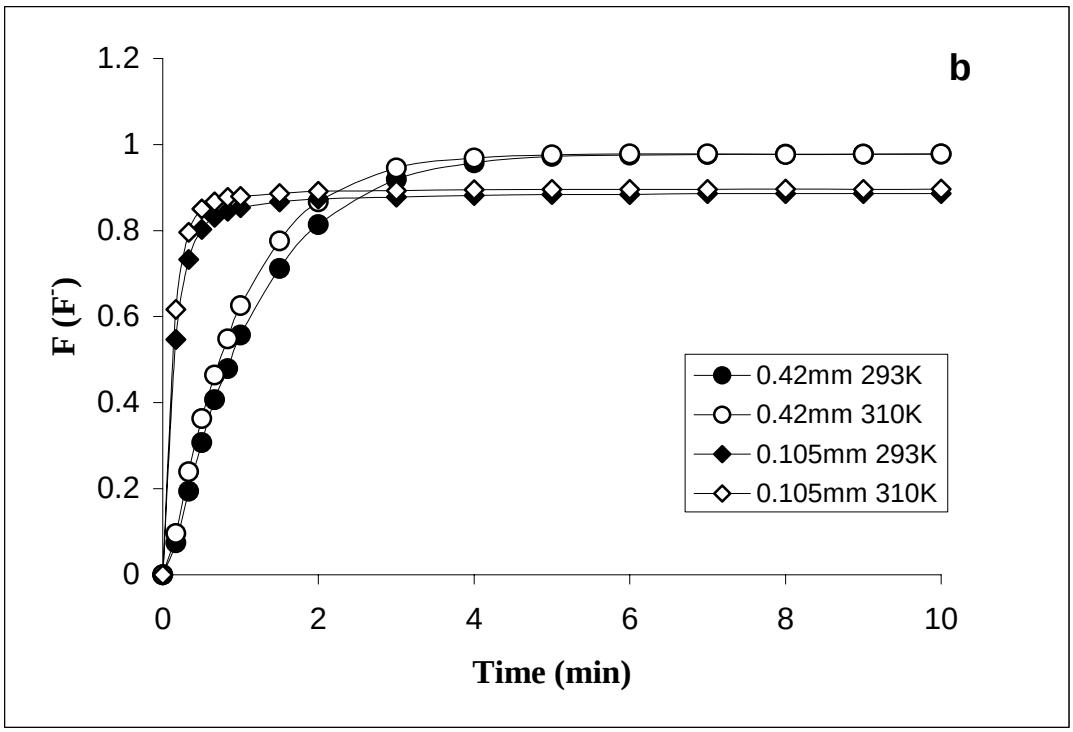
b
1.2
1
0.8
0.6
0.4
0.2
0
F (F')
0
2
4
6
8
10
Time (min)
0.42mm 293K
0.42mm 310K
0.105mm 293K
0.105mm 310K

Figure 4

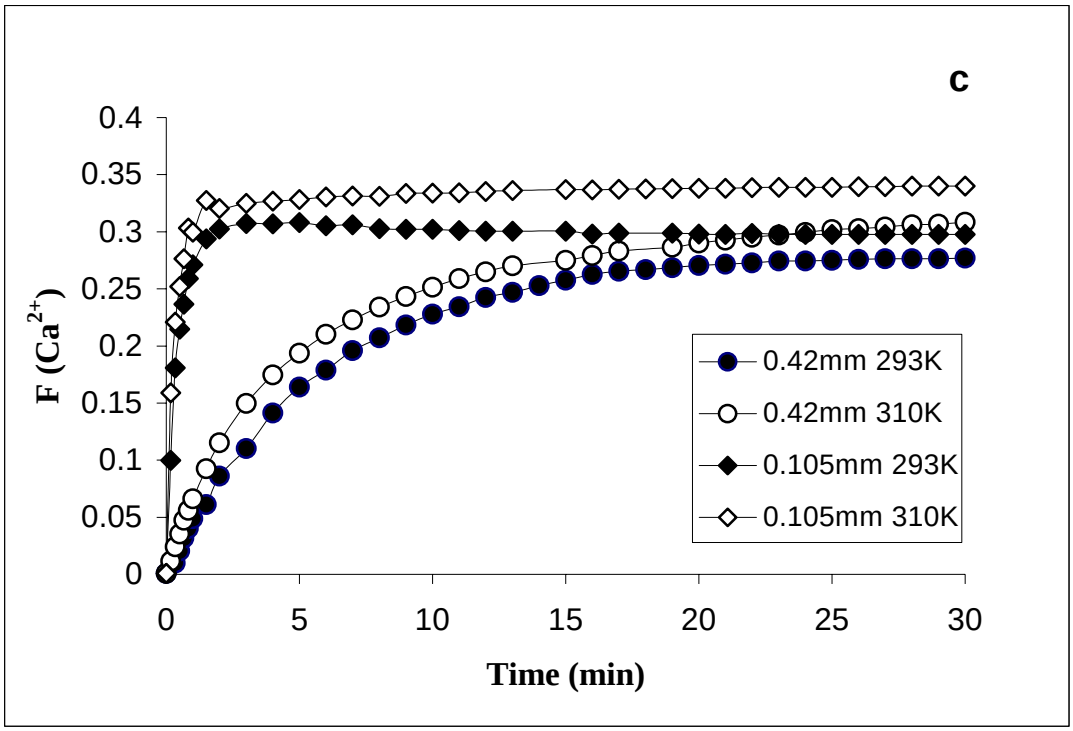
c
0.4
0.35
0.3
0.25
0.2
0.15
0.1
0.05
0
F (Ca2+)
0
5
10
15
20
25
30
Time (min)
0.42mm 293K
0.42mm 310K
0.105mm 293K
0.105mm 310K

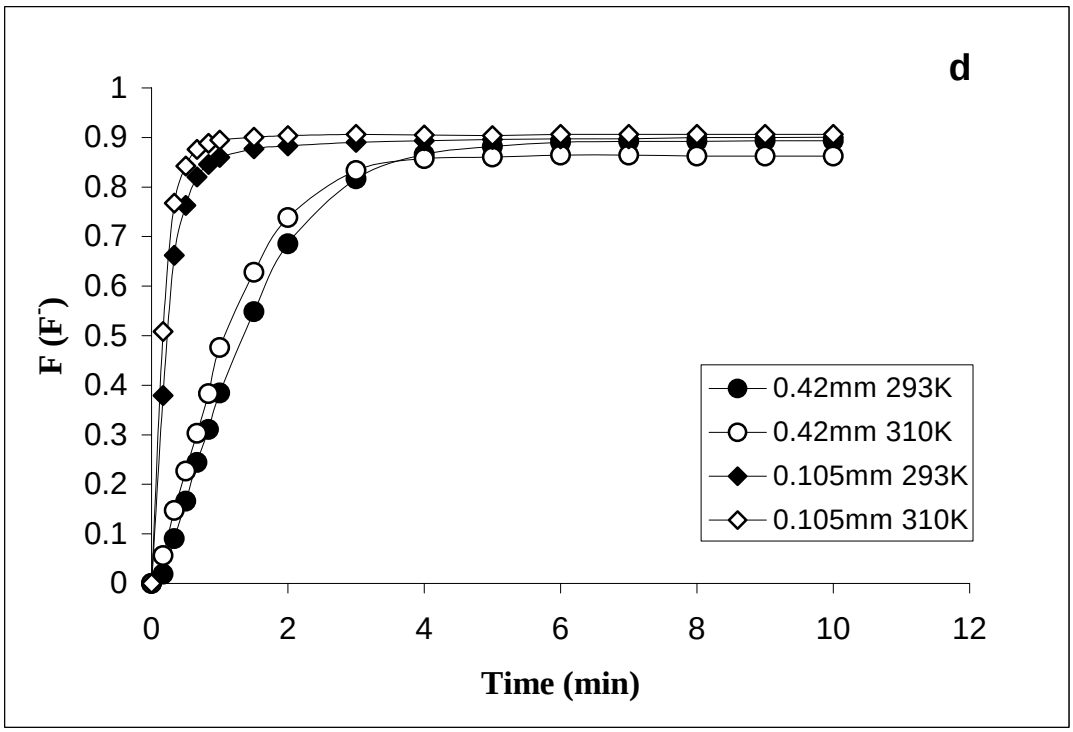
d
1
0.9
0.8
0.7
0.6
0.5
0.4
0.3
0.2
0.1
0
F (F-)
0
2
4
6
8
10
12
Time (min)
0.42mm 293K
0.42mm 310K
0.105mm 293K
0.105mm 310K

Figure 4

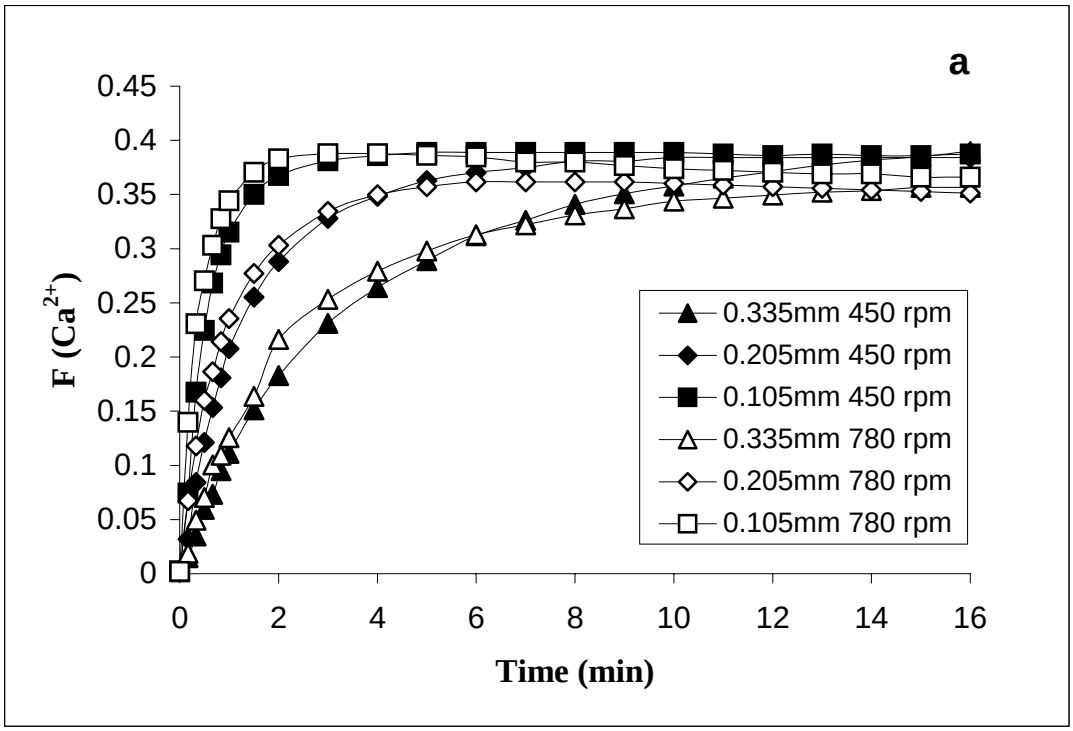
a
0.45
0.4
0.35
0.3
0.25
0.2
0.15
0.1
0.05
0
F (Ca2+)
0
2
4
6
8
10
12
14
16
Time (min)
0.335mm 450 rpm
0.205mm 450 rpm
0.105mm 450 rpm
0.335mm 780 rpm
0.205mm 780 rpm
0.105mm 780 rpm

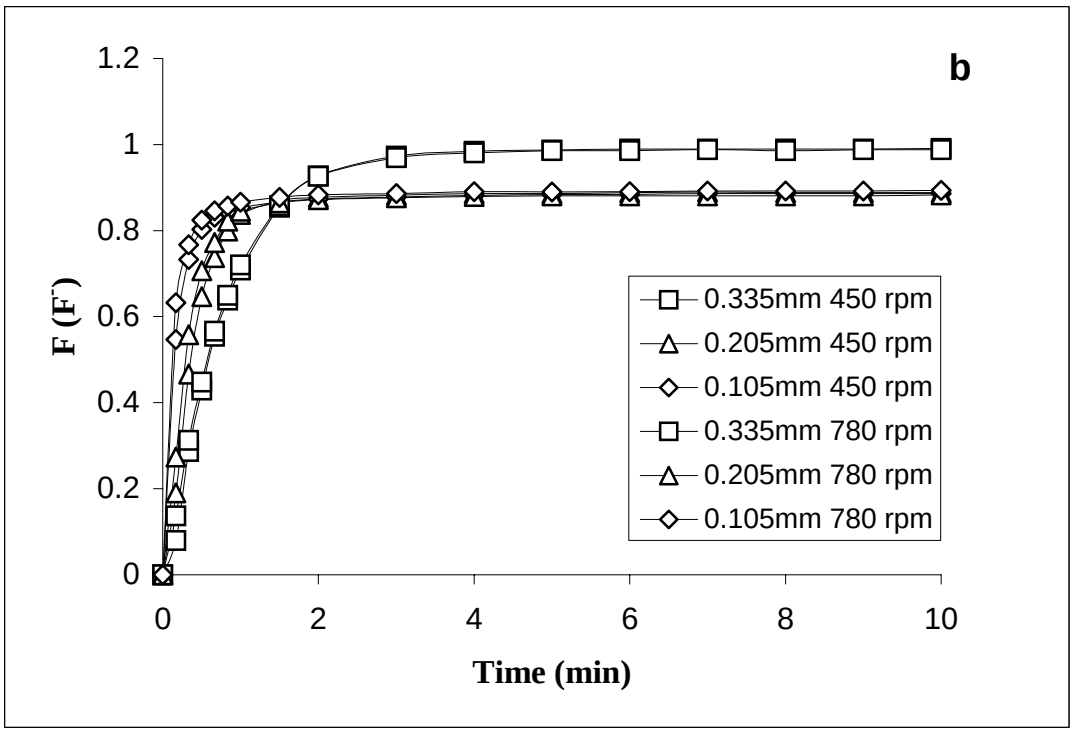
b
1.2
1
0.8
0.6
0.4
0.2
0
F (F-)
0
2
4
6
8
10
Time (min)
0.335mm 450 rpm
0.205mm 450 rpm
0.105mm 450 rpm
0.335mm 780 rpm
0.205mm 780 rpm
0.105mm 780 rpm

Figure 5

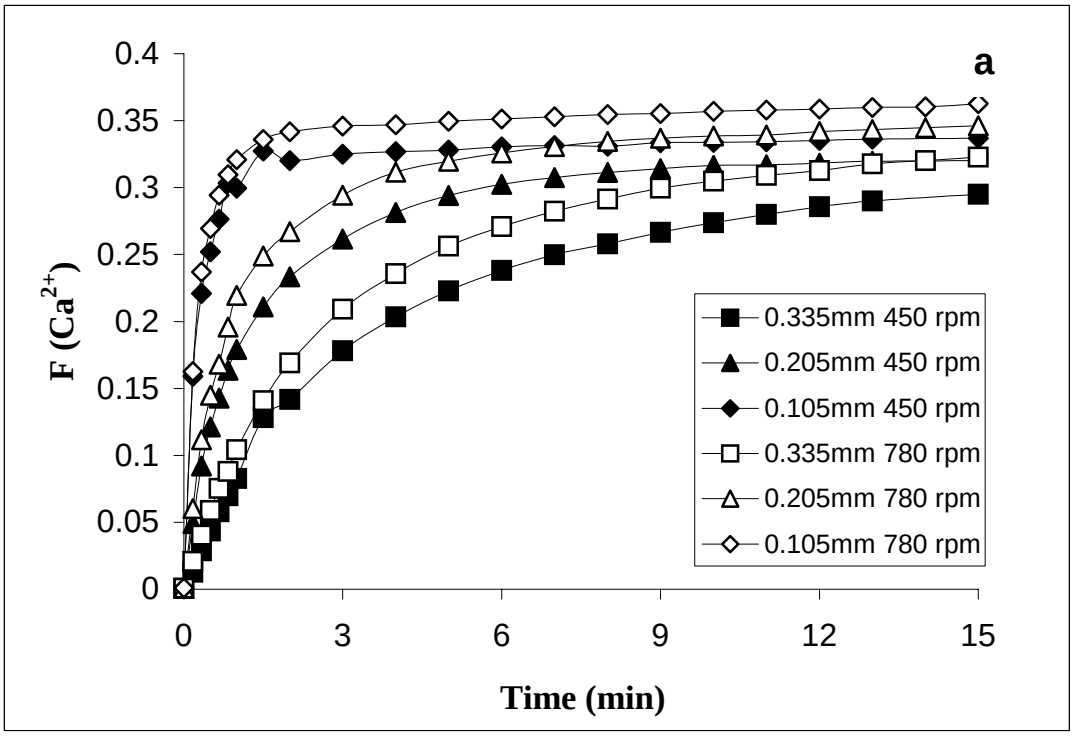
a
0.4
0.35
0.3
0.25
0.2
0.15
0.1
0.05
0
F (Ca2+)
0
3
6
9
12
15
Time (min)
0.335mm 450 rpm
0.205mm 450 rpm
0.105mm 450 rpm
0.335mm 780 rpm
0.205mm 780 rpm
0.105mm 780 rpm

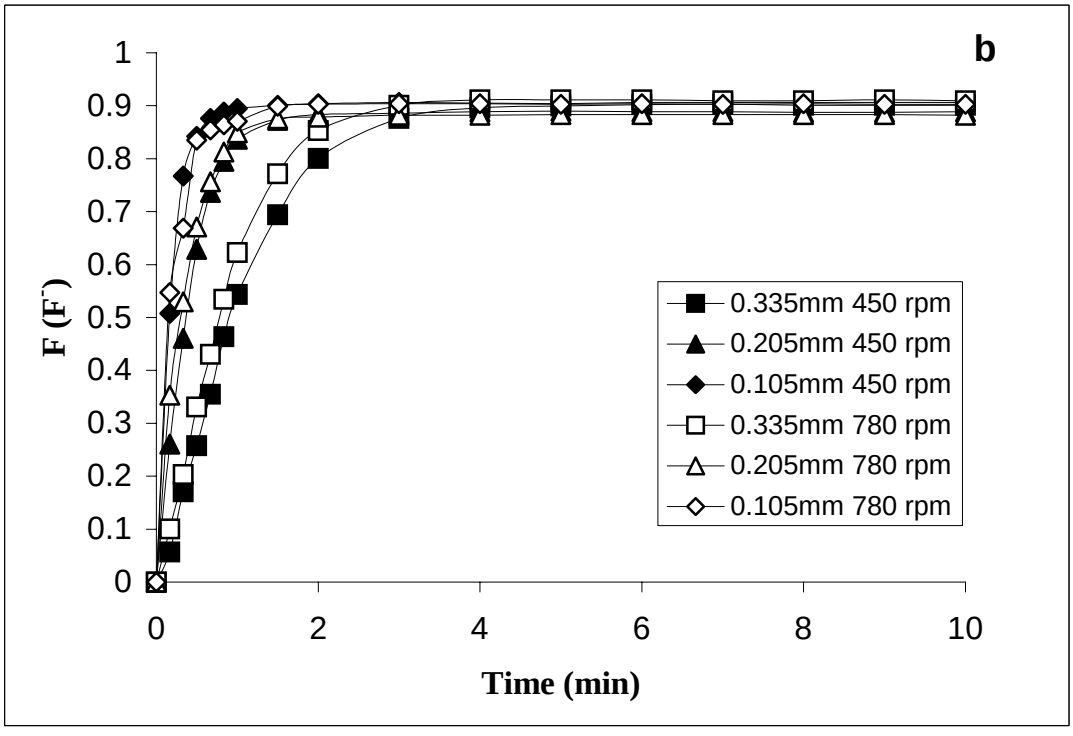
b
1
0.9
0.8
0.7
0.6
0.5
0.4
0.3
0.2
0.1
0
F (F-)
0
2
4
6
8
10
Time (min)
0.335mm 450 rpm
0.205mm 450 rpm
0.105mm 450 rpm
0.335mm 780 rpm
0.205mm 780 rpm
0.105mm 780 rpm

Figure 6

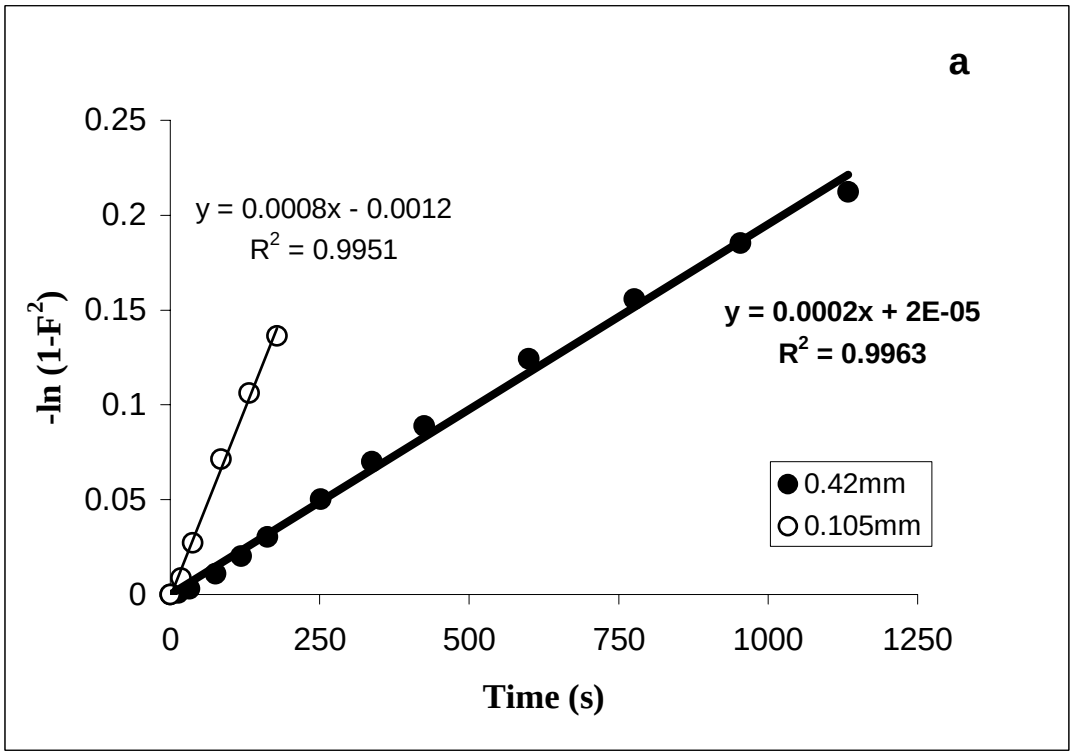
a
0.25
0.2
0.15
0.1
0.05
0
-ln (1-F2)
y = 0.0008x - 0.0012
R2 = 0.9951
y = 0.0002x + 2E-05
R2 = 0.9963
0.42mm
0.105mm
0
250
500
750
1000
1250
Time (s)

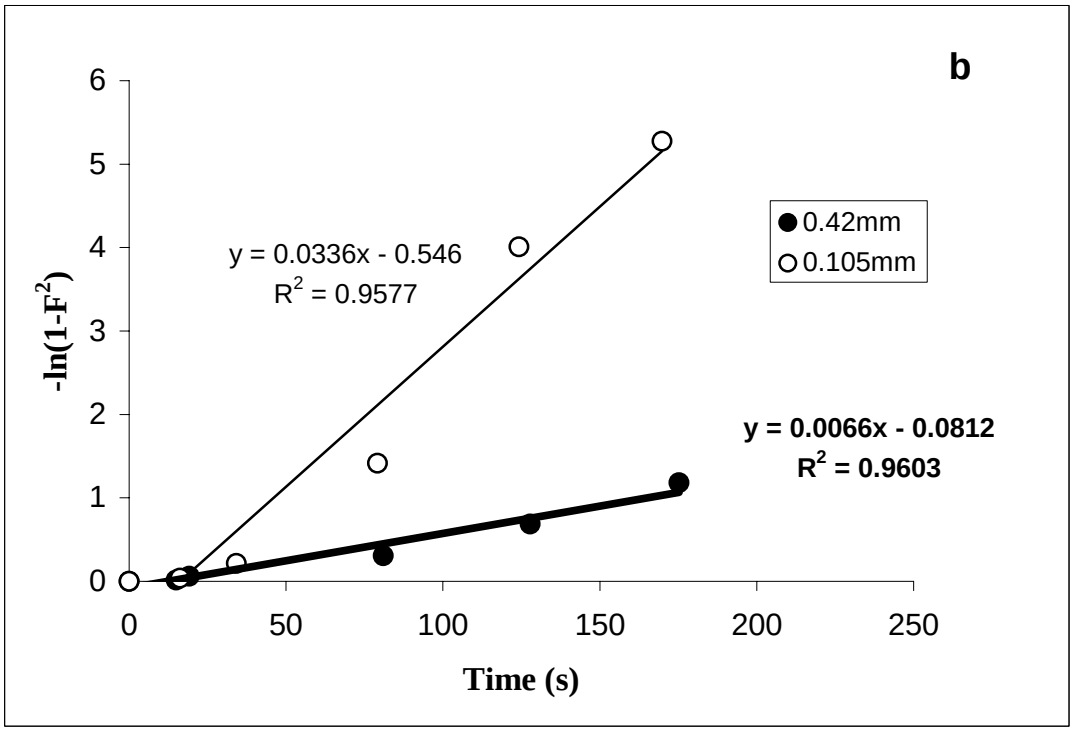
b
6
5
4
3
2
1
0
-ln(1-F2)
y = 0.0336x - 0.546
R2 = 0.9577
y = 0.0066x - 0.0812
R2 = 0.9603
0.42mm
0.105mm
0
50
100
150
200
250
Time (s)

Figure 7

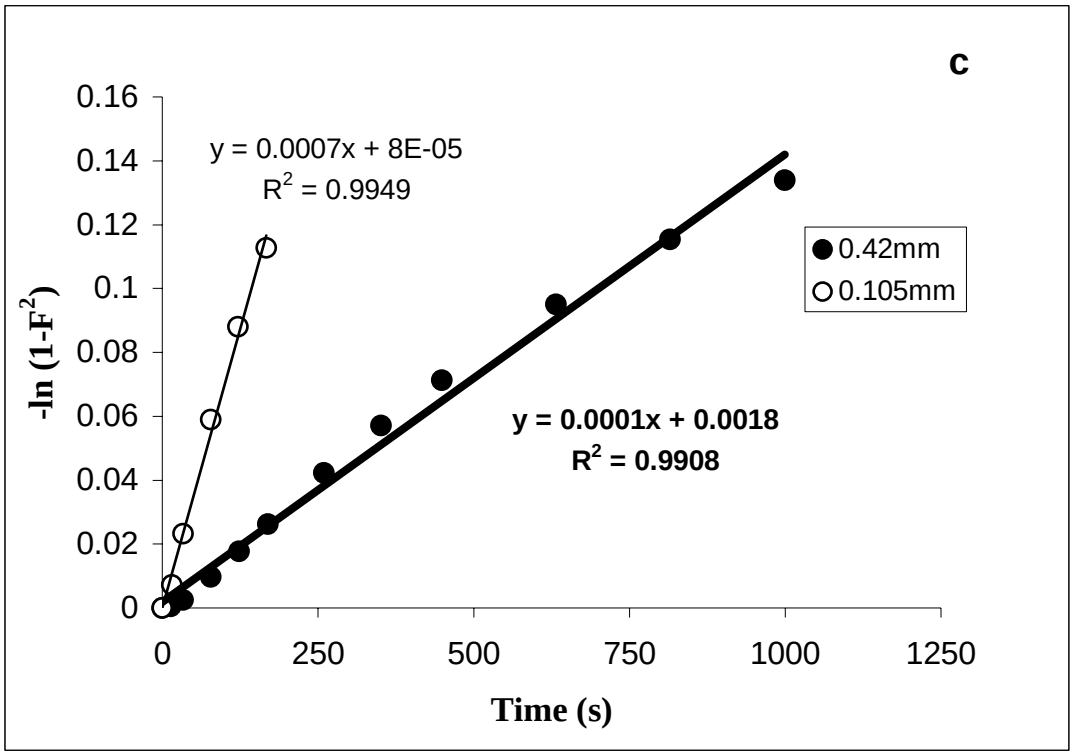
c
0.16
0.14
0.12
0.1
0.08
0.06
0.04
0.02
0
-ln (1-F2)
y = 0.0007x + 8E-05
R2 = 0.9949
0.42mm
0.105mm
y = 0.0001x + 0.0018
R2 = 0.9908
0
250
500
750
1000
1250
Time (s)

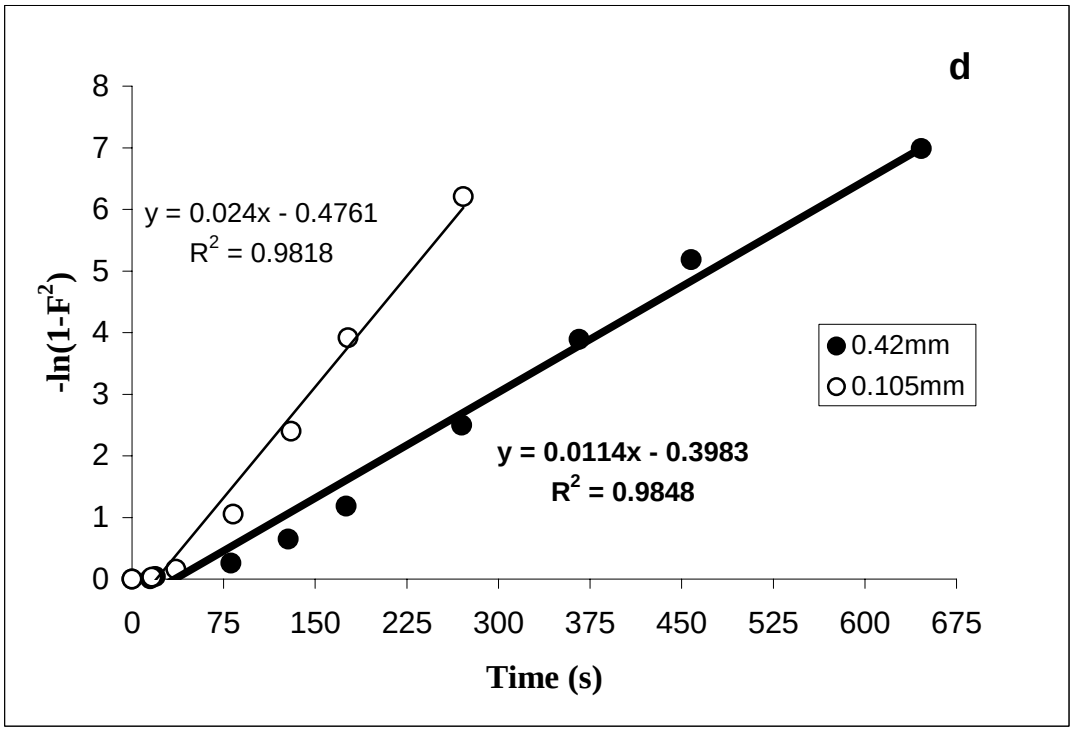
d
8
7
6
5
4
3
2
1
0
-ln(1-F2)
y = 0.024x - 0.4761
R2 = 0.9818
0.42mm
0.105mm
y = 0.0114x - 0.3983
R2 = 0.9848
0
75
150
225
300
375
450
525
600
675
Time (s)

Figure 7

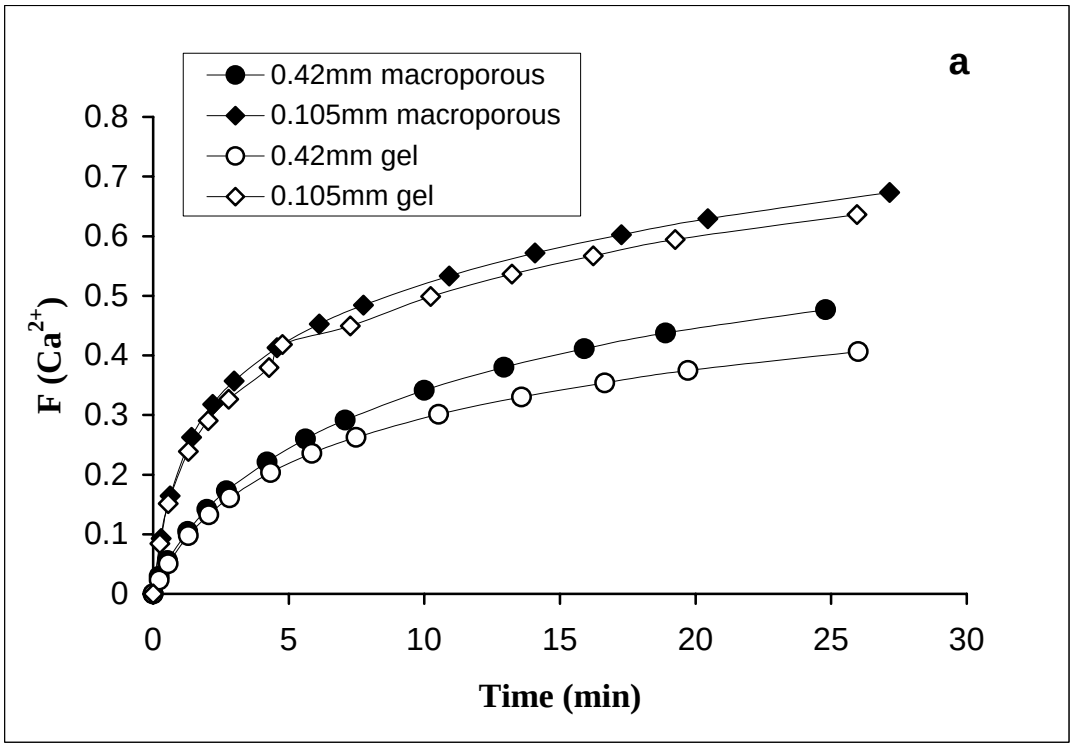
a
0.42mm macroporous
0.105mm macroporous
0.42mm gel
0.105mm gel
F (Ca2+)
0.8
0.7
0.6
0.5
0.4
0.3
0.2
0.1
0
0
5
10
15
20
25
30
Time (min)

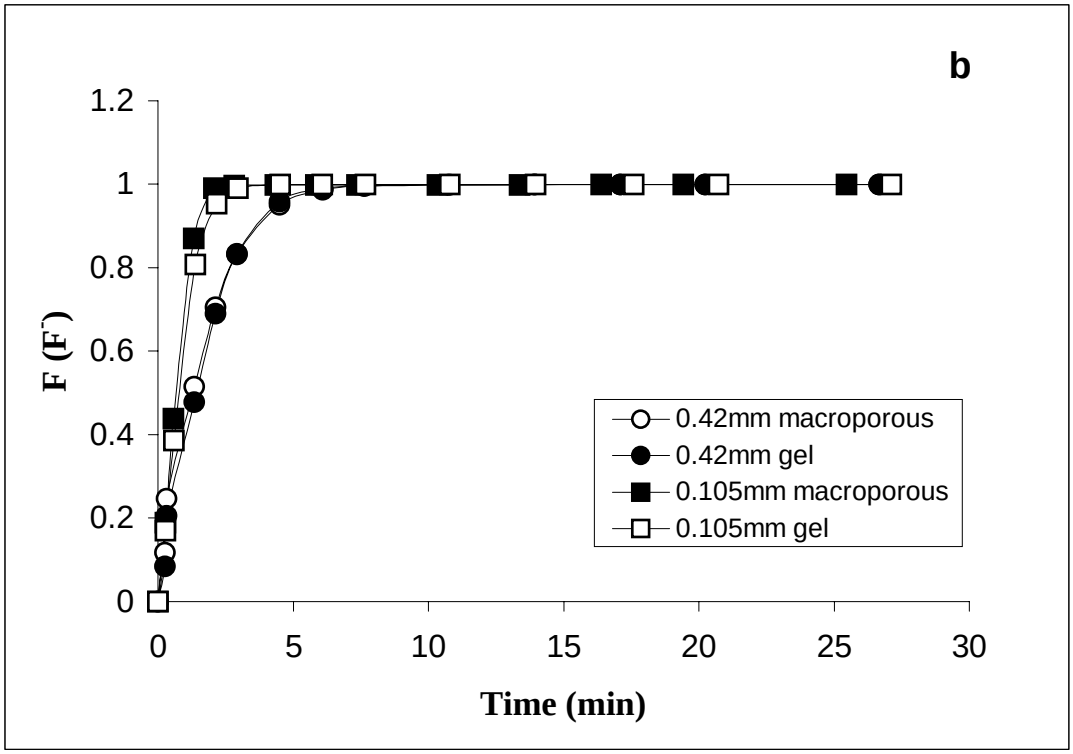
b
F (F-)
1.2
1
0.8
0.6
0.4
0.2
0
0.42mm macroporous
0.42mm gel
0.105mm macroporous
0.105mm gel
0
5
10
15
20
25
30
Time (min)

Figure 8

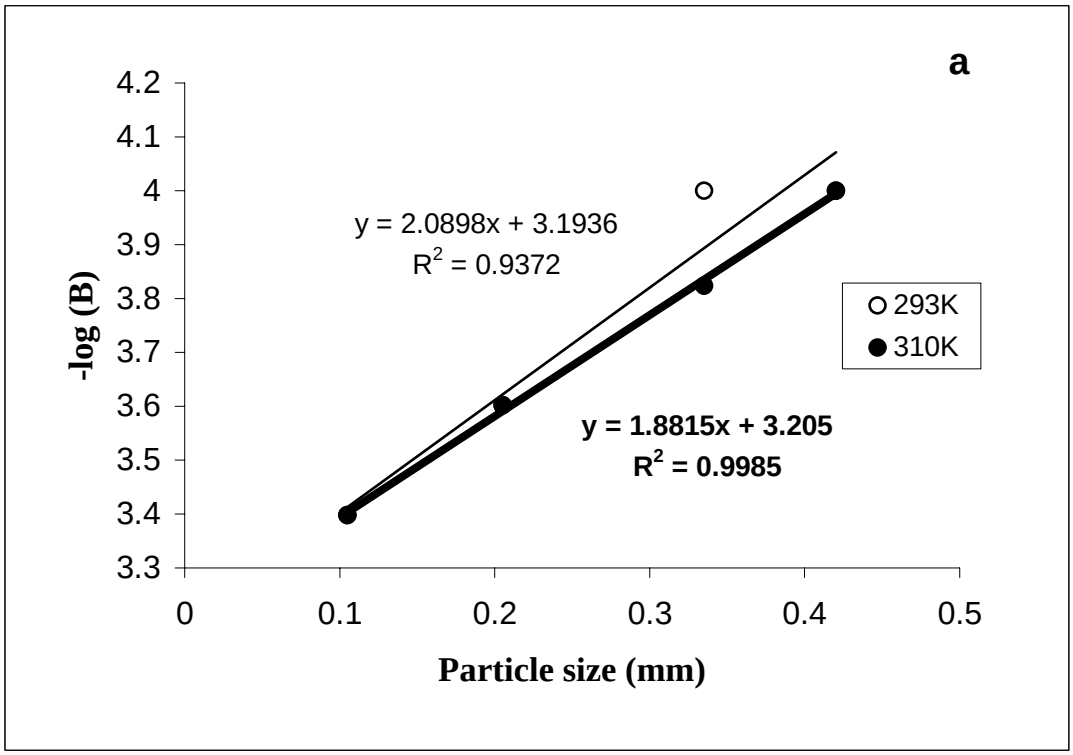
a
4.2
4.1
4
3.9
3.8
3.7
3.6
3.5
3.4
3.3
-log (B)
y = 2.0898x + 3.1936
R2 = 0.9372
293K
310K
y = 1.8815x + 3.205
R2 = 0.9985
0
0.1
0.2
0.3
0.4
0.5
Particle size (mm)

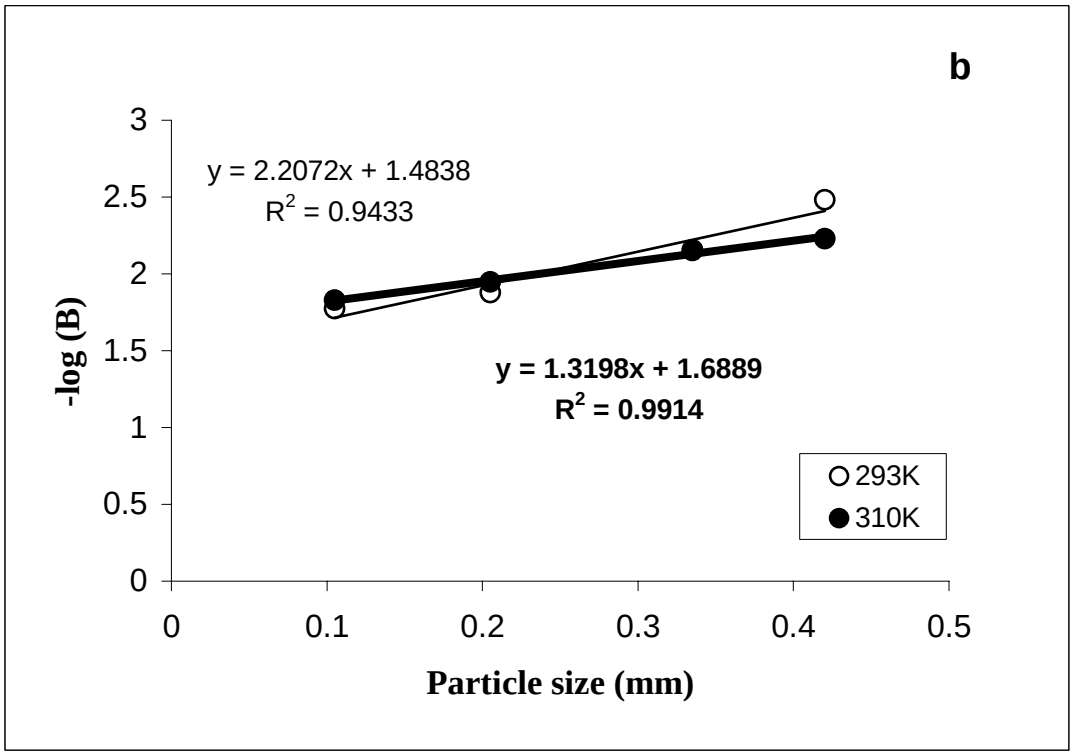
b
3
2.5
2
1.5
1
0.5
0
-log (B)
y = 2.2072x + 1.4838
R2 = 0.9433
y = 1.3198x + 1.6889
R2 = 0.9914
293K
310K
0
0.1
0.2
0.3
0.4
0.5
Particle size (mm)

Figure 9

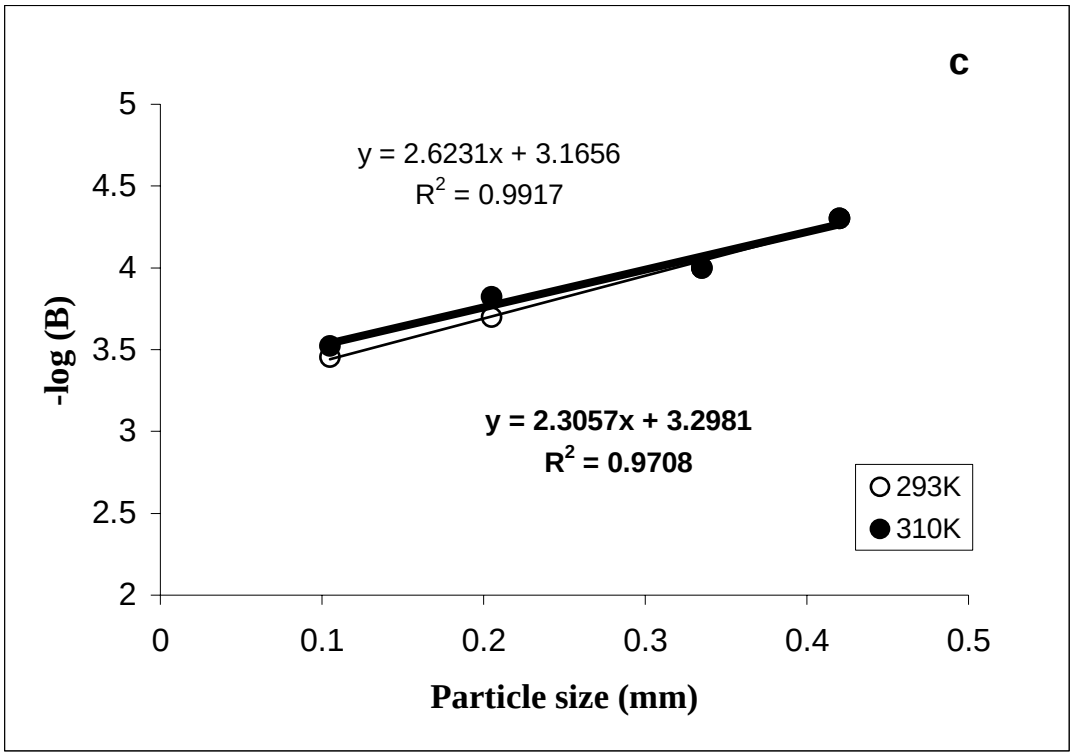
c
y = 2.6231x + 3.1656
R2 = 0.9917
y = 2.3057x + 3.2981
R2 = 0.9708
293K
310K
-log (B)
Particle size (mm)
5
4.5
4
3.5
3
2.5
2
0
0.1
0.2
0.3
0.4
0.5

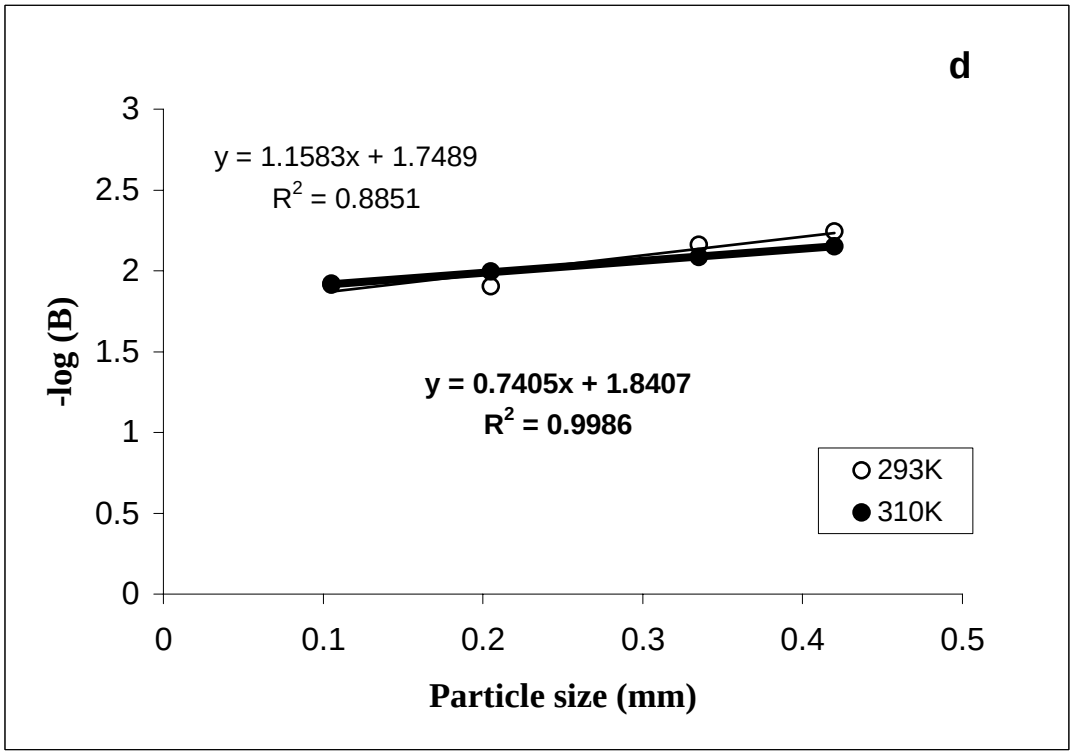
d
y = 1.1583x + 1.7489
R2 = 0.8851
y = 0.7405x + 1.8407
R2 = 0.9986
293K
310K
-log (B)
Particle size (mm)
3
2.5
2
1.5
1
0.5
0
0
0.1
0.2
0.3
0.4
0.5

Figure 9

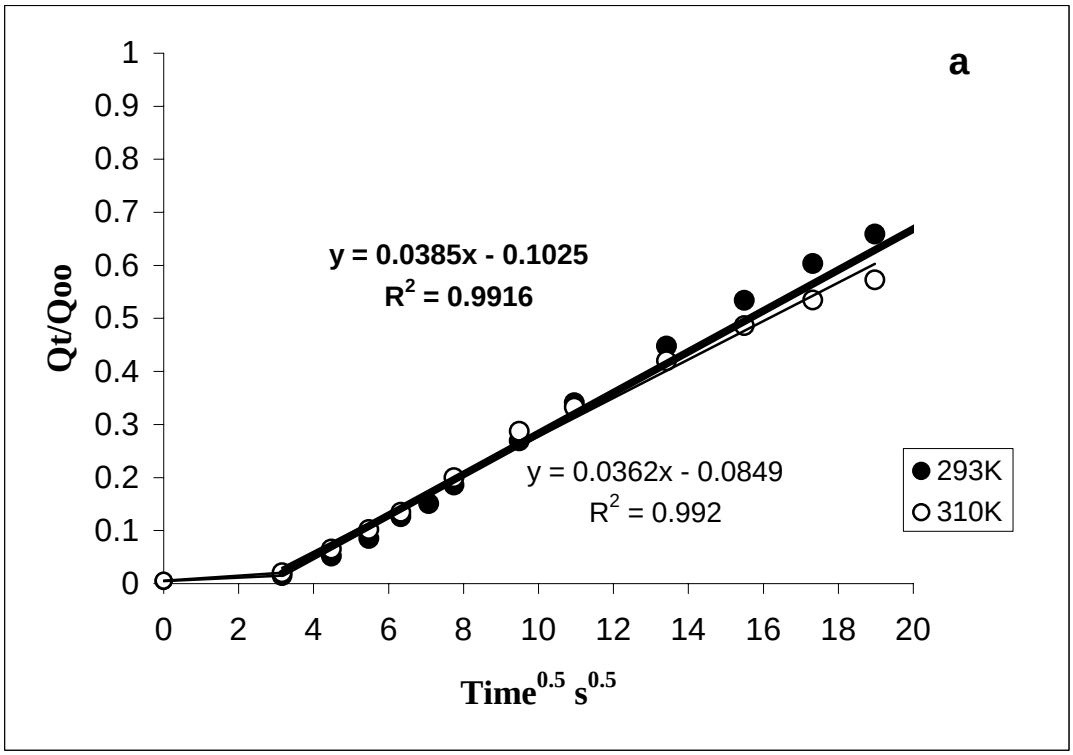
a
y = 0.0385x - 0.1025
R2 = 0.9916
y = 0.0362x - 0.0849
R2 = 0.992
293K
310K
Qt/Qoo
Time0.5 s0.5

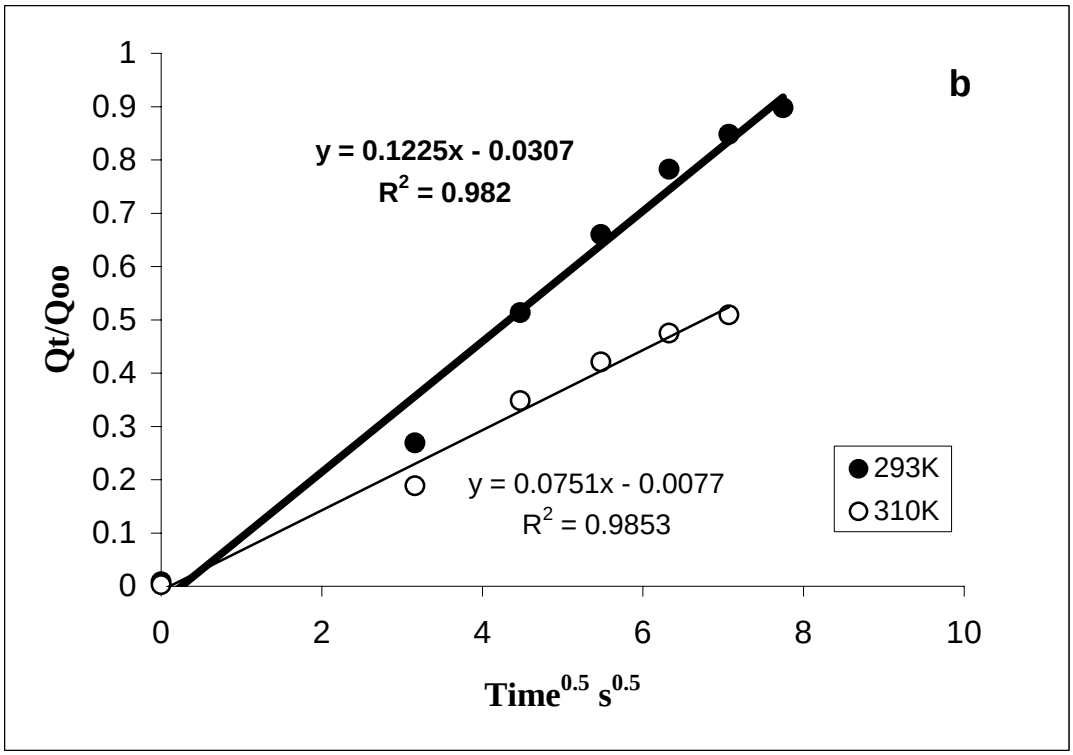
b
y = 0.1225x - 0.0307
R2 = 0.982
y = 0.0751x - 0.0077
R2 = 0.9853
293K
310K
Qt/Qoo
Time0.5 s0.5

Figure 10

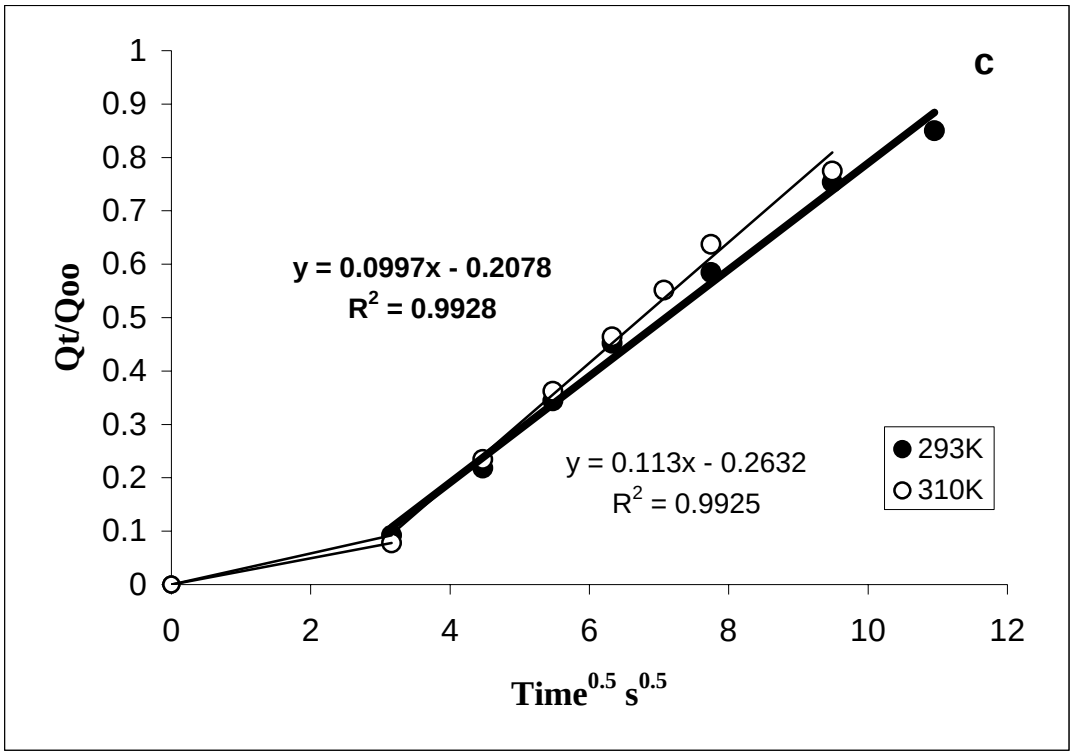
c
y = 0.0997x - 0.2078
R2 = 0.9928
y = 0.113x - 0.2632
R2 = 0.9925
293K
310K
Qt/Qoo
Time0.5 s0.5
0
0.1
0.2
0.3
0.4
0.5
0.6
0.7
0.8
0.9
1
0
2
4
6
8
10
12

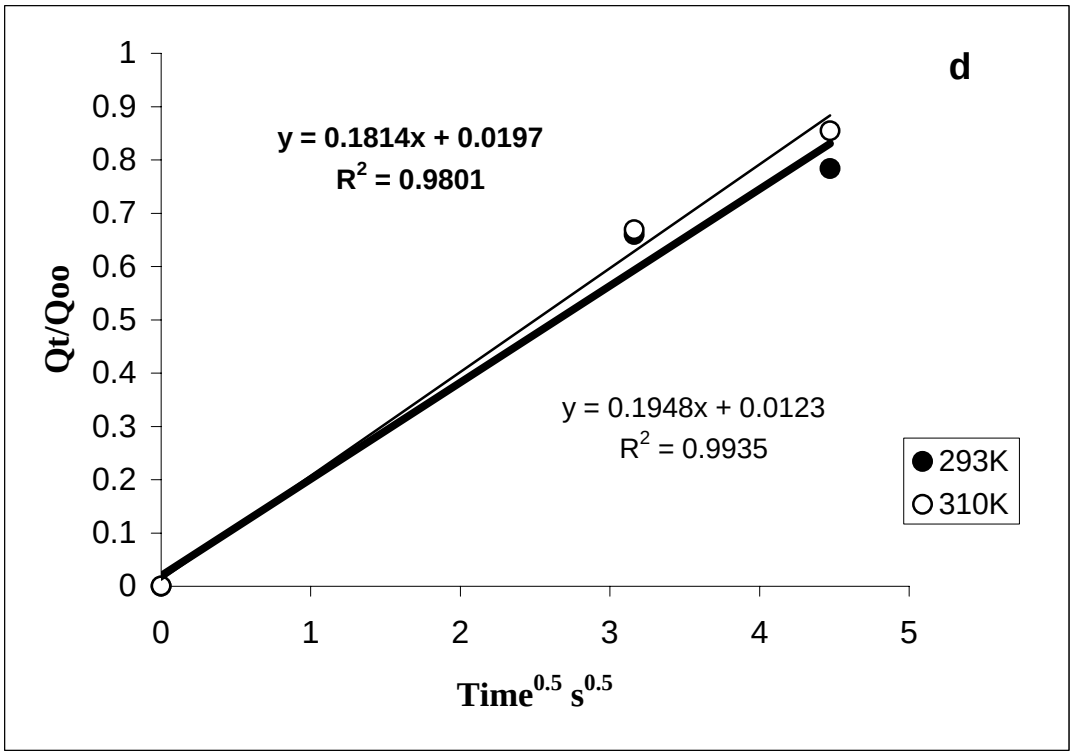
d
y = 0.1814x + 0.0197
R2 = 0.9801
y = 0.1948x + 0.0123
R2 = 0.9935
293K
310K
Qt/Qoo
Time0.5 s0.5
0
0.1
0.2
0.3
0.4
0.5
0.6
0.7
0.8
0.9
1
0
1
2
3
4
5

Figure 10

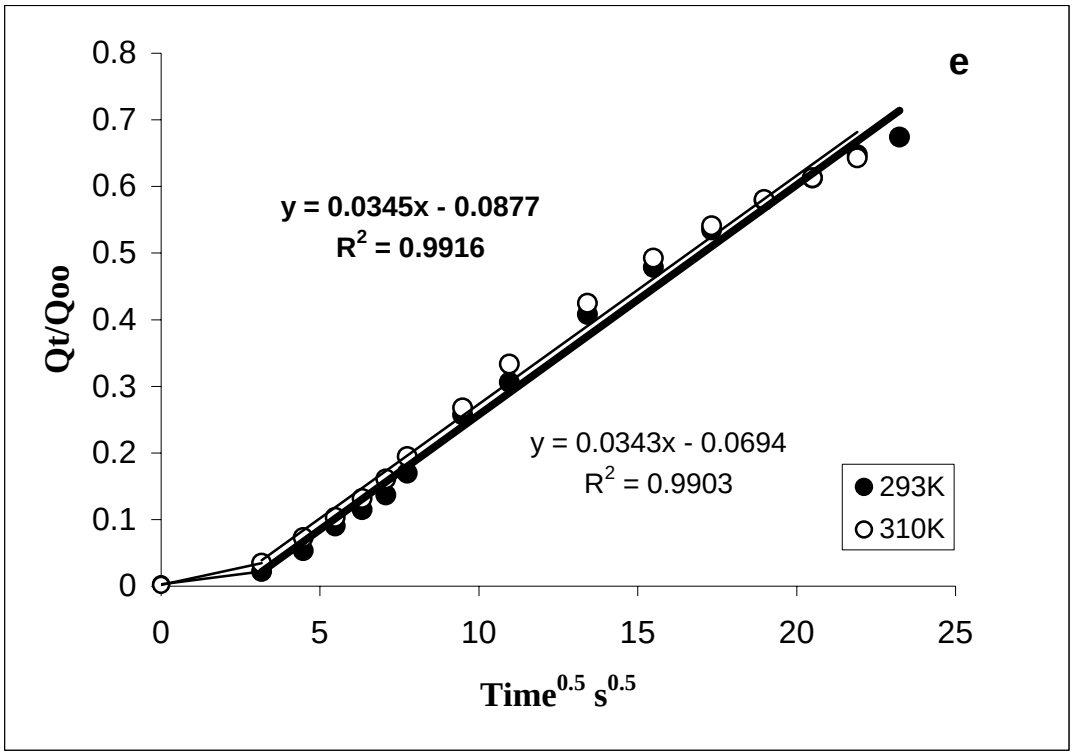
e
y = 0.0345x - 0.0877
R2 = 0.9916
y = 0.0343x - 0.0694
R2 = 0.9903
293K
310K
Qt/Qoo
Time0.5 s0.5
0
0.1
0.2
0.3
0.4
0.5
0.6
0.7
0.8
0
5
10
15
20
25

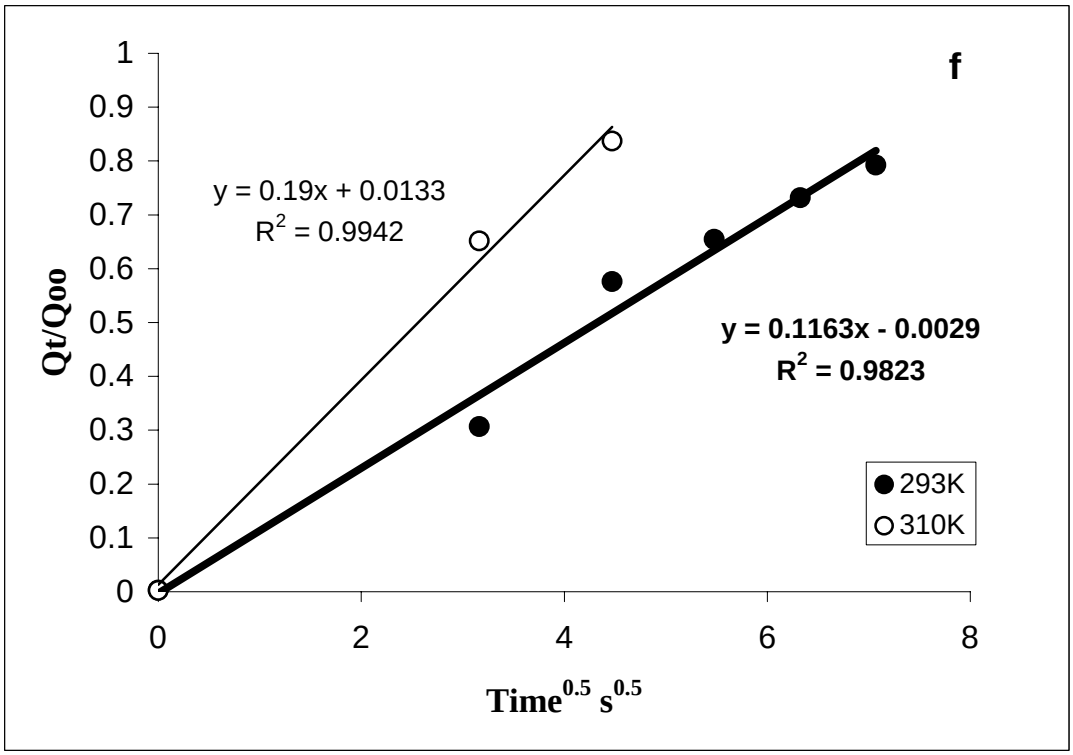
f
y = 0.19x + 0.0133
R2 = 0.9942
y = 0.1163x - 0.0029
R2 = 0.9823
293K
310K
Qt/Qoo
Time0.5 s0.5
0
0.1
0.2
0.3
0.4
0.5
0.6
0.7
0.8
0.9
1
0
2
4
6
8

Figure 10

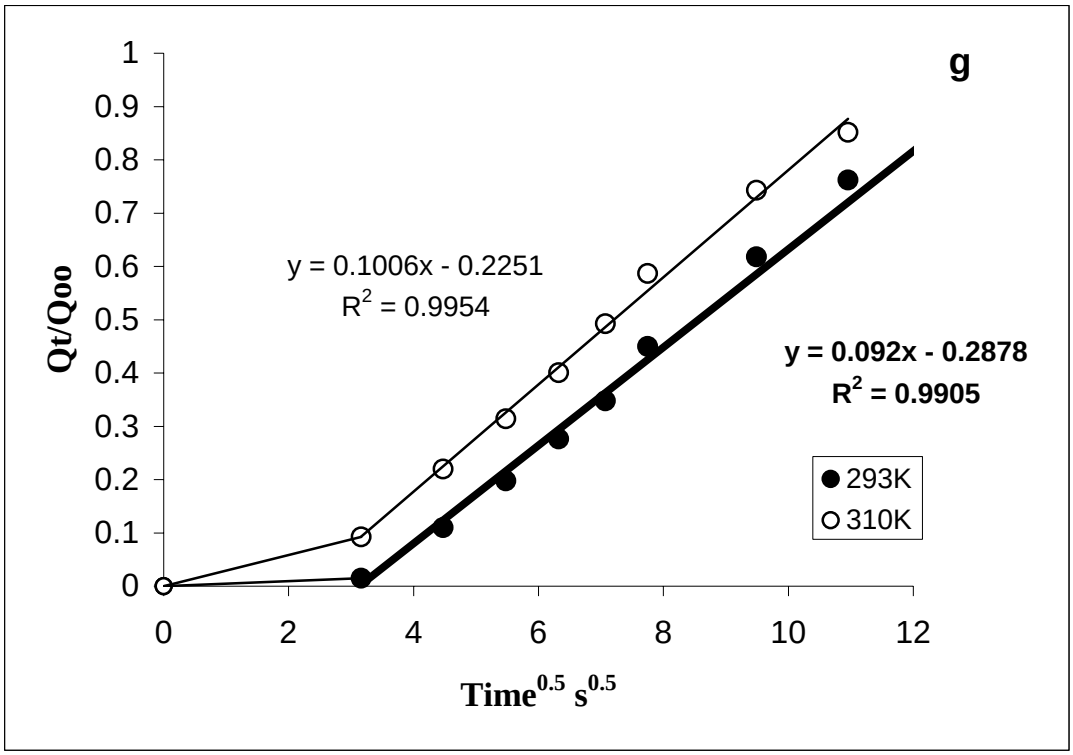
g
y = 0.1006x - 0.2251
R2 = 0.9954
y = 0.092x - 0.2878
R2 = 0.9905
293K
310K
Qt/Qoo
Time0.5 s0.5

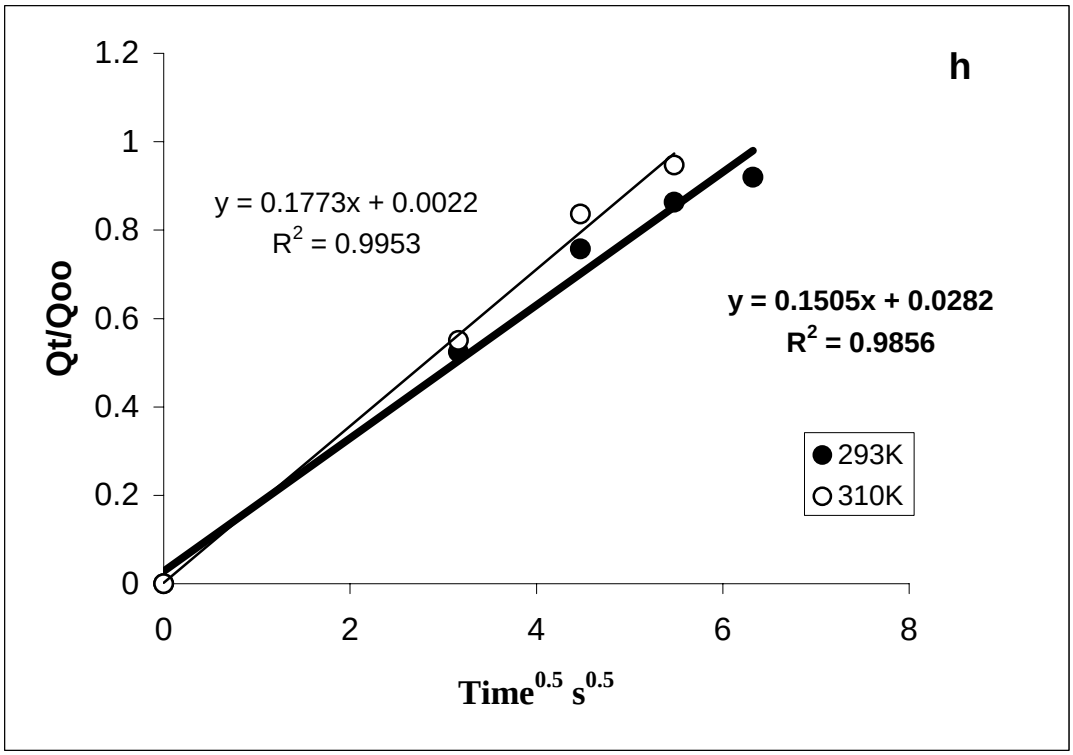
h
y = 0.1773x + 0.0022
R2 = 0.9953
y = 0.1505x + 0.0282
R2 = 0.9856
293K
310K
Qt/Qoo
Time0.5 s0.5

Figure 10

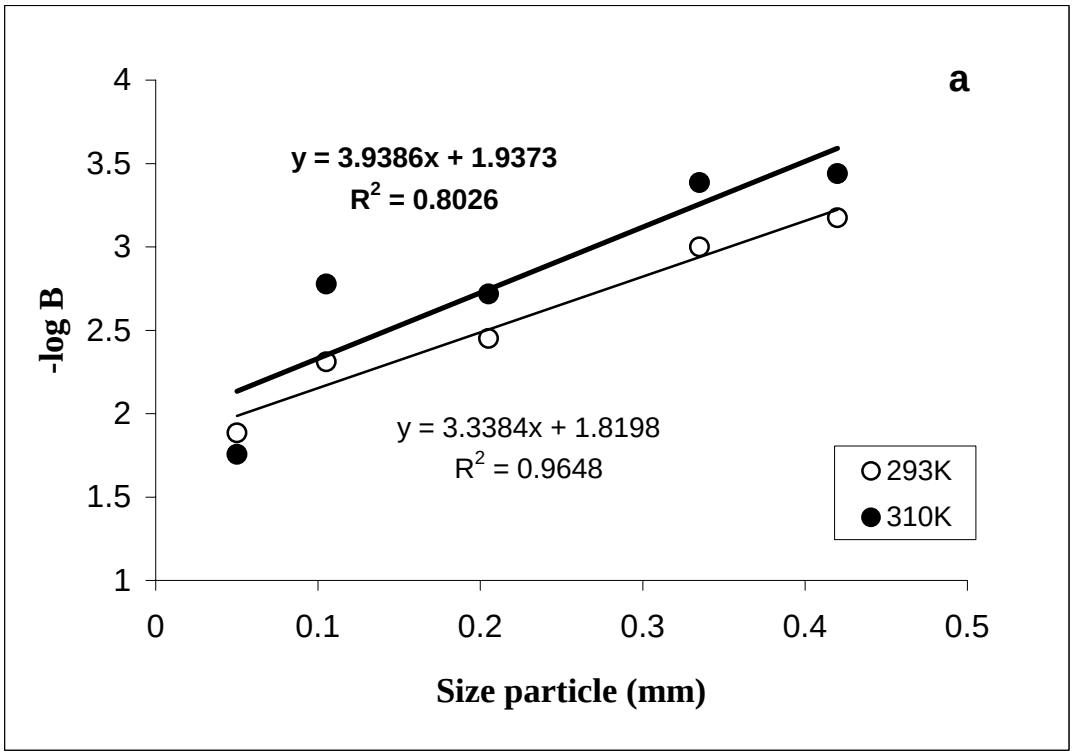
a
y = 3.9386x + 1.9373
R2 = 0.8026
y = 3.3384x + 1.8198
R2 = 0.9648
293K
310K
-log B
Size particle (mm)
4
3.5
3
2.5
2
1.5
1
0
0.1
0.2
0.3
0.4
0.5

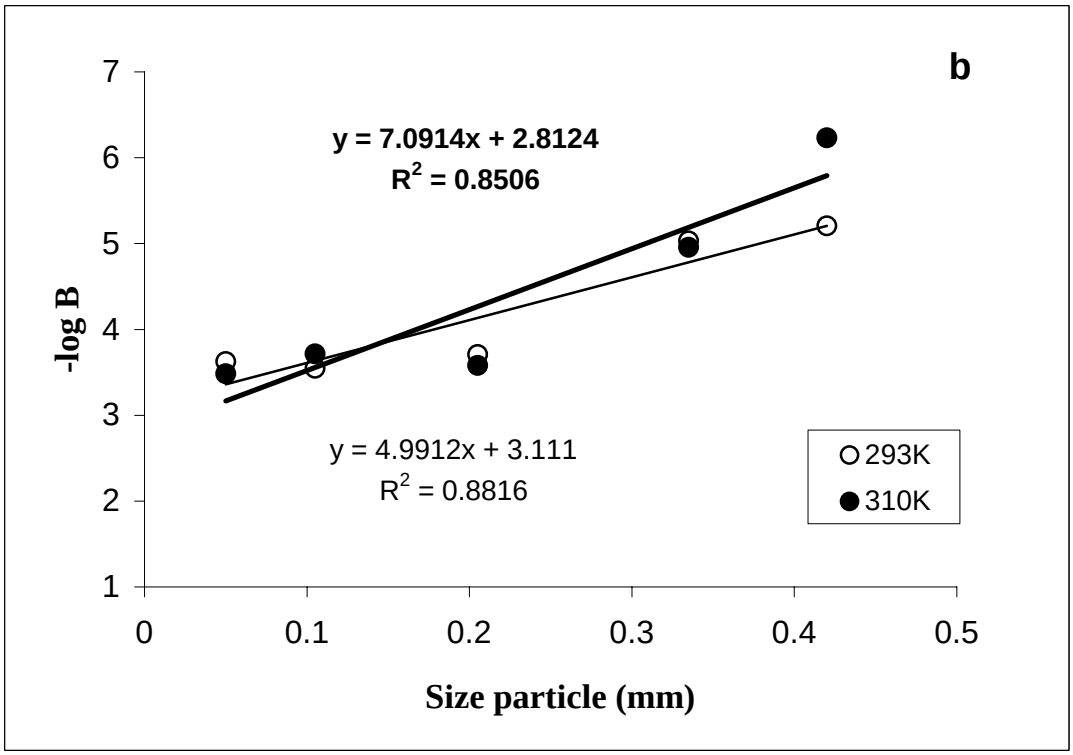
b
y = 7.0914x + 2.8124
R2 = 0.8506
y = 4.9912x + 3.111
R2 = 0.8816
293K
310K
-log B
Size particle (mm)
7
6
5
4
3
2
1
0
0.1
0.2
0.3
0.4
0.5

Figure 11

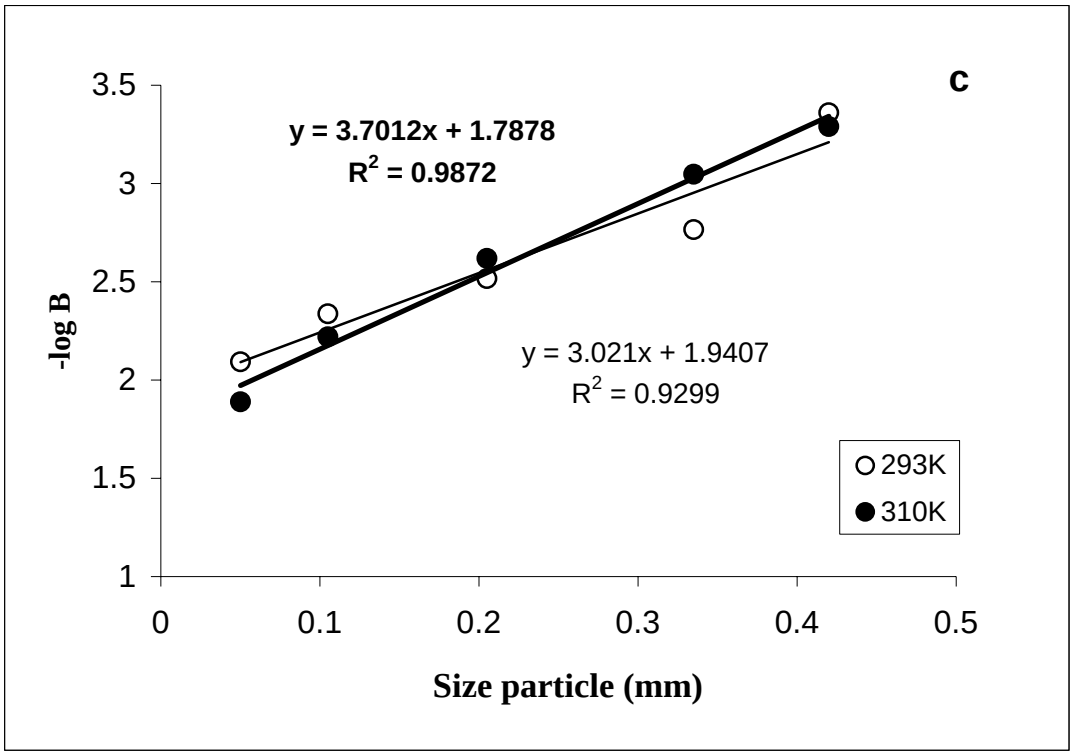
c
y = 3.7012x + 1.7878
R2 = 0.9872
y = 3.021x + 1.9407
R2 = 0.9299
293K
310K
-log B
Size particle (mm)
3.5
3
2.5
2
1.5
1
0
0.1
0.2
0.3
0.4
0.5

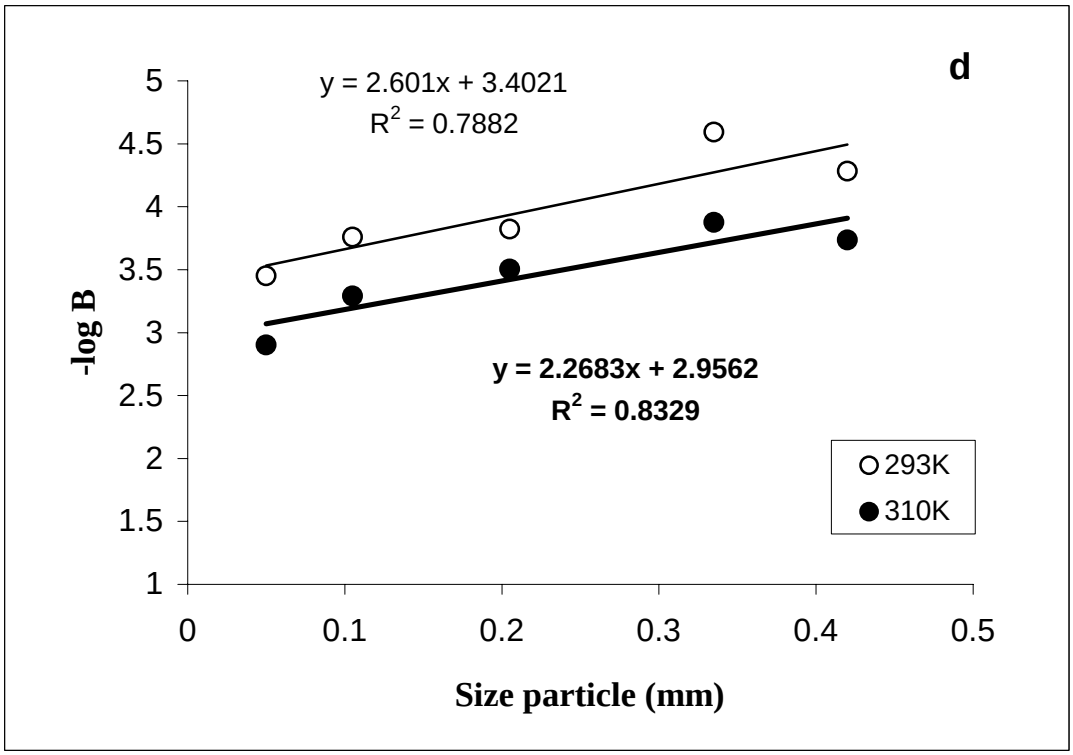
d
y = 2.601x + 3.4021
R2 = 0.7882
y = 2.2683x + 2.9562
R2 = 0.8329
293K
310K
-log B
Size particle (mm)
5
4.5
4
3.5
3
2.5
2
1.5
1
0
0.1
0.2
0.3
0.4
0.5

Figure 11

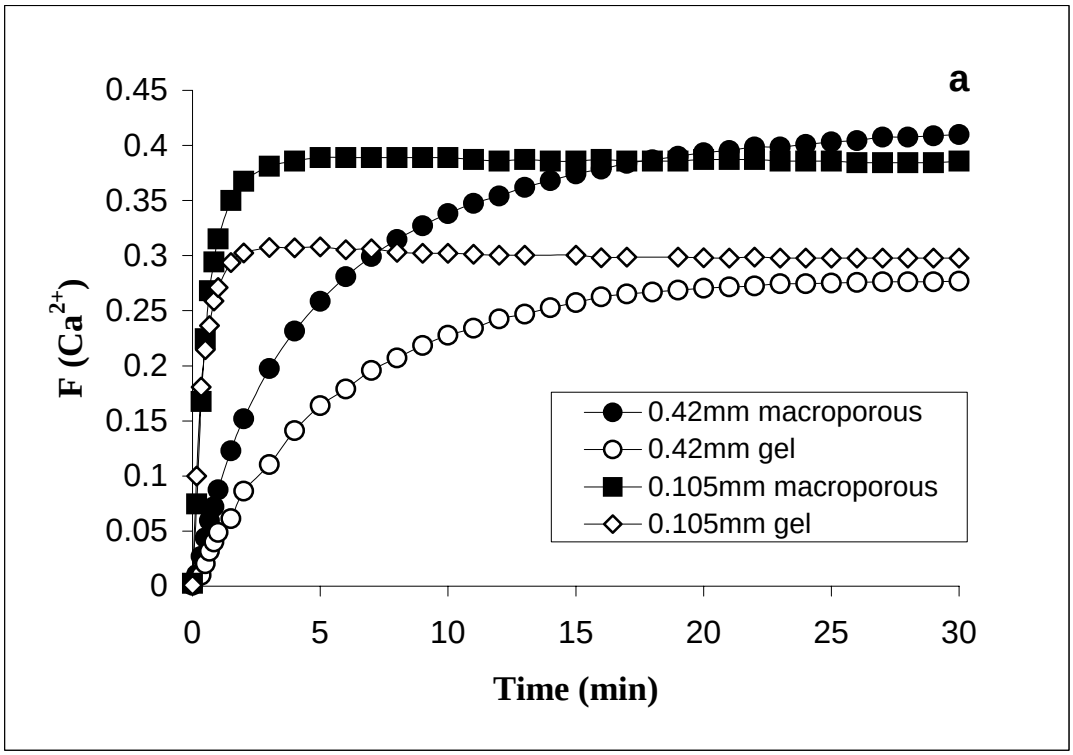
a
0.45
0.4
0.35
0.3
0.25
0.2
0.15
0.1
0.05
0
F (Ca2+)
0
5
10
15
20
25
30
Time (min)
0.42mm macroporous
0.42mm gel
0.105mm macroporous
0.105mm gel

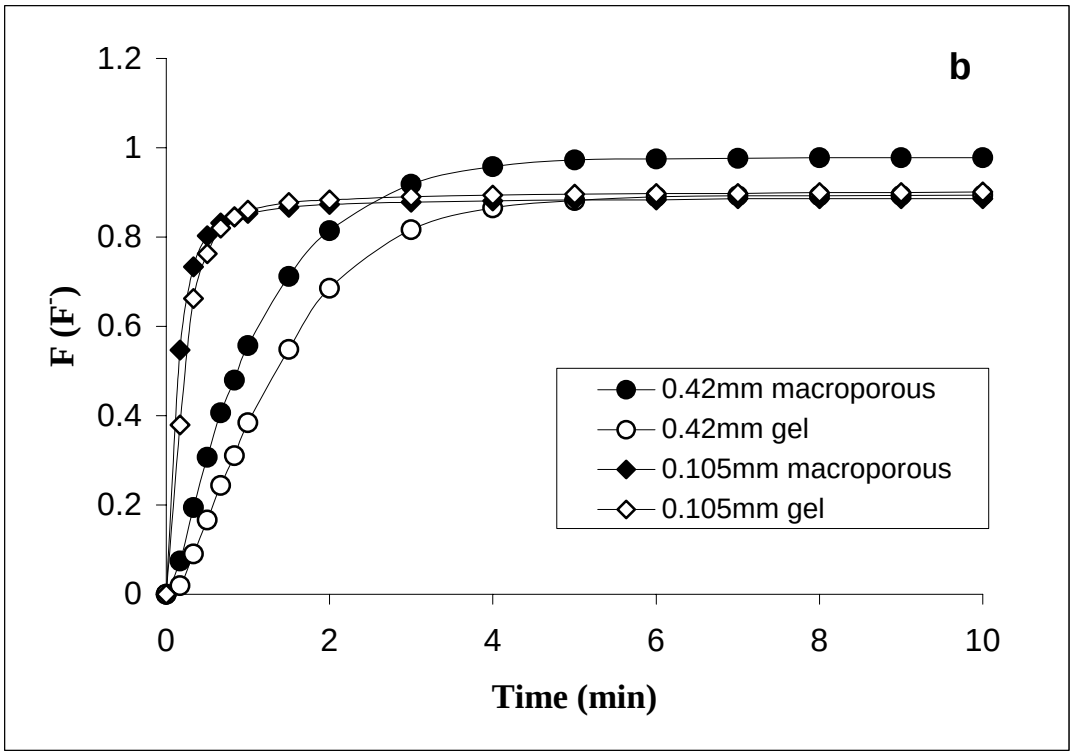
b
1.2
1
0.8
0.6
0.4
0.2
0
F (F-)
0
2
4
6
8
10
Time (min)
0.42mm macroporous
0.42mm gel
0.105mm macroporous
0.105mm gel

Figure 12

ANNEX 4

sci
where science meets business

Journal of Chemical Technology and Biotechnology
ISSN: 1097-4660 online; 0268-2575 print

Society of Chemical Industry
14/15 Belgrave Square
London SW1X 8PS UK
T: +44 (0)20 7598 1500
F: +44 (0)20 7235 0887
E: jctb@soci.org
W: www.soci.org

Dr Manuel Valiente
Department de Química
Untat Analitica
Centre GTS
Universitat Autònoma de Barcelona
Facultat de Ciéncies, Edifici Cn
E-08193 Bellaterra
Spain

14 July 2003

Dear Dr Valiente

JCTB 57/2003 Calcium and fluoride release from ion exchange polyphasic systems

Thank you for returning your amended manuscript. I am pleased to inform you that your paper has now been accepted for publication, and has been forwarded to our publishers, John Wiley & Sons. To speed up the process of publication, if you have not already done so, please supply **an electronic copy of the final version of your paper on PC disk, or by email**, in a format compatible with MS Word 97 to the **below** address.

Enclosed you will find the *Copyright Transfer Agreement Form* which must be signed (preferably by *all* the authors) and returned to the publishers.

In due course you will receive your *proofs* from the publishers, please check them very carefully and return them as soon as possible so as not to delay publication.

Samantha Moore
John Wiley & Sons, Ltd.
The Atrium
Southern Gate
Chichester
West Sussex PO19 8SQ

Tel: +44 (0)1243 770 383
Fax: +44 (0)1243 770 144
Email: smoore@wiley.co.uk

If you have any queries about the status of your paper please contact Samantha Moore.

Yours sincerely

Jennifer Quamina
Editorial Assistant
Tel: +44 (0) 20 7598 1555
Fax: +44 (0) 20 7235 0887
Email: jctb@soci.org

SCI founded 1881
Incorporated by Royal Charter 1907
Registered Charity 206883

Journal of Chemical Technology and Biotechnology *J Chem Technol Biotechnol* **78**:000–000 (online: 2003)
DOI: 10.1002/jctb.906

Calcium and fluoride release from ion exchange polyphasic systems

Anna Torrado and Manuel Valiente*

Departament de Química, Unitat Analítica, Centre GTS, Universitat Autònoma de Barcelona, Facultat de Ciències, Edifici Cn, E-08193 Bellaterra (Barcelona), Spain

Abstract: The present study concerns the kinetics of ion exchange accompanied by CaF_2 precipitation in tri-phasic and quadri-phasic systems involving a weak base anionic exchanger and a carboxylic cationic exchanger in the F^- and Ca^{2+} forms, respectively, in contact with a solution of artificial saliva. It was shown that in both systems the rate of Ca^{2+} release from the cationic exchanger is much lower than that of F^- from the anionic one. The rate of release for both ions, controlled by intraparticle diffusion, has been characterized by a Fick's law model. The kinetic parameters of effective rate of release (*B*) and diffusion coefficient (*D*) of the respective ion in the resin phase depend on the type of resin and the presence of different numbers of phases. The amount of the precipitate crystallizing on the surface of the resin beads depends on the type of the ion exchange resin, its particle size and on the ratio of resin components. By varying this ratio and the particle size of the ion exchangers it is possible to accomplish the precipitation mostly on the larger surface of the ionic exchanger.

Keywords: ion exchange; kinetics release; polyphasic system; calcium fluoride

1 INTRODUCTION

The most traditional forms of investigation in the field of ion exchange are habitually bi-phasic systems. These systems involve, as a rule, a solid or liquid ion exchanger and a liquid solution. The presence of additional phases in such systems, either by addition of new phases or by possible formation during the ion exchange process, will substantially complicate the study. Despite this, a new tri-phasic system can show some advantages in comparison with the traditional ion exchange process. The best known tri-phasic systems are the catalytic systems,[1–3] which consist of a solid phase and two immiscible liquids (S–L–L systems). Recently, new studies based on the AIR (Aqua Impregnated Resins) concept have appeared. They attempt to convert S–L–L systems to the corresponding bi-phasic system, where resins impregnated with an aqueous solution (AIR) are contacted with an organic solution. In this way, a batch operation process can be transformed to a dynamic one by using a column procedure. Successful results have been obtained in the selective separation and recovery of metal ions using the AIR technique.[4–6] Another type of tri-phasic system used classically are the solid–solid–liquid systems (S–S–L systems) which are known as mixed resin beds. These are widely used for water deionization,[7–9] synthesis,[10] liquid chromatographic separations[11] and for other purposes. However, the precipitation of poorly soluble substances in the resin bed increases the resistance to mass transfer in the resin phase because of the precipitate coating the exchanger beads. This problem has been addressed by either the addition of precipitation inhibitors, or by the use of sectional columns or counter-current units.[12]

On the other hand, a combination of ion exchange materials loaded with required ions can be effectively applied as an ion release system to solve different remineralization problems. Thus, a sustained release of nutrients for plants has been successfully obtained by using an appropriate ion exchange blending.[13] A similar approach can be used on the remineralization of organomineral dental tissues.[14,15] Fluoride has been proved to be effective for the prevention of dental caries in various forms and concentrations, and its reactivity with the mineral components of sound and carious dental enamel has been associated with both increased resistance to acid demineralization and increased rates of remineralization *in vitro* and *in vivo*.[16,17] Several studies report the deposition of CaF_2 on the surface of human enamel after treatment with fluoridated solutions.[18,19] The hypothesis that CaF_2 uptake by

* Correspondence to: Manuel Valiente, Departament de Química, Unitat Analítica, Centre GTS, Universitat Autònoma de Barcelona, Facultat de Ciències, Edifici Cn, E-08193 Bellaterra (Barcelona), Spain
E-mail: manuel.valiente@uab.es
Contract/grant sponsor: Spanish Ministry of Science and Technology; contract/grant number: PPQ2002-04 267-C03-01
Contract/grant sponsor: Universitat Autònoma de Barcelona
(*Received 18 February 2003; revised version received 13 June 2003; accepted 9 July 2003*)

dental enamel acts as a fluoride reservoir for a long period of time and that it enhances fluorapatite formation has been defended. However, it is not firmly established that CaF_2 formed as a result of topical fluoride application is the basic element in the prevention and control of dental caries.[20] As is known, the rate at which the components are released is a key parameter to successful crystal growth.[21,22] Because in our case this is a primary objective related to enamel restoration, ion exchange resins mixed bed systems let to control• the concentration of ions released to the solution. So, the characterization of this release process will be of key importance in optimizing a successful application in a dental treatment.

The aim of the present work is to study the kinetics of ion exchange accompanied by CaF_2 precipitation in tri-phasic and quadri-phasic systems involving a weak base anionic exchanger and a carboxylic cationic exchanger, respectively in the F^- and Ca^{2+} forms, in contact with a solution of artificial saliva.

2 EXPERIMENTAL

2.1 Materials

Highly purified ion exchange resins, carboxylic type, Lewatit S8528 ($pK_a = 4.5–5$), and tertiary amine types, Lewatit S3428 and MP62 ($pK_a = 7–8$), with macroporous structures, were kindly supplied by Bayer Hispania Industrial, SA Solutions of $CaCl_2$ (1 mol dm^{-3} and 0.3 mol dm^{-3}), KCl (0.01 mol dm^{-3}), NaCl (0.008 mol dm^{-3}), NaF (0.9 mol dm^{-3}), $NaNO_3$ (0.5 mol dm^{-3}), NaOH (2.2 mol dm^{-3}), and EDTA (0.1 mol dm^{-3}; pH = 8• adjusted with NH_3) were prepared from the corresponding Panreac (Barcelona) pro analysis quality solid salts. HCl (1 mol dm^{-3}) and HAc (0.8 mol dm^{-3}) solutions were prepared by dilution of the corresponding concentrated Panreac pro analysis quality acid. In all cases, deionized water of Milli-Q quality (Millipore, USA) was used.

2.2 Instrumentation

The release of F^- was determined by potentiometry using an ion selective electrode, Orion (USA), whereas Ca^{2+} was measured spectrophotometrically by inductively coupled plasma atomic emission spectroscopy (ICP–OES) using an ARL model 3410 minitorch (USA). All the samples were analyzed with an uncertainty lower than 1.5% and all the experiments were carried out in triplicate.

Qualitative analysis of the elements present in the polymer surface was carried out by an X-ray elemental analysis. This technique takes advantage of the X-rays emitted by a sample covered with carbon, after being bombed by a primary electron beam from an SEM (Scanning Electron Microscopy) instrument (Jeol model JSM-6300, Japan) equipped with an X-Ray Energy Dispersive Spectrometer (EDS) (Link ISIS-200, England) to generate the X-ray spectra.

2.3 Resins loading

Resins were conditioned by following a standard procedure.[23] The conversion of the resins to the desired ionic form was carried out in columns under dynamic conditions by flowing aqueous solutions of the corresponding concentrations through the resin bed. After complete loading, the resin phase was successively washed with water to remove the excess of electrolyte solution, quantitatively removed from the column and separated from water by filtration, followed by drying in an oven (60–70 °C). Resins in the different ionic forms were kept in hermetically sealed vials.

2.4 Resins capacity

Determination of the specific capacity of the different resins towards Ca^{2+} and F^- was carried out under dynamic conditions in columns following a standard procedure.[24] A weighed portion of each resin was introduced in a 10 cm column (8 mmØ) and the counterion of interest was eluted with HCl in the case of the cationic resin and with $NaNO_3$ in the anionic one. Eluate was collected periodically in volumetric flasks and analyzed. The results of the analysis were used to determine the specific capacity of the resins, q_s, according to the equation:

$$q_s = \frac{VC_i}{W_i} \quad (1)$$

where V is the total volume of eluted solution, C_i is the concentration of the solution containing the eluted ion and W_i is the weight of resin loaded with this ion. The specific capacities determined experimentally are shown in Table 1.

2.5 Grinding and sieving

A fraction of each type of resin was ground in a mechanical agate mortar Retsch RMO (Germany) and sieved using a set of standard stainless steel sieves in a mechanical siever, CISA (Spain). Thus, separate fractions of the resins were collected with particle sizes of diameter 0.42 mm, 0.5–0.42 mm and 0.16–0.05 mm.

2.6 Ion exchange kinetics

The study of ion exchange kinetics for the different systems was carried out under dynamic conditions using the 'shallow bed' technique.[25] A small portion of loaded resin was introduced into a column connected to a thermostat and a solution of artificial saliva

Table 1. Specific capacity of the resins towards Ca^{2+} and F^-

	Capacity (mmol g^{-1})	
	Ca^{2+}	F^-
Lewatit S8528	3.11 ± 0.03	—
Lewatit MP62	—	2.91 ± 0.04
Lewatit S3428	—	2.53 ± 0.03

at 310K with a relatively high concentration of the exchanging ion (solution of concentration 1g dm^{-3} KCl and 0.5g dm^{-3} NaCl, pH = 5.5) passed through the resin bed at a high flow rate (~30 cm^3 min^{-1}•). All the resulting eluate was collected in volumetric flasks, analyzed and these analytical data transformed to the degree of conversion, Ψ, by using the equation:•

$$\Psi = \frac{\sum_{t_i=1}^{t_n} c_i v_i}{q_\infty} \qquad (2)$$

where v_i corresponds to the volume of the eluate sample i, c_i to its concentration and $q_\infty = mq_s$ is the total capacity of the resin where m is the resin sample weight and q_s (mmol g^{-1}) the specific capacity of the resin towards the immobilized ion as determined in Section 2.4.

In the case of tri-phasic systems, a further elution after the first artificial saliva desorption and washing with water was carried out by using either a 0.1M EDTA solution at pH 8 for cationic resins, or a 0.5M $NaNO_3$ solution for anionic resins.

In the case of quadri-phasic systems with mixed bed resins mixtures (composed of both anionic and cationic exchangers with different particle sizes), after the artificial saliva desorption and washing with water, the mixed bed system was separated in the two resin components by sieving. Separated resin samples with larger particle sizes were transferred quantitatively to a column and either the EDTA or $NaNO_3$ solution was passed through the column depending on the type of ion exchanger. During elution, the CaF_2 precipitate remained on the surface of the resin beads and only the Ca^{2+} or F^- still immobilized in the polymeric matrix was eluted by the respective solutions.

On the basis of the analytical results, the CaF_2 mass precipitated on the surface of the exchanger beads (P) was calculated by:

$$P(\text{mg}) = \frac{(q_\infty - q_f)MW_{CaF_2}}{2} \qquad (3)$$

where q_f is the total number of mmol of F^- released to the solution, q_∞ is the total capacity of the resin and, MW_{CaF2} is the molecular weight of CaF_2.

All samples were additionally washed with water, dried and kept for Scanning Electron Microscopy (SEM) analysis with the instrument equipped with an X-Ray Energy Dispersive Spectrometer (EDS), as described in Section 2.2.

To investigate the influence of the mixed bed composition on the Ψ value for both the anionic and cationic exchanger components, kinetic experiments were performed on mixtures of the resins at different ratios. For comparison, tri-phasic systems (loaded resin, target counterion solution and solid CaF_2) were studied at the same anionic to cationic ratios. The ratios Ca^{2+}:F^- studied, expressed in terms of milliequivalents, were 4:1, 2:1, 1:1, 1:2 and 1:4. In the case of tri-phasic systems, the concentrations of Ca^{2+} and F^- in solution (direct solubilization of the corresponding solid salts in the artificial saliva) are shown in Table 2. The main parameters of the systems investigated are given in Table 3.

3 RESULTS AND DISCUSSION

The experimental data have been expressed in terms of degree of conversion, Ψ, versus time.

The corresponding curves for systems 1, 4 and 5–8 (Table 3) are presented in Figs 1a and 1b and indicate that the conversion rates of the cationic exchangers are much lower than that of anionic exchangers both in the bi-, tri- and, quadri-phasic systems. This can be explained by the different selectivity of the cationic and anionic exchange resins towards the target exchanging ions.[26] It is also observed that the increase in the number of phases leads to an increase in Ψ values in the case of cationic ion exchangers, and a decrease in the case of anionic exchangers. To interpret these results the following facts are considered: the results obtained for the tri-phasic and quadri-phasic systems include both the shifting of the equilibrium in systems where ion exchange is accompanied by precipitation (in this case CaF_2, • • $Kps = 2.7 \times 10^{-11}$) and the coating of the surface of the resin beads with the precipitate. The formation of solid CaF_2 follows the actual equilibrium conditions in the related systems. Thus, the concentrations of fluoride and calcium play an important role. In the case of fluoride (Fig 1b), the observed decrease is due to the presence of Ca^{2+} at different conditions. Thus, in the tri-phasic system, Ca^{2+} is at relatively low concentration in the solution of artificial saliva, whereas in the quadri-phasic system, the resin is loaded with Ca^{2+} and provides a higher local concentration of this ion when meeting the released fluoride in the artificial saliva flowing through the mixed bed of resins. These results correlate with those obtained for Ca^{2+} (Fig 1a) since the observed higher release of this cation in the quadri-phasic system, within the relative low volume of the resin, leads to a lower concentration of fluoride because of the formation of the solid CaF_2 under these conditions. In the case of Ca^{2+}, the observed increase in the degree of conversion in comparison with the bi-phasic system may be attributed to the 'supersaturation' effect that occurs in the mixed bed system. This supersaturation

Table 2. Ca^{2+} and F^- concentration in the desorption solution of tri-phasic systems studied

Ca^{2+}:F^- ratios	R_2-Ca^{2+}:F^- solution system (mol dm^{-3})	$R-F^-$:Ca^{2+} solution system (mol dm^{-3})
4:1	5.6×10^{-4}	1.0×10^{-3}
2:1	8.4×10^{-4}	7.0×10^{-4}
1:1	9.6×10^{-4}	4.4×10^{-4}
1:2	1.1×10^{-3}	2.6×10^{-4}
1:4	1.2×10^{-3}	1.5×10^{-4}

Table 3. Parameters of ion exchange systems under investigation

System No	Resin 1, Ionic form, Granulation (mm)	Resin 2, ionic form, granulation (mm)	Desorbing solution	Precipitate	Number of phases	Overall reaction[a]
1	S8528 Ca^{2+}-form 0.42	—	KCl + NaCl	—	2	R_2-Ca + $2Na^+/K^+$ = 2R-Na/K^+Ca^{2+}
2	—	MP62 F-form 0.105	KCl + NaCl	—	2	R-F + Cl^- = R-Cl + F^-
3	S8528 Ca^{2+}-form 0.105	—	KCl + NaCl	—	2	R_2-Ca + $2Na^+/K^+$ = 2R-Na/K + Ca^{2+}
4	—	S3428 F-form 0.45	KCl + NaCl	—	2	R-F + Cl^- = R-Cl + F^-
5[a]	S8528 Ca^{2+}-form 0.42	—	KCl + NaCl + NaF	CaF_2	3	R_2-Ca + 2NaF = 2R-Na/K + CaF_2
6[a]	—	S3428 F-form 0.45	KCl + NaCl + $CaCl_2$	CaF_2	3	2R-F + $CaCl_2$ = 2R-Cl + CaF_2
7	S8528 Ca^{2+}-form 0.42	MP62 •F^--form 0.105	KCl + NaCl	CaF_2	4	R_2-Ca + 2R-F + 2Na/KCl = 2R-Na/K + 2R-Cl + CaF_2
8	S8528 Ca^{2+}-form 0.105	S3428 F^--form 0.45	KCl + NaCl	CaF_2	4	R_2-Ca + 2R-F + 2Na/KCl = 2R-Na/K + 2R-Cl + CaF_2

[a] NaCl and KCl have not been taken into account in the overall reaction despite being involved in the ion exchange process.

stabilizes the solution within the column interstitial space and the eluate collected can start to crystallize either spontaneously,[27,28] or after a certain period of time.[10] Thus, both Ca^{2+} and F^- would benefit from such an effect, but it is only noticed for Ca^{2+} because of its low Ψ values. For F^-, the degree of conversion is very high so the supersaturation effect is not appreciated.

Results obtained in a previous study using interruption tests[29] have shown that the rate-determining step of the ion exchange processes on individual resins is intraparticle diffusion. Taking into account these findings, data collected in Figs 1a and 1b of the present study have been treated by a specific kinetic model valid for the description of ion exchange processes controlled by an intraparticle diffusion mechanism in dynamic systems.[30]

The model is based on a Fick's law adapted to ion exchange resins composed of spherical beads by using the equation:

$$-\ln(1-\Psi^2) = 2\frac{D\pi^2}{r^2}t = 2Bt \qquad (4)$$

where B is the effective rate of release related to the diffusion coefficient, D, by the equation:

$$B = \frac{D\pi^2}{r^2} \qquad (5)$$

and r and t are the resin particle radius and time respectively.

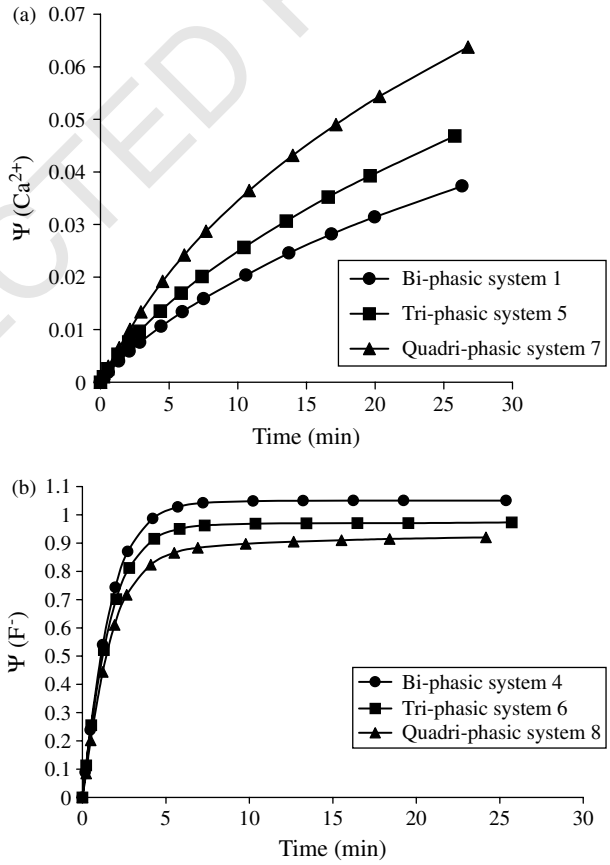

Figure 1. (a) Kinetics of Ca^{2+} release from cationic resin in Ca^{2+}-form of 0.42 mm particle size in the 1:1 Ca^{2+}:F^- ratio. (b) Kinetics of F^- release from anionic resin in F^--form of 0.45 mm particle size in the 1:1 Ca^{2+}:F^- ratio.

The observed linear dependencies of experimental data in terms of $-\ln(1-\Psi^2)$ vs t verify the intraparticle diffusion control of the ion exchange process.

The results obtained in terms of B values are presented in Table 4. As can be appreciated, the increase in $B(Ca^{2+})$ with the number of phases corresponds to the shift of the equilibrium reaction because of the formation of solid CaF_2. On the contrary this solid formation causes a decrease in $B(F^-)$, ie, the presence of the corresponding equilibrium diminishes the rate of fluoride release. In addition, the remarkable difference on diffusivity of both ions in the respective resin phase is revealed. This difference can also be characterized in terms of the diffusion coefficient, D, calculated by eqn (5). The corresponding values are presented in Table 5.

The influence of the resin affinity for the different ions is emphasized by the significant difference in the respective diffusion coefficients.

The relative proportion of anionic and cationic exchange resins in these mixed bed systems has a remarkable influence on the respective Ψ values. Thus, kinetic experiments using mixtures of different proportions of the resins as described above were carried out to elucidate such influences. The results of this series of experiments are shown in Figs 2a, 2b, 3a and 3b. As seen, as more Ca^{2+} is present in the resins mixture, the more solid CaF_2 is formed and consequently less Ca^{2+} is released into the solution phase (due to the influence of the related ion exchange reaction) and this outcome is independent of the particle size of the resins. Therefore, the intraparticle diffusion barrier is not a relevant process compared with the precipitating reaction.

In these figures, the dependence of the release rate of the ions with particle size can be observed. A comparison of the rates of Ca^{2+} and F^- release from the size fractions 0.42/0.45 and 0.105 mm shows that the decrease in the resin particle size increases the rate of ion release. This follows from the increase in the amount of surface contact between the solution and functional groups in the polymeric matrix as the particle size diminishes. This fact is clearly shown in the case of the cationic ion exchanger. Again, the relatively sharper increase of the Ca^{2+} release rate is seen to be more relevant because of the low value of its degree of conversion.

In the corresponding tri-phasic systems, the results obtained at the same Ca^{2+}:F^- ratios, plotted in Figs 4 and 5, support the above findings.

Table 4. Effective rates of release, B, of Ca^{2+} and F^- in the resin phase

	$B(s^{-1})$	
System type	B (Ca^{2+} 0.42 mm) $\times 10^6$	B (F^- 0.45 mm) $\times 10^3$
Bi-phasic	0.4	4.3
Tri-phasic	0.5	3.6
Quadri-phasic	1.5	2.3

Table 5. Diffusion coefficients, D, of Ca^{2+} and F^- in the resin phase

	D ($m^2\ s^{-1}$)	
System type	D (Ca^{2+} 0.42 mm) $\times 10^{15}$	D (F^- 0.45 mm) $\times 10^{11}$
Bi-phasic	2.0	2.2
Tri-phasic	2.2	1.8
Quadri-phasic	6.7	1.1

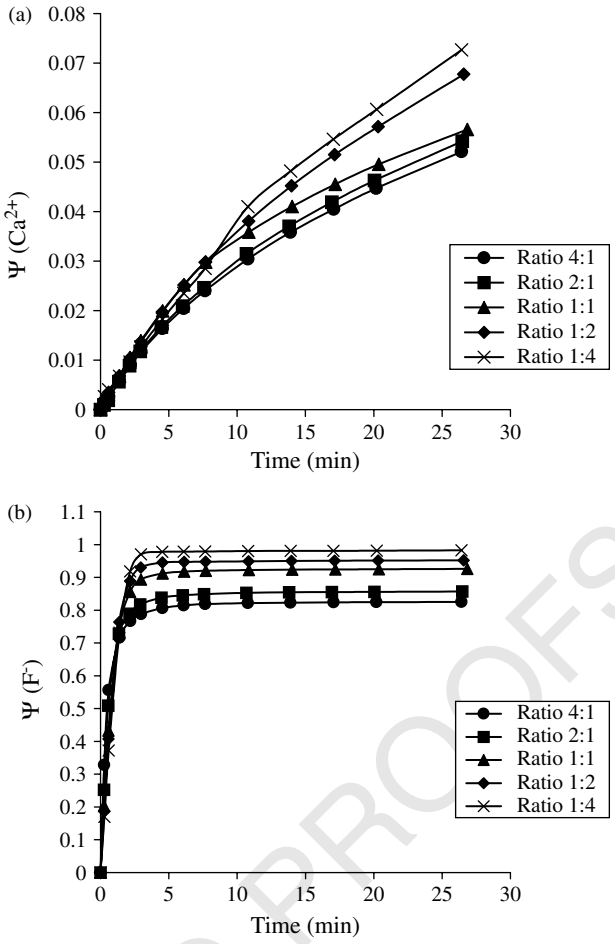

Figure 2. (a) Kinetics of Ca^{2+} release from cationic resin in Ca^{2+}-form in mixed beds R_2-Ca^{2+} (0.42 mm):R-F^- (0.105 mm) of different composition. (b) Kinetics of F^- release from anionic resin in F^--form in mixed beds R_2-Ca^{2+} (0.42 mm):R-F^- (0.105 mm) of different composition.

3.1 Formation of solid CaF_2

Several experiments were carried out to study the formation of the solid CaF_2. Thus, the results obtained using EDTA solutions (10% v/v, pH 8) are shown in Figs 6a–6d. The higher conversion degree obtained for Ca^{2+}, under these conditions, shows that EDTA diminishes the formation of CaF_2 by competition with fluoride for calcium ions. Furthermore, the total quantity of Ca^{2+} and F^- recovered, obtained as the sum of both the kinetic release experiment and the additional stripping with the corresponding

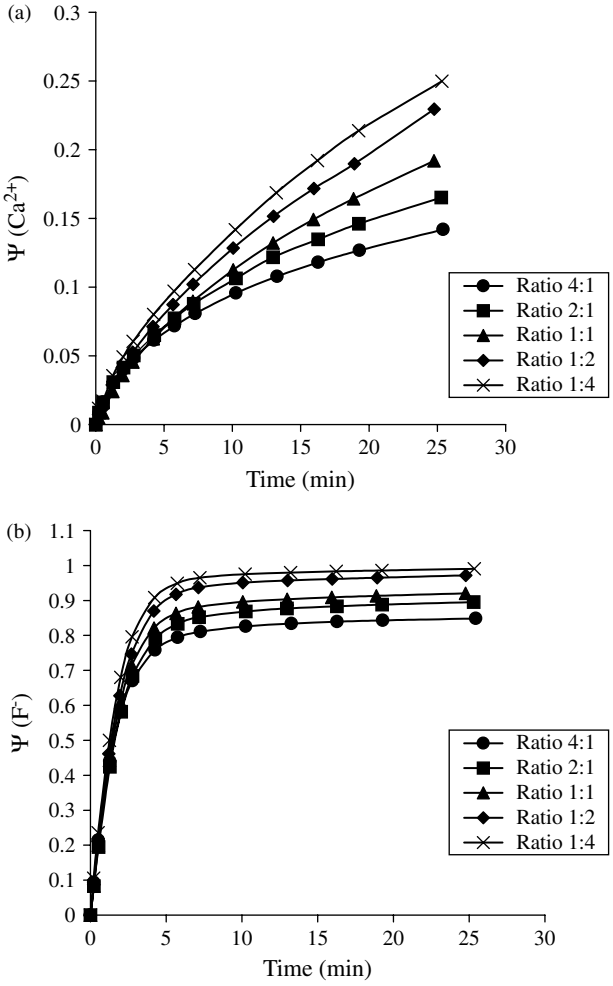

Figure 3. (a) Kinetics of Ca^{2+} release from cationic resin in Ca^{2+}-form in mixed beds R_2-Ca^{2+} (0.105 mm):R-F^- (0.45 mm) of different composition. (b) Kinetics of F^- release from anionic resin in F^--form in mixed beds R_2-Ca^{2+} (0.105 mm):R-F^- (0.45 mm) of different composition.

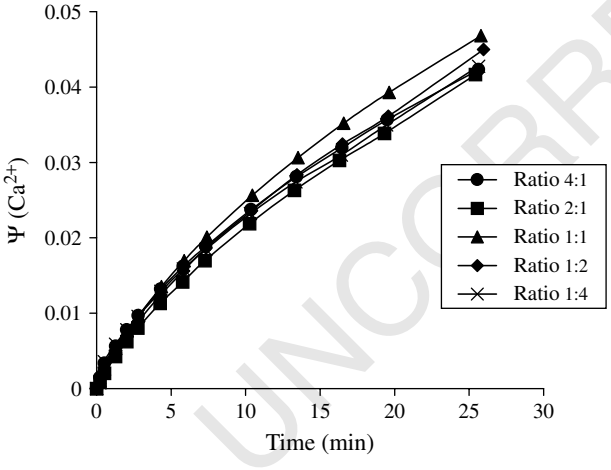

Figure 4. Kinetics of Ca^{2+} release from cationic resin in Ca^{2+}-form of 0.42 mm particle size in tri-phasic systems of different composition.

solution, is lower than the number of ions initially immobilized on the respective ion exchange resins. It was also demonstrated that neither the EDTA nor the $NaNO_3$ stripping solutions are capable of dissolving

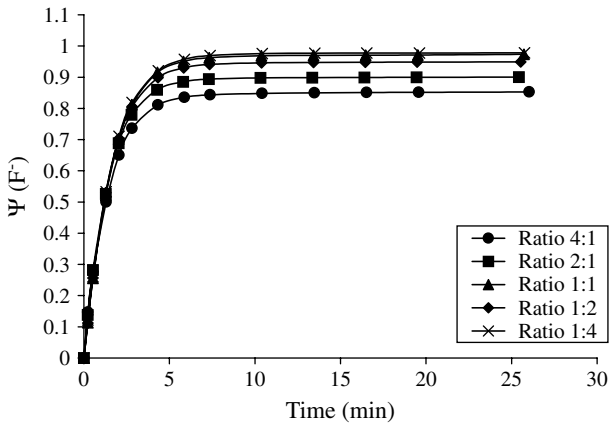

Figure 5. Kinetics of F^- release from anionic resin in F^--form of 0.45 mm particle size in tri-phasic systems of different composition.

CaF_2 at the working pH. On the contrary, complete desorption of both Ca^{2+} and F^- is achieved from the corresponding ion exchangers when the above solutions are used. Accordingly, the observed lack of Ca^{2+} and F^- and the low solubility of CaF_2 support its precipitation on the surface of the exchanger beads.

As a consequence of the previous findings, the amount of CaF_2 precipitated on the exchanger beads in the quadri-phasic systems 7 and 8 has been determined (Fig 7). Note that this amount of CaF_2 has been obtained by potentiometric measurements of fluoride, since Ca^{2+} was determined by atomic emission spectroscopy (ICP–OES), where both Ca^{2+} free in solution and present as suspended particles of CaF_2 are jointly determined. In fact, some precipitate can be observed in the first aliquots of the desorption solution due to the high flux rate flowing through the resin bed that carries away some of the solid precipitated on the exchanger beads.

To verify the above results, comparative analysis of the data of calcium determination by both potentiometric (ISE) and atomic emission spectroscopy was performed. As seen in Fig 8, the higher conversion values for Ca^{2+} when the solutions are analyzed by ICP–OES support the presence of solid CaF_2.

Additional confirmation of the formation of solid CaF_2 is reflected in the concave curves shown in Figs 9 and 9b, where the concentrations of Ca^{2+} or F^- with time in the desorption solutions for systems 5 and 6 are plotted. Indeed, during the first 0.5–2 min a decrease in either Ca^{2+} or F^- concentration, in the respective system, reveals the formation of solid CaF_2.

Finally, acidic treatment of both cationic and anionic resins from systems 7 and 8 (1:1 Ca^{2+}:F^- ratio) after the kinetic •experiments indicates the presence of fluoride mainly in the larger resin granules (Table 6), that can directly be assigned to the CaF_2 precipitated on the surface of the exchanger beads.

Note that in system 7 the quantity of CaF_2 precipitated is considerably higher and is concentrated on the cationic exchanger. According to previous findings,[31] the formation of these crystals in a mixture

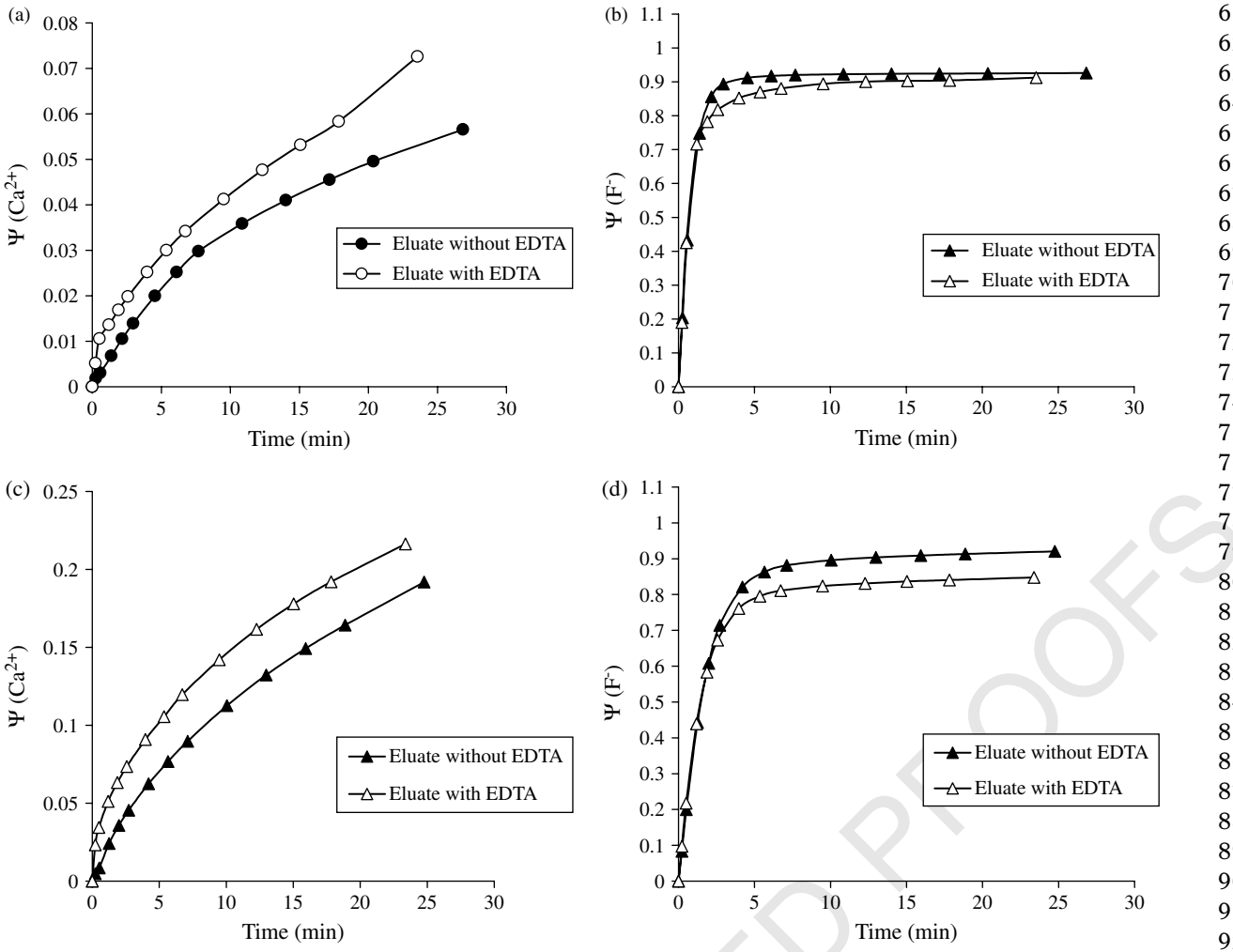

Figure 6. (a) Kinetics of Ca^{2+} release from cationic resin in Ca^{2+}-form in mixed bed R_2-Ca^{2+} (0.42 mm):R-F^- (0.105 mm) of 1:1 ratio. (b) Kinetics of F^- release from anionic resin in F^--form in mixed bed R_2-Ca^{2+} (0.42 mm):R-F^- (0.105 mm) of 1:1 ratio. (c) Kinetics of Ca^{2+} release from cationic resin in Ca^{2+}-form in mixed bed R_2-Ca^{2+} (0.105 mm):R-F^- (0.45 mm) of 1:1 ratio. (d) Kinetics of F^- release from anionic resin in F^--form in mixed bed R_2-Ca^{2+} (0.105 mm):R-F^- (0.45 mm) of 1:1 ratio.

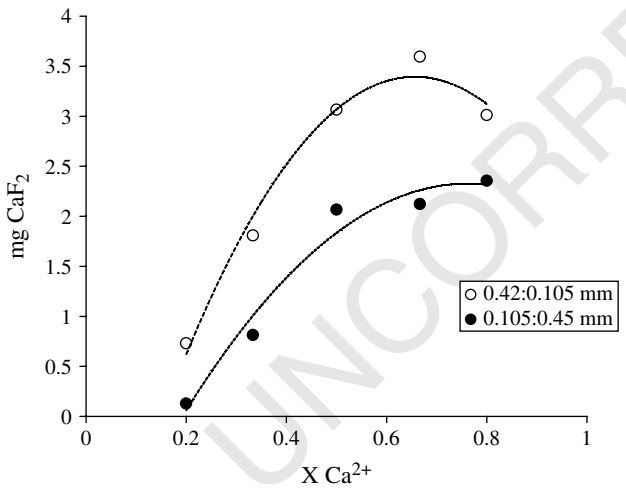

Figure 7. Dependence of the formation of crystalline solid CaF_2 with mixed bed systems R_2-Ca^{2+} (0.42 mm):R-F^- (0.105 mm) and R_2-Ca^{2+} (0.105 mm):R-F^- (0.45 mm) composition.

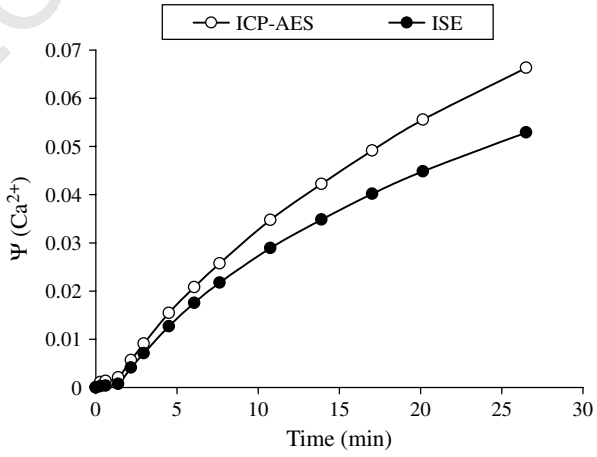

Figure 8. Kinetics of Ca^{2+} release from cationic resin in Ca^{2+}-form in mixed bed R_2-Ca^{2+} (0.42 mm):R-F^- (0.105 mm) of 1:1 ratio. Detection techniques comparison: ion selective electrode (ISE) and atomic emission spectroscopy (ICP).

of ion exchange resins mainly takes place on the surface of the resin characterized by the lowest kinetics of release and largest particle size. In fact, under the experimental conditions employed, rapid accumulation of F^- in the solution surrounding the ion exchangers, in comparison with Ca^{2+}, can be

Table 6. Mass of CaF_2 precipitated on the surface of the ion exchangers

	R_2-Ca		R-F	
	0.42 mm (system 7)	0.105 mm (system 8)	0.45 mm (system 8)	0.105 mm (system 7)
mg CaF_2	2.33 ± 0.05	0.067 ± 0.002	0.233 ± 0.005	0.130 ± 0.003

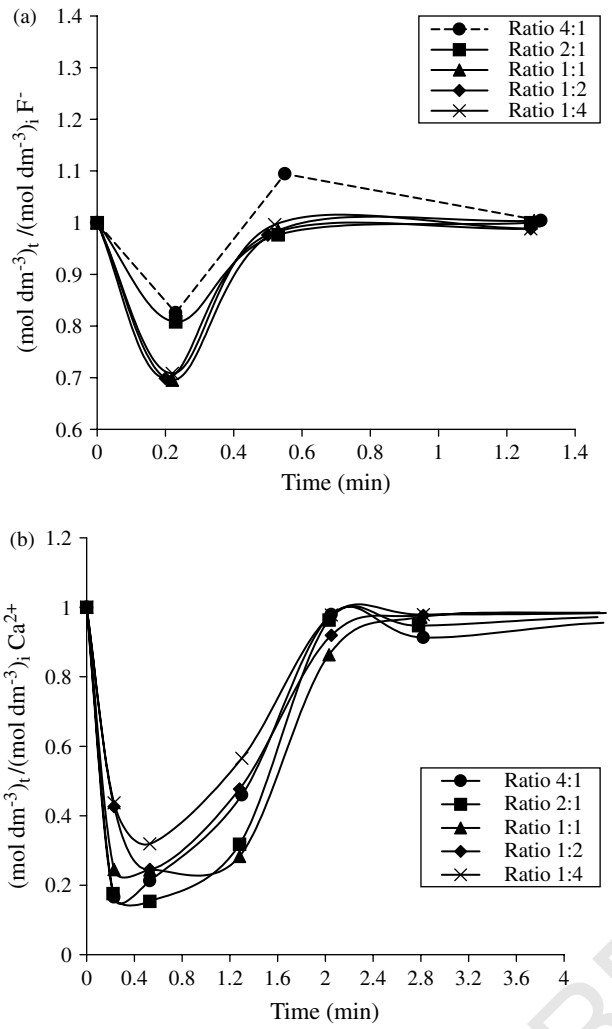

Figure 9. (a) Variation of the concentration of F^- with time in the desorption solutions used in tri-phasic systems R_2-Ca^{2+} (0.42 mm):F^- (solution). (b) Variation of the concentration of Ca^{2+} with time in the desorption solutions used in tri-phasic systems R-F^- (0.45 mm):Ca^{2+} (solution).

expected and thus promotes the formation of solid CaF_2 on the surface of the cation exchanger. However, the contribution of the bead surface is remarkable since in system 8 the precipitate of CaF_2 is observed on the particles of larger size and not on those with a slower release• rate.

Following the previous description and taking into account size and rate of ion release, the formation of CaF_2 follows the sequence:

$$R_2\text{-Ca } 0.42\text{mm}\bullet > \text{R-F } 0.45\text{mm} > R_2\text{-Ca } 0.105\text{mm} > \text{R-F } 0.105\text{mm}$$

In addition, the data in Fig 7 show that the increase in the cationic component in the •mixture increases the amount of CaF_2 formed, so the mass of crystalline solid formation is dependent on the lower releasable ion, ie calcium. Thus because the rate of release is also dependent on the resin surface, system 8, which is formed by the cationic resin in Ca^{2+}-form with the smallest particle size, should lead to the highest CaF_2 formation. However, none of the experiments have confirmed this expectation. In this case, the supersaturation taking place within the column interstitial space clearly depends on the extent of such space, which is far higher in system 8 than in system 7 because the lower density of, the anionic resin leads to a higher bed volume when the largest particles are used.

3.2 SEM characterization

The results obtained can be further confirmed by the scanning electron microscopy images shown in Fig 10. As seen from the figure, the crystals formed on the surface of the cationic ion exchanger of 0.42 mm particle size can be clearly seen; indeed a smaller amount is observed in the image of the 0.45 mm particle size anionic ion exchanger and practically nothing in the resins of 0.105 mm particle size. Other SEM images of ion exchangers of large size from the ratios Ca^{2+}:F^- 4:1 and 1:4 obtained from both systems 7 and 8, also show (Fig 11), in comparison with systems 1 and 2, the presence of CaF_2 crystals on the surface of the ion exchanger. Further analysis by SEM–EDS and the fact that the system does not chemically allow formation of any other solids (no ions other than calcium and fluoride are present in the polymeric matrices) have confirmed the presence of CaF_2 crystals on the ion exchangers' surface.

4 CONCLUSIONS

From the results obtained, the following conclusions can be drawn.

1. The ion exchange kinetics in tri-phasic and quadri-phasic systems involving a weak base anionic exchanger in F^--form and a weak acid cationic exchanger in Ca^{2+}-form is accompanied by CaF_2 precipitation and shows that in both systems the rate of Ca^{2+} release from the cationic exchanger is lower than that of F^- from the anionic resin.
2. The release rate of calcium and fluoride ions is controlled by intraparticle diffusion and has been characterized by a Fick's law model. The

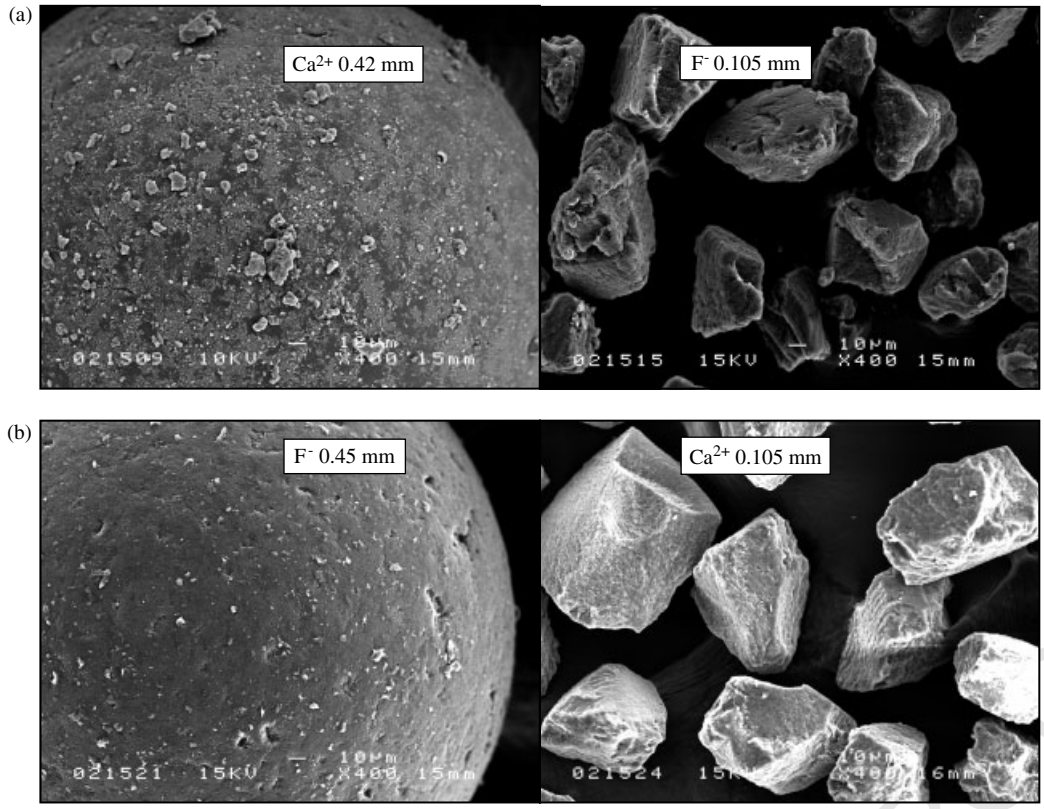

Figure 10. SEM images from mixed bed systems 7 and 8 (1:1 ratio) after desorption. (a) System 7: R_2-Ca^{2+} (0.42 mm):R-F^- (0.105 mm). (b) System 8: R_2-Ca^{2+} (0.105 mm):R-F^- (0.45 mm).

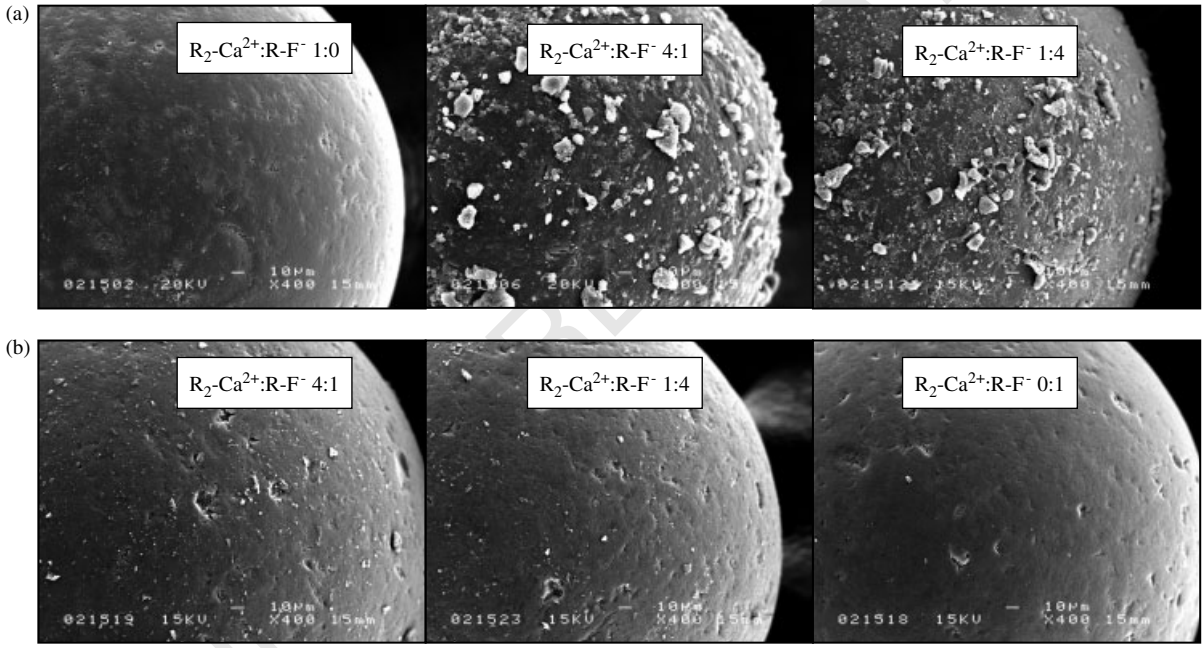

Figure 11. SEM images from mixed bed systems 7 and 8 of different composition after desorption. (a) R_2-Ca^{2+} (0.42 mm) of system 7 (R-Ca^{2+} : R-F^- ratios: 1:0, 4:1 and, 1:4). (b) R-F^- (0.45 mm) of system 8 (R-Ca^{2+} : R-F^- ratios: 4:1, 1:4 and, 0:1).

quantitative terms of effective rate of release (B) and diffusion coefficient (D) of the respective ions in the resin phase clearly depend on the type of resin and the presence of different numbers of phases.

3. The amount of precipitate crystallizing on the surface of resin beds depends on the type of the ion exchange resin, the respective particle size •and on the ratio of resin components (cationic/anionic) mainly in the case of a quadri-phasic system containing a mixed resin bed.
4. By Varying the ratio of type of resins and their particle size it is possible to accomplish

the precipitation mostly on the larger surface of the ionic exchanger. Under supersaturation conditions, when the solution leaves the resin column, precipitation takes place mainly in the solution phase after a certain period of time.

ACKNOWLEDGEMENTS

This work was supported by the Spanish Ministry of Science and Technology (research project PPQ2002-04267-C03-01). AT acknowledges the Universitat Autònoma de Barcelona for the FI Research Grant to support her studies.

REFERENCES

1 Regen SL, Triphase catalysis. Kinetics of cyanide displacement on 1-bromooctane. *J Am Chem Soc* **98**:6270–6274 (1976).
2 Regen SL and Besse JJ, Liquid–solid–liquid triphase catalysis. Consideration of the rate-limiting step, role of stirring, and catalyst efficiency for simple nucleophilic displacement. *J Am Chem Soc* **101**:4059–4063 (1979).
3 Wu HS and Tang JF, Formation and hydrolysis of 4-methoxyphenylacetic acid butyl ester reacting from 4-methoxyphenylacetic acid and *n*-bromobutane using triphase catalysis. *J Molec Catal A* **145**:95–105 (1999).
4 Muraviev D, Oleinikova M and Valiente M, Aqua-impregnated resins. 1. Mass transfer active interfaces in bi- and triphase systems involving solid polymer and two immiscible liquid phases. *Langmuir* **13**:4915–4922 (1997).
5 Oleinikova M, Muraviev D and Valiente M, Aqua-impregnated resins. 2. Separation of polyvalent metal ions on iminodiacetic and polyacrylic resins using bis(2-ethylhexyl)phosphoric and bis(2-ethylhexyl) dithiophosphoric acids as organic eluents. *Anal Chem* **71**:4866–4873 (1999).
6 Muraviev D, Torrado A and Valiente M, Extraction of non-extractable ionic species in aqua impregnated resin systems, in *Proceedings of ISEC '99*, Barcelona, Spain. Vol 2, pp 1291–1295 (2001).
7 Kataoka T, Muto A and Nishiki T, Theoretical analysis of mass transfer of deionization by cation and anion mixed-ion exchange resins—A batchwise contact. *J Chem Eng Japan* **27**:375–381 (1994).
8 Harries RR, Ion exchange kinetics in ultra pure water systems. *J Chem Technol Biotechnol* **51**:437–447 (1991).
9 Noh B II, *et al*,• Parametric studies on the performance of mixed-bed ion exchange at ultralow concentrations—1. Multicomponent system. *Korean J Chem Eng* **16**:737–744 (1999).
10 Muraviev D, Noguerol J, Gaona J and Valiente M, Clean Ion-exchange technologies 3. Temperature-enhanced conversion of potassium chloride and lime milk into potassium hydroxide on a carboxylic ion exchanger. *Ind & Eng Chem Res* **38**:4409–4416 (1999).
11 Pietrzyk DJ, Senne SM and Brown DM, Anion–cation separations on a mixed-bed ion-exchange column with indirect photometric detection. *J Chromatogr* **546**:101–110 (1991).
12 Gorshkov VI, Ion exchange methods for ultra purification of inorganic, organic, and biological substances. *Solv Extr & Ion Exch* **16**:1–73 (1998).
13 Soldatov VS, Ion exchanger mixtures used as artificial nutrient media for plants, in *Ion Exchange for Industry*, ed by Streat M. Ellis Horwood, Chichester, pp 652–658 (1988).
14 Naumann G, Pieper G and Rehberg HJ, Dental composition and appliances containing anti-carious ion exchange resins. US Patent 3,978,206 (1976).
15 Valiente M, Muraviev D and Zvonnikova LV, Material remineralizante de tejidos organominerales. Spanish Patent 9700016 (1997).
16 Corpron RE, *et al*, *In vivo* remineralization of artificial enamel lesions by fluoride dentifrice or mouthrinse. *Caries Res* **20**:48–55 (1986).
17 White DJ, Reactivity of fluoride dentifrices with artificial caries III. Quantitative aspects of acquired acid resistance (AAR): F uptake, retention, surface hardening and remineralization. *J Clin Dent* **3**:6–14 (1991).
18 Gerould CH, Electron microscope study of the mechanism of a fluoride deposition in teeth. *J Dent Res* **24**:223–233 (1945).
19 Wefel JS and Harless JD, The effect of topical fluoride agents on fluoride uptake and surface morphology. *J Dent Res* **60**:1842–1848 (1981).
20 Benediktsson S, *et al*, The effect of contact time of acidulated phosphate fluoride on fluoride concentration in human enamel. *Arch Oral Biol* **27**:567–572 (1982).
21 Brice JC, Diffusive and kinetic processes in growth from solution. *J Crystal Growth* **1**:(1967).
22 Pamplin BR, *Crystal Growth*. Pergamon Press, Oxford (1975).
23 Dorfner KA,• *Ion Exchangers*, ed by Dorfner K Walter der Gruyter Publisher, Berlín, •p 128 (1991).
24 Dorfner KA, *Ion Exchangers*, ed by Dorfner K Walter der Gruyter Publisher, Berlín, p 328• (1991).
25 •Dorfner KA, *Ion Exchangers*, ed by Dorfner K Walter der Gruyter Publisher, Berlín, p 94• (1991).
26 Korkisch J, *Handbook of Ion Exchange Resins: Their Application to Inorganic Analytical Chemistry*. CRC Press, Inc, Florida, Vol 1, •p 16 (1989).
27 Muraviev D, *et al*, Clean ion-exchange technologies. I. Synthesis of chlorine-free potassium fertilizers by an ion-exchange isothermal supersaturation technique. *Ind Eng Chem Res* **37**:1950–1955 (1998).
28 Khamizov RKh, *et al*, Clean ion-exchange technologies. 2. Recovery of high-purity magnesium compounds from seawater by an ion-exchange isothermal supersaturation technique. *Ind Eng Chem Res* **37**:2496–2501 (1998).
29 Muraviev D, Torrado A and Valiente M, Kinetics of release of calcium and fluoride ions from ion-exchange resins in artificial saliva. *Solv Extr & Ion Exch* **18**:345–374 (2000).
30 Streat M and Naden D, Ion exchange in uranium extraction, in *Ion Exchange and Sorption Processes in Hydrometallurgy. Critical Reports on Applied Chemistry*,ed by Streat M and Naden D. John Wiley & Sons, Chichester, pp 1–55 (1987).
31 Muraviev D, Sverchkova OYU, Voskresensky NM and Gorshkov VI, Kinetics of ion exchange in polyphase systems including crystallizing substances. *React Polym* **17**:75–88 (1992).

QUERIES TO BE ANSWERED BY AUTHOR (SEE MARGINAL MARKS)

IMPORTANT NOTE: Please mark your corrections and answers to these queries directly onto the proof at the relevant place. Do NOT mark your corrections on this query sheet.

Query No.	Query
Q1	Please clarify
Q2	Confirm pH 8 refers only to EDTA?
Q3	Confirm amendment?
Q4	Define t
Q5	Confirm OK, not K_{ps} or Kp_s,
Q6	Define symbol
Q7	F or F^-
Q8	Please clarify
Q9	Confirm amendment
Q10	What does R indicates
Q11	Please clarify
Q12	Please clarify
Q13	‘‘Please provide names of all contributors rather than et al’’
Q14	?KA or K
Q15	Closing page nos
Q16	Closing page nos
Q17	?Chapter titles
Q18	Closing page nos
Q19	Closing page nos